

THESIS FOR THE DEGREE OF DOCTOR OF PHILOSOPHY

Production and Characterization of ZrN and PuN Materials for
Nuclear Fuel Applications

Marcus Hedberg



Department of Chemistry and Chemical Engineering

CHALMERS UNIVERSITY OF TECHNOLOGY

Gothenburg, Sweden 2016

Production and Characterization of ZrN and PuN Materials for Nuclear Fuel Applications

MARCUS HEDBERG

ISBN 978-91-7597-465-1

© MARCUS HEDBERG, 2016

Doktorsavhandlingar vid Chalmers tekniska högskola.

Ny serie Nr 4146

ISSN: 0346-718X

Department of Chemistry and Chemical Engineering

Chalmers University of Technology

SE-412 96 Gothenburg

Sweden

Telephone +46 (0)31-772 1000

Cover:

Powder X-ray diffractogram of produced PuN powder compared against the diffraction pattern of pure PuN according to the Powder Diffraction File (PDF) database.

Printed by:

Chalmers Reproservice

Gothenburg, Sweden

2016

Production and Characterization of ZrN and PuN Materials for Nuclear Fuel Applications

MARCUS HEDBERG

Department of Chemistry and Chemical Engineering

Chalmers University of Technology

Abstract

At the heart of a nuclear reactor resides its fuel. The chemical composition of the nuclear fuel affects the performance of several key properties important for the overall operation and safety performance of the reactor. The energy-producing reactors presently operational in the world utilize oxide-based nuclear fuel, which has been the dominating fuel form throughout the history of commercial nuclear power. The concept of nitride-based nuclear fuel is not new and development in the field, together with studies on actinide nitride properties, has been conducted for 50-60 years, although in limited scale compared to oxides. Nitride-based nuclear fuel possess properties making it an interesting fuel form in light water reactors as well as liquid metal cooled reactors envisioned for fourth generation nuclear power systems. In generation four reactor systems nitride-based fuel is an interesting fuel option both in UN-based liquid metal cooled breeding reactors as well as in reactors dedicated to the burning of transuranic actinides present in the used fuel of current light water reactors. This thesis focuses on the studies of inert matrix fuels mainly for non-breeding reactor purposes. In this work preparation and characterization of nitride fuel matrices of ZrN, ZrPuN and PuN have been studied. The internal gelation method has been applied for formation of oxide microsphere precursor material and carbothermal reduction has been applied for nitride production. Nitride fuel pellet purity and final density have been studied through cold pressing and sintering as well as ZrCN pellet formation from microspheres through spark plasma sintering. Investigations of nitride purity estimations through powder X-ray diffraction data has been performed. Am losses during the production route of PuN pellets by both internal gelation and powder synthesis has been investigated. Production of reasonably pure PuN through carbothermal reduction is possible and purities up to $\text{PuN}_{0.99}\text{C}_{0.01}$ have been reached. Carbide formed in ZrN was more stable and in the Zr system nitride purities of about $\text{ZrN}_{0.85}\text{C}_{0.15}$ were achieved. Conventional pressing and sintering of ZrCN microspheres did not reach densities above about 50% of theoretical density while spark plasma sintering of ZrCN of similar purity reached about 85% TD. PuN powder could be conventionally pressed and sintered to almost 80% of TD. It has been shown that ZrCN materials can be accurately composition estimated by XRD data while quaternary (Zr,Pu)(C,N) material estimations overestimated nitride purity somewhat. During PuN synthesis about 4% Am was lost during carbothermal reduction. Sintering in N_2 atmosphere resulted in total losses of about 11% Am while sintering in Ar atmosphere yielded losses of about 50% Am.

Keywords: Nuclear fuel, Zirconium Nitride, Plutonium Nitride, Internal gelation, Carbothermal reduction

List of Publications

The thesis is based on the work contained in the following articles, referred to by Roman numerals in the text:

- I. Hedberg, M., Ekberg, C., Studies on plutonium-zirconium co-precipitation and carbothermal reduction in the internal gelation process for nitride fuel preparation, 2016, Journal of Nuclear Materials 479, pp. 608-615
Contribution: Main author, all experimental work.

- II. Hedberg, M., Cologna, M., Cambriani, A., Somers, J., Ekberg, C., Zirconium carbonitride pellets by internal sol gel and spark plasma sintering as inert matrix fuel material, 2016, Journal of Nuclear Materials 479, pp. 137-144
Contribution: Main author, most experimental work.

- III. Hedberg, M., Streit, M., Ekberg, C., Effects of carbide impurities on the lattice parameter of mixed zirconium nitrides, Submitted to Progress in Nuclear Engineering
Contribution: Main author, part of the experimental work.

- IV. Hedberg, M., Ekberg, C., A comparative study of nitride purity and Am fabrication losses in PuN materials by the powder and internal gelation production routes, 2016, Submitted to Journal of Nuclear Materials
Contribution: Main author, all experimental work.

Table of Contents

1.	Introduction	1
1.1.	Objectives	2
2.	Background	5
2.1.	The concepts of fast and thermal nuclear reactors	5
2.2.	Chemical forms and properties of nuclear fuel	6
2.2.1.	Oxide fuel	6
2.2.2.	Nitride fuel	7
2.2.3.	Carbide fuel	9
2.2.4.	Inert matrix fuels	9
2.3.	Fuel type geometries	10
2.4.	Gelation based techniques for microsphere production	11
2.4.1.	The external gelation process	11
2.4.2.	The ORNL process	11
2.4.3.	The IChTJ (INCT) process and the double extraction process.....	11
2.4.4.	The internal gelation process.....	12
2.5.	Nitride production techniques	12
2.5.1.	The cyclic hydriding/nitriding process	12
2.5.2.	Oxidative ammonolysis	13
2.5.3.	Reactive ball milling.....	13
2.5.4.	Nitride formation from metal halides	13
2.5.5.	Carbothermal reduction	13
3.	Theory	15
3.1.	The internal gelation process.....	15
3.2.	Carbothermal reduction and nitride formation	17
3.3.	Pellet formation and sintering	19
3.3.1.	Mechanical pressing and sintering	19
3.3.2.	Spark plasma sintering	21
3.4.	Characterization techniques.....	21
3.4.1.	Scanning Electron Microscopy.....	21
	Energy Dispersive X-ray Spectroscopy.....	22
3.4.2.	X-ray diffraction.....	22
3.4.3.	Elemental analysis based on inert gas fusion and/or combustion.....	22
3.4.4.	Computer X-ray tomography for density gradient evaluation.....	22
3.4.5.	HPGe gamma spectrometry.....	22
3.5.	Composition estimations of solid solutions.....	23

4.	Methods and experimental procedures	27
4.1.	Preparation of zirconium containing sols and microspheres	27
4.2.	Preparation of Zr/Pu mixed sols and gelation of microspheres	28
4.3.	Preparation of Pu sol and gelation of microspheres	30
4.4.	Nitridation of microspheres and powders	31
4.4.1.	Carbothermal reduction of Zr-based microspheres	32
4.4.2.	Carbothermal reduction of mixed Zr/Pu microspheres	33
4.4.3.	Preparation and carbothermal reduction of PuO ₂ powders	33
4.4.4.	Carbothermal reduction of Pu-based microspheres	33
4.5.	Pellet fabrication and sintering	33
4.5.1.	Conventional cold pressing of pellets	33
4.5.2.	Sintering of pelletized compacts	34
4.5.3.	Spark plasma sintering on nitrided Zr microspheres	34
5.	Results and discussion	35
5.1.	Dispersion stabilization	35
5.2.	Microsphere production	37
5.2.1.	Production of Zr based microspheres	37
5.2.2.	Gelation of mixed Zr/Pu sols	40
5.2.3.	Production of Pu based microspheres	44
5.3.	Light element quantification by EDX	46
5.4.	Light element quantification and XRD measurements	47
5.5.	Composition determinations by Vegard's law and mixed nitride influence on lattice parameter	49
5.5.1.	Ternary ZrCN materials	49
5.5.2.	Quaternary ZrPuCN materials	50
5.6.	Pellet formation and sintering	53
5.6.1.	Conventional pressing and sintering of Zr-based microspheres	53
5.6.2.	Spark plasma sintering of Zr-based microspheres	62
5.6.3.	Pellet formation of mixed Zr/Pu microspheres	69
5.6.4.	PuN pellets produced from powders and internal gelation	73
5.7.	Am volatilization in PuN matrix pellets	78
6.	Summary and Conclusions	81
7.	Future Work	83
8.	Acknowledgements	85
9.	References	87

1. Introduction

Electricity is a prerequisite for modern life as known today. The integration of electrical equipment within the developed world is so profound that today's accustomed lifestyle is impossible without it. Yet electricity as a type of energy is seldom, if ever, enjoyed by the final consumer in its inherent energy form. When electricity is consumed it is generally converted into other forms of energy. For example it can be used for propulsion by conversion into mechanical energy powering the electrical engines of a train, for heating applications by powering a stove or an electrical heating radiator, for production of electromagnetic radiation, whether it is in the form of light from a light bulb or information carrying light such as radio waves. The key point and greatness of electricity is thus the ability to convert it into the correct type of energy desired at any given moment, coupled with the rapid and efficient energy distribution accessible from an electric power grid. If following this power grid upstream, it is by the thermo-dynamical principle of energy conservation a necessity to find an electricity generating source putting energy into the electrical grid. There are several different ways in which this electricity generating source can be constructed and what fuel is utilized. On a worldwide scale, both in the past and still in the present, the dominating energy source has been the combustion of fossil materials such as coal and oil [WEC 13]. Due to the increase in awareness regarding global environmental effects caused by combustion of carbon-based fuels, such as global warming and ocean acidification, both by CO₂ release, more attention and focus is constantly being shifted towards lower carbon footprint techniques. Among such techniques one can include for example hydro-, wind-, solar- and also nuclear power.

At the end of 2014, 438 nuclear reactors for commercial power production purposes were operational, amounting to a production capacity of 376.2 GW(e) [IAE 15]. On the non-power producing side there were 247 operational research reactors at the end of 2014 [IAE 15]. In Sweden 10 power producing reactors, comprising 7 boiling water reactors (BWR) and 3 pressurized water reactors (PWR), generated 62.3 TWh, corresponding to 41.5% of the electricity consumption during 2014 [IAE 15].

As most techniques for the production of virtually anything there are advantages and disadvantages. This holds true also for electricity production by nuclear power. The general benefits of nuclear power include large scale production capacity, low carbon emission and high energy density of the fuel used, i.e. it is possible to extract a lot of energy from a small volume of fuel. The main disadvantages of nuclear energy generally does not concern negative effects during every day operation. The two big disadvantages of nuclear power are potential release of artificial radioactivity into the environment during accident conditions and the requirement for safe storage of the used nuclear fuel for a time period in the range of 100 000 years [SKB 11]. By introducing recycling of nuclear fuel into the nuclear fuel cycle the required storage time of the final waste can instead be reduced to about 1000 years [BON 75]. Depending on the design of a recycle-integrated nuclear fuel cycle, the composition of new fuel from recycled material can be, and in some cases will be, unsuitable for use in the current generation of commercial reactors [SOM 11]. One highly important parameter in the design of nuclear energy systems is the chemical composition of the nuclear fuel. The composition of the fuel will affect important properties, such as what temperature the fuel will keep its integrity before

meltdown occurs and how well the fuel chemically resists the core coolant in cases of fuel rod rupture.

The fuel from which a nuclear power plant extracts energy is generally uranium and to lesser degree also some plutonium. All of the Swedish reactors and the vast majority of the other 428 operational power-producing reactors use nuclear fuel in the chemical form of oxide.

A nuclear reactor can be, and in several early reactors was, driven by metallic fuel [RIN 86]. Partially due to higher chemical and thermal stability, the metallic uranium-based fuels were successively abandoned and replaced by nuclear energy development based on UO_2 fuel instead [RIN 86]. Throughout the history of commercial nuclear power production UO_2 -based nuclear fuel has therefore been the default choice and dominating fuel type, resulting in an experience base that vastly exceeds that of any other fuel type [LOV 06].

Oxide-based nuclear fuels are however not a superior chemical form of nuclear fuel in every way imaginable. Alongside the development of oxide nuclear fuel several other fuel types have been under development throughout the history of nuclear power, even if most of these fuels have not made it to the commercial power production level yet. Among these fuels nitride-based nuclear fuel is one option. In metal nitride nuclear fuel, instead of metal bonding to oxygen, the material is made up of metal bonding to nitrogen atoms, hence the name nitride. A metal nitride will have mechanical and chemical properties that differs from that of the corresponding metal oxide. This means that the metal nitride may acquire some properties that are superior to that of the metal oxide in the context of nuclear fuel fabrication and performance, but also that other properties may be inferior in the same respects. In the end it is thus not the case that any single nuclear fuel type is, or will be, the superior choice in every given nuclear reactor and nuclear fuel cycle. That is why it is of interest and importance to continue development and research into the field of nuclear fuel and not simply settle for the standard oxide fuel dominant in nuclear power today.

In potential future recycle-integrated fuel cycles, it may be desirable to avoid processes requiring handling of highly radioactive powders during fabrication of trans-uranium containing fuels. This can be achieved by applying solution-based gelation processes. Such an approach would also be inherently compatible with solvent extraction-based recycling processes for used nuclear fuel.

1.1. Objectives

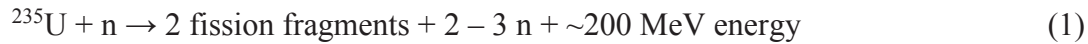
In this work the focus has been aimed towards production and characterization of (Zr,Pu)N-based inert matrix fuel (IMF). Work has been performed within production of the inert matrix ZrN, the actual plutonium-containing IMF (Zr,Pu)N and also production of pure PuN materials and pellets. Work has mainly been performed within the area of nitride production from material produced by internal gelation methods but powder route synthesis has also been studied. The coupling between internal gelation and nitride fabrication has previously been studied to a limited degree and mostly with respect to the uranium system. Studies regarding the production of Zr, Zr,Pu and Pu nitrides starting from the internal gelation process are however scarce. The scope of the work has been focused on extending the existing knowledge in the field of production of (Zr,Pu)N nuclear fuel to include pellet fabrication from the nitrated

microsphere state. This includes studies of both cold pressing techniques as well as Spark plasma sintering of nitride microspheres, the latter so far being a technique most commonly applied to studies of fine powder systems in the nuclear fuel field.

2. Background

2.1. *The concepts of fast and thermal nuclear reactors*

A nuclear reactor operates by a self-sustaining, neutron induced, fission chain reaction. During a fission event, fission fragments are formed together with release of on average 2-3 neutrons and energy. Using ^{235}U as example a fission reaction can be expressed as



Fission cross sections and fission probabilities are dependent not only on the type of nucleus being irradiated with neutrons but also on the kinetic energy of the neutrons used during irradiation [NOR 12]. Nuclear power plants can be constructed to in principle operate on either thermal or fast neutrons. Which of the actinides, and which of their respective isotopes, that can effectively be used as fuel depends on if the nuclear reactor used operates using a thermal or a fast neutron spectrum [NOR 12].

Nuclear reactors can be divided into two major sub groups, Fast and thermal neutron reactors. In the thermal neutron reactor, such as the BWR and the PWR, transuranic actinides are produced by successive neutron capture and beta minus decay reactions. Some of the nuclides produced, such as ^{239}Pu and ^{241}Pu for example, are fissile in a thermal neutron reactor [WAL 11]. Such nuclides can therefore be recovered and used as fuel in thermal reactors. Production of mixed oxide fuel (MOX) is an example of such a recovery process. Other nuclides formed when using UO_2 fuel in thermal reactors, such as ^{237}Np , ^{240}Pu , ^{241}Am , ^{243}Am and ^{244}Cm for example, are not readily split by thermal neutrons. Thermal reactors are therefore generally not considered an optimal choice for transmutation of minor actinides even if concepts do exist for transmutation of, for example, Am in thermal reactors [CHA 99].

In fast neutron reactor systems the moderation of neutrons is not desired. As a result water is not used as core coolant and liquid metal or gas are used instead. The nuclei that can be utilized as fuel in a fast neutron reactor include among others the nuclides previously mentioned, such as ^{237}Np , ^{240}Pu , ^{242}Pu , ^{241}Am , ^{243}Am and ^{244}Cm . This makes fast neutron reactors a candidate solution for transmutation of minor actinides produced in commercial power reactors, producing additional electricity in the process. A high-energy neutron spectrum has the advantage of being able to effectively use a larger number of actinide nuclei as nuclear fuel. The fast reactors have not really reached commercialization. So far the fast neutron reactors have mostly remained at the research stage and as prototype reactors in the civil sector and in the military as propulsion systems for submarines [BLA 88, WAL 12].

2.2. *Chemical forms and properties of nuclear fuel*

There are several viable chemical forms useable as nuclear fuel. As already stated, oxide is the fuel type that has become the “standard” fuel type for commercial power production. Other fuel types include nitride- and carbide- based fuel.

A basic principle of any material being considered for use from a chemistry perspective in nuclear fuel applications, is that the material should be compatible with other materials present within the reactor core. The fuel should thus be compatible with the cladding material used in case of fuel swelling and pellet cladding interaction. In case of cladding material rupture the fuel type used should also preferably be chemically compatible with the reactor core coolant used. In the case of moderated reactors the coolant to be resisted is most often water, while in liquid metal-cooled fast neutron reactor concepts the coolant can vary between options such as sodium, lead and lead-bismuth eutectic. Other important properties include fissile material density, melting temperature, thermal conductivity and heat capacity. The fissile material density of the fuel affects properties, such as macroscopic cross sections. These are properties that can also be affected by degree of enrichment of a certain nuclide, such as ^{235}U in UO_2 fuel for example. It is however the density of the chemical fuel form used that sets limiting boundaries for these kinds of properties. The melting temperature of the fuel is a governing property for how large the gap will be between the operational temperature of the fuel and the point where meltdown will occur. Thermal conductivity is also a property that influences the margin to meltdown in the fuel. A fuel with low thermal conductivity will experience large thermal gradients within the fuel pellets over the radial direction, causing the center of the pellet to be much hotter than the surface. If the thermal conductivity is high the temperature profile of the fuel pellets will be much flatter and the same surface temperature during operation as compared to the “low thermal conductivity” case will result in lower center line temperatures, and thereby increased margin to fuel failure. The heat capacity of the fuel influences how quickly the core responds to some transient behaviors and how fast the temperature changes in the core.

2.2.1. *Oxide fuel*

Oxide is the most commonly used chemical form of nuclear fuel and the fuel type that dominates in power producing applications [BLA 89]. The basic fuel for power production is UO_2 made up of uranium that has been enriched in ^{235}U up to around 3-5%, compared to the 0.72% abundance in uranium found in nature. In heavy water-moderated reactors such as the Canada Deuterium Uranium (CANDU) type for example, no enrichment is necessary and natural uranium can be used as fuel [RIN 86]. UO_2 crystallizes within the FCC- CaF_2 [ALL 67] type structure, with uranium forming the FCC structure and the oxygen atoms situated in the tetrahedral holes in between the uranium atoms. The theoretical density of UO_2 is 10.97 g/cm^3 [HAY 12]. The heat capacity of UO_2 increases with temperature and between 1000 and 2000 °C the heat capacity increases from about 85 to 115 J/K·mole [POP 00]. The melting temperature of UO_2 is 2847 °C [HAY 12]. The thermal conductivity of UO_2 decreases with increasing temperature, falling from about 2.8 to 2.1 W/K·m between 1000 and 2000 °C [POP 00]. A benefit of the UO_2 based fuel is that it is chemically compatible with water but it does however react with sodium [BAN 12].

Mixed oxide fuel (MOX) is an oxide fuel type containing both UO_2 and PuO_2 , where the plutonium has been recovered from used UO_2 fuel, where it was formed in successive neutron capture and β^- decays of ^{238}U . In MOX fuel the isotopes ^{239}Pu and ^{241}Pu are used as fissile material while the ^{238}Pu , ^{240}Pu and ^{242}Pu isotopes are present but not fissile in a thermal neutron spectrum. Recovery of plutonium for reuse in moderated reactors cannot be done repeatedly between irradiation cycles using the same fuel. Even if some new ^{239}Pu and ^{241}Pu is formed in every cycle the net plutonium vector will degrade, as the Pu composition will shift to more of the non-fissile isotopes in every cycle. In a fast neutron reactor perspective MOX has been the reference fuel in several reactor concepts [ARA 12].

Just as with UO_2 , PuO_2 crystallizes within the FCC- CaF_2 structure [BEG 90]. The density is 11.5 g/cm^3 [HAY 12]. The heat capacity is similar to UO_2 and also increases with increasing temperature [POP 00, VÄL 14]. The thermal conductivity decreases with increasing temperature, from about 3 to $2.2 \text{ W/K}\cdot\text{m}$ [GIB 71]. The melting temperature of PuO_2 is $2428 \text{ }^\circ\text{C}$ [ADA 85]. PuO_2 is chemically inert towards water but, as with UO_2 , PuO_2 reacts with sodium [PIL 89, BYK 15].

2.2.2. Nitride fuel

Nitride-based nuclear fuel possess several characteristics that makes it superior to the conventional oxide. Actinide nitrides exist as mono nitride MeN type compounds and uranium, neptunium and thorium nitrides can also exist as sesquinitrides, where U and Np can form U_2N_3 and Np_2N_3 phases and Th can form Th_2N_3 and Th_3N_4 phases. U_2N_3 can exist in two different phases; one body center cubic (BCC) $\alpha\text{-U}_2\text{N}_{3+x}$ Mn_2O_3 type phase and a $\beta\text{-U}_2\text{N}_{3-x}$, La_2O_3 type, hexagonal phase, while Np_2N_3 forms one La_2O_3 -type hexagonal structure. Th_2N_3 also forms a hexagonal structure of La_2O_3 -type and Th_3N_4 forms a Th_3P_4 -type hexagonal phase. Uranium and neptunium can also exist as an FCC- CaF_2 type MeN_2 phase. It is however the mono nitride phases that are of interest in nuclear fuel applications [ARA 12, OLS 65, ARO 66, STO 64]. The mono nitrides of Th, U, Np, Pu, Am and Cm all form FCC- NaCl type structures. The FCC- NaCl structure is similar to the FCC- CaF_2 structure and the actinides are arranged in an FCC arrangement, but instead of the tetrahedral sites, like in the UO_2 case, the nitrogen populates the octahedral sites in the structure [SMA.05]. Pu does not form any sesquinitride phase but in the U-Pu-N system sesquinitrides have been observed up to 15% Pu metal content [LOR 68].

Actinide nitride properties of interest for nuclear fuel purposes that are superior to those of corresponding oxides include thermal conductivity, higher density and better chemical compatibility to liquid metal coolants, such as lead and sodium. The thermal conductivity of actinide nitrides are higher compared to that of the corresponding oxides. UN has a thermal conductivity that changes from about 25 to $28 \text{ W/K}\cdot\text{m}$ between 1000 and $2000 \text{ }^\circ\text{C}$ [KLE 99, ARA 92]. Firstly this is advantageous compared to UO_2 , since the far higher thermal conductivity allows for flatter temperature profiles within the fuel during in pile operation, and therefore also lower centerline temperatures. Secondly there is a significant difference in trend behavior between UO_2 and UN thermal conductivities when the temperature rises. The thermal conductivity of UO_2 decreases with increasing temperature, which means that the heat removal becomes worse as temperatures increase. In UN on the other hand the thermal conductivity increases with increasing temperature. In case of an overpower transient UN-based fuel will thus become more efficient in removing heat, slowing the temperature increase, while UO_2 intrinsically gets worse as the temperature rises. In PuN the same trend can be observed as in

UN, displaying increasing thermal conductivity with increasing temperature. The thermal conductivity of PuN is lower than that of UN however, being about 11 W/K·m at 1000 °C and having a lower rate of change as a function of temperature [ARA 92, SUZ 98]. NpN and AmN also follow the same trend of increasing thermal conductivity with increasing temperature [ARA 98, NIS 08]. High thermal conductivity is beneficial for effective heat removal in the nuclear fuel and influences the operational temperature of the fuel during in pile operation. To maintain a high threshold to melting of the fuel it is important at what temperature the fuel actually melts. Metallic fuel for example will have very high thermal conductivity but the far lower melting point compared to e.g. oxide will result in a lower margin to melting, despite high thermal conductivity. The melting temperatures of UN and PuN are both high compared to those of UO₂ and PuO₂ but in nitrides the surrounding partial pressure of N₂ will influence the melting temperature. At a partial pressure of 1 bar N₂, both UN and PuN decompose rather than melting; UN at 2780 °C [OLS 63, BUG 64] and PuN at 2570 °C [OET 67]. At an N₂ partial pressure of 3 bar UN melts congruently at 2830 °C [BEN 70] while PuN melts incongruently up to an N₂ partial pressure of 24-25 bar [OLS 64].

The density of UN and PuN exceed that of UO₂ and PuO₂. The densities of UN and PuN are 14.3 and 14.4 g/cm³ respectively [HAY 90, HAY 12]. One benefit of higher fuel density is that the fissile material density can be increased in the fuel, which allows for more compact core constructions. In breeding purposes, increased fissile material density can also help to lower the doubling time of the fuel, thanks to high energy density [ROG 03]. The decrease of fraction-light elements in mono nitride compared to dioxide fuel also decreases the softening of the neutron spectrum, which can be desired in fast neutron reactor concepts.

Nitride-based nuclear fuel also benefits from being chemically compatible with liquid metal coolants, such as sodium and lead. Coolant interactions between nitride fuel and liquid metals are more extensively studied for sodium as coolant [BLA 88, ROG 03] but liquid lead has also shown chemical compatibility with UN and UPuN [ROG 03].

Not all characteristics of nitride fuel are superior to oxide, however, and there are several drawbacks that have to be taken into consideration. One downside with nitride-based nuclear fuel is that there will be formation of ¹⁴C in the fuel due to (n,p) reactions in ¹⁴N. Formation of ¹⁴C can be managed during fuel reprocessing, separated out and immobilized as elemental carbon or as carbonates [YIM 06]. Formation of ¹⁴C is thus a manageable problem but it is however counter intuitive to the principle of one of the general key features of generation IV systems. One big advantage of the fourth generation nuclear power system is to use what currently is considered waste, such as the minor actinides, as fuel. In a system envisioned to reduce the amount of final radioactive waste it is inherently undesirable to produce an additional new radioactive waste fraction. In addition to the production of additional radioactive waste the neutron economy becomes worse due to the (n,p) reaction [MAT 91]. The ¹⁴N problem can be overcome however by isotope enrichment and production of fuel containing ¹⁵N instead, to decrease the issues of ¹⁴C production and neutron economy. ¹⁵N is only a minor part of the nitrogen present in the environment and the costs associated with nitrogen enrichment prior to fuel fabrication adds to the fabrication costs.

Nitrides are not chemically compatible with water. At elevated temperature UN is not chemically stable towards water or steam. UN hydrolyses in contact with any of these, forming UO₂ and NH₃ in the process. This is an issue concerning use of UN as a fuel material in water-

cooled reactor systems since rupture of a cladding tube would result in deterioration of the mechanical integrity of the fuel pellets [RAM 91].

Production of nitride-based nuclear fuels is more complicated compared to that of oxides. Due to the tendency of actinide nitrides to be oxidized by the oxygen and hydrolyzed by the water vapor in the air, nitrides have to be fabricated using inert atmosphere conditions, requiring closed production systems such as glove box systems for example. Apart from the deterioration of the produced nitrides in air there is also a fire hazard connected with open handling of for example UN powders due to the material being pyrophoric [EVA 63]. Issues connected with materials being pyrophoric can be approached by inert atmosphere handling but the problem can also be decreased by avoiding and minimizing handling of high surface material forms such as powders. An alternative could be producing nitride fuel in the form of spherical fuel kernels that can either be compacted into traditional pellets or filled into fuel rods as individual spheres.

2.2.3. Carbide fuel

Carbides are a fuel category that have great similarities to nitrides. Compared to oxides the monocarbides, like the nitrides, of U and Pu possess higher thermal conductivity and higher fissile material density. The carbides of U can exist, similarly to the nitrides, as UC, U₂C₃ and UC₂. The carbides of Pu differ from the nitrides in that apart from the mono carbide PuC, also Pu₃C₂, Pu₂C₃ and PuC₂ can be formed. PuC does generally exist as a hypo-stoichiometric compound and stoichiometric PuC dissociates to hypo-stoichiometric PuC and Pu₂C₃. Like the nitrides, the monocarbides of U and Pu crystallize in the FCC-NaCl structure and form solid solutions of the Me(N,C) type. UC₂ has a tetragonal structure up to about 1730 °C, where a cubic structure is adopted instead. The U₂C₃ sesquicarbide possesses a cubic BCC structure [STO 67]. PuC₂ is reported to exist in a tetragonal structure, while Pu₂C₃ is reported to crystallize in a cubic structure [STO 67]. It has however been reported that PuC₂ actually forms a cubic FCC structure, with the tetragonal structure being a meta-stable modification observed on cooling to room temperature [AKH 69]. Carbide-based nuclear fuel has disadvantages compared to nitride nuclear fuel. The melting temperature of UC is about 2500 °C, which is somewhat lower than that of UN. The melting temperature of PuC is about 1600 °C, and thus is far lower than that of PuN [MAT 86]. General disadvantages of carbide fuels compared to oxides are similar to those of nitrides, such as higher vapor pressure, pyrophoricity of fine powders and no inherent chemical compatibility with H₂O. Advantages of carbides compared to nitrides include easier fabrication, since no need for isotopic enrichment of N₂ is required. Carbides have not been the focus within this work and will therefore not be treated in similar depth as nitrides. In this work carbide presence has been addressed mostly as an undesired impurity during the fabrication of nitrides.

2.2.4. Inert matrix fuels

An inert matrix fuel is a fuel that contains a material that is present as a solid phase diluent and that is not fissile or fertile itself. One reason for wanting to use an inert matrix in the fuel is in cases where it is desired to lower the fissile material density and lower fuel in pile temperature [KLE 99]. Inert matrices can be used both as single phase and multiphase systems. In single

phase fuel, the actual fuel forms a solid solution with the inert matrix, resulting in a single crystalline phase. In multiphase systems the inert matrix will form a phase separate from that of the fuel. In multiphase systems the homogeneity of the final fuel is achieved by mixing grains of the inert matrix and the fuel to achieve as homogeneous distribution of the fissile material as possible. There are different types of solid phase diluents that can be used for fuel purposes. CERCER (ceramic in ceramic) is a fuel type where the ceramic fuel (fuel that is not metallic) is diluted with a ceramic material. CERMET (ceramic in metallic) is a fuel form where the fuel is present as a ceramic and the solid diluent is a metal.

ZrN is a material that is considered to be a promising candidate for use as inert matrix for actinide nitride fuels such as (Zr,Pu)N [LED 96, BUR 01, DAU 97, STR 03]. ZrN crystallizes within the face center cubic (FCC)-NaCl system and forms a solid solution with actinide mono nitrides, allowing the production of a single crystalline phase in the fuel [KLE 99]. Zr is a good material for inert matrix use due to its low absorption cross section for neutrons. As the actinide nitrides ZrN possess high thermal conductivity, making it possible to blend in without deteriorating the heat conductivity of the fuel [KLE 99], which is one of the properties that make nitrides interesting in the first place. The melting temperature of ZrN depends on the N₂ pressure in the surrounding atmosphere and is 3250 °C at 1 bar N₂ partial pressure and increases to 3700 °C at 60 bar N₂ [ERO 76], making ZrN suitable for inert matrix purposes also with respect to melting point.

2.3. Fuel type geometries

The most commonly used geometrical form of nuclear fuel is that of pellets that are stacked in a cladding tube. It is however not a necessity to use fuel in the form of pellets. There are several other viable fuel geometries and some are based on using microspheres for fuel fabrication. A microsphere is a spherical particle that generally has a diameter in the range of about 100-2000 μm. Examples of such fuel geometries include sphere-pac fuel where different microsphere size fractions are poured directly into a fuel rod [BAR 08]. Vibration packed (VIPAC) fuel is a fuel version where the fuel is directly poured into the fuel rods. Vipac fuel differs from sphere-pac fuel in that vibration of the fuel rod is applied during filling to increase the density of the fuel filling. Vipac fuel does not have to be based on microspheres, however, but can be produced from other geometries such as irregularly shaped crushed fuel material for example [FRE 72, HEL 06]. Another example of fuel geometry is microspheres embedded in a graphite matrix [CHA 08]. A version of microsphere-based fuel used for embedding in graphite matrices is tristructural-isotropic (TRISO) fuel kernels. In TRISO fuel, fuel microspheres are covered in several protective barriers. The microsphere is covered with a porous graphite layer followed by two pyrolytic carbon layers with a SiC layer in between [CHA 06]. In such fuel the porous graphite layer is added, amongst other things to provide a void for fission gasses and accommodate microsphere swelling. The SiC layer is present to act as a barrier against diffusion [BAK 13]. In cases when pellets are a desired final fuel form it can be of interest to produce the pellets from microspheres rather than powders. These reasons include benefits of being able to work with powder-free processes, which can lower the radiotoxic hazards associated with fine radioactive powders [GAN 93]. Production of microspheres is performed starting from aqueous metal solutions. This can be an advantageous feature, if producing new fuel in connection with

solvent extraction-based recycling processes. The output from such separation processes would be similar to the input feed in microsphere production processes.

2.4. *Gelation based techniques for microsphere production*

Several different kinds of gelation based processes have been developed for microsphere production. All existing gelation processes are however based on the starting material being an aqueous solution containing dissolved metals that one wants to produce microspheres from.

2.4.1. *The external gelation process*

In the external gelation process an actinide-containing sol is prepared by addition of viscosity modifying and surface tension modifying agents such as polyvinylalcohol and tetrahydrofurfurylalcohol [FU 04, VER 07]. There are several slightly differing processes that can be categorized as being external gelation processes, such as the KFA, which was developed for the production of U-Th oxide microspheres, and the SNAM process [BRA 70, NAE 79, GAN 86]. No gelation agents are added to the sol during external gelation. The sol is broken up into droplets using a nozzle or a rotating cup. The droplets fall through ammonia vapor, causing a thin “crust” to form on the surface of the droplet, before falling into aqueous ammonia solution. The surface formed in the ammonia vapor helps the sphere to retain its shape when falling into the ammonia solution and diffusion of hydroxide ions into the sphere causes pH increase and metal precipitation. This is the reason why the process is called external gelation, since the microspheres produced are solidified from the outside and inwards as the hydroxide diffuses into the microspheres. External gelation has for example been used for the production of uranium-based microspheres and also for mixes of U,Th, U,Pu and U,Pu,Am [GAN 86, CAR 14].

2.4.2. *The ORNL process*

The ORNL process was developed at Oak Ridge National Laboratory in the U.S during the 1960s [WYM 68, LOT 68]. The process works by producing a sol consisting of aqueous actinide solution dispersed in 2-ethyl-1-hexanol (2EH). The aqueous solution forms small spherical droplets in the 2EH. Water migrates from the aqueous droplets into the 2EH and as the droplets lose water the metals solidify, forming solid kernels. Surfactants such as the nonionic surfactant SPAN-80 are added to the 2EH to avoid sphere coalescence and clustering [WYM 68].

2.4.3. *The IChTJ (INCT) process and the double extraction process*

The IChTJ process is similar to the ORNL process. The process originates from the 1970s and the IChTJ institute in Poland and the process has been used for the production of microspheres for nuclear fuel applications but also in other areas, such as the production of spherical hydroxyapatite particles for example [DEP 92, BRY 15]. Within the nuclear material application field the actinides in solution are complexed with ascorbic acid and the pH of the solution adjusted to about 4 with NH_4OH . Just as in the ORNL process, the gelation is performed by water extraction into 2EH, forcing gelation by dehydration [BRY 14]. In the double extraction process a primary aliphatic amine, typically Primene JMT, is added to the 2EH prior to gelation. The primary amine is present in the 2EH to extract nitric acid out of the

droplets simultaneously with the water extraction. The benefit of adding the nitric acid extraction is that the formed microspheres will contain lower amounts of nitrate, which can cause microsphere fracturing during thermal treatment.

2.4.4. The internal gelation process

The internal gelation process was originally developed at the Keuring Electrotechnische Materialen Arnkem (KEMA) laboratories in the Netherlands [BRU 70, KAN 74]. The process was originally developed for production of uranium oxide microspheres but has since been applied to a variety of different metal mixtures, such as U, U,Pu, Zr, Zr,Ce and Zr,Pu for example, and the method has been applied for the production of different varieties of oxide, carbide and nitride microspheres [POU 09, POU 03, BEN 08, STR 04, MUK 90]. The method starts from metal nitrate solution, which is cooled to about 0-4 °C [VAI 87]. Urea is added to the sol as a metal complexation agent and hexamethylenetetramine (HMTA) is added as the gelation agent. The sol is then introduced as droplets into a heated immiscible heat carrier, such as silicone oil for example. Depending on the sol composition the oil is heated to between 50-100 °C [POU 09, VAI 08]. Heat transfer over the phase boundary from the oil to the aqueous droplets causes HMTA to degrade, causing an increase in pH, resulting in gelation/precipitation of the metal inside of the droplet [APA 12]. Unlike the external gelation process, where no gelation agent is present inside the sol, the gelation process in this case propagates within the droplets without any material diffusion across the sphere surface being a necessity, hence the name internal gelation. The internal gelation method is the sol gel production method that has been applied within this work and will be described in closer detail in the theory part of this work.

2.5. Nitride production techniques

Nitrides are generally less thermodynamically stable than oxides, resulting in oxides being common material types observable in nature while nitrides have to be produced in air- and moisture-free environments to exist without being more or less rapidly oxidized. If the nitrides produced are desired to have low oxygen content the production should be performed under inert atmosphere conditions. Material storage should also be done under inert atmosphere in the case of storage of high surface materials, such as powders or high porosity structures. Different production techniques for nitrides all come with different advantages and disadvantages, making selection of production technique dependent on the intended field of application. Techniques available that have been more or less tested for nitride production within the nuclear field include cyclic hydriding/nitriding, oxidative ammonolysis, reactive ball milling, ammonolysis from halogens and carbothermal reduction. Among these techniques carbothermal reduction is the technique that has been identified as a technique more easily practical for scaling up from laboratory to pilot or industrial production scale [BER 89].

2.5.1. The cyclic hydriding/nitriding process

The cyclic hydriding/nitriding process is a method that starts from metallic raw material as input into the process. The method is based on comminuting metallic ingots into fine powders by cyclic hydriding/dehydriding. The metal is heated in hydrogen gas to form metal hydride and then dehydrided in inert gas, such as argon, to reform the metal. Metals experiencing big

differences in density between the metallic and hydride state, such as uranium, can in this way be converted from larger solid shapes into fine powders. If the metal and hydride are more similar in density, as for zirconium for example, milling steps may have to be used in the process to achieve fine powders [PAR 11]. When the material has been properly pulverized it can be nitrided by heating in flowing N_2 from either the metallic or hydride state [OI 72]. The process produces powder grains of individual metal nitrides and if mixed nitride solid solutions are desired powder blending and solid solution formation by sintering is required. The method has the advantage of avoiding carbon impurities during fabrication but the fine powders produced increase the sensitivity to oxidation. The process requires inert conditions to avoid oxygen impurities. The method has been applied for production of dense high purity UN pellets [MAL 14, JOH 16]. Starting from metallic materials and only using gas phase reactants is a way to avoid impurities in the final material but a downside is that handling metallic actinide materials can be associated with issues regarding proliferation resistance. The method can also be used for preparation of PuN [BRO 55].

2.5.2. *Oxidative ammonolysis*

Oxidative ammonolysis is a reaction route that starts from actinide oxides rather than metals. When producing UN, UO_2 powder is blended with NH_4HF_2 at room temperature to produce NH_4UF_8 . By reacting the NH_4UF_8 with NH_3 at elevated temperature UN_2 is produced and subsequently converted to UN by heating in inert atmosphere [YEA 08]. Oxidative ammonolysis has also been applied for the production of NpN and attempts have been made to produce ThN. In the case of ThN however a ThNF species forms even during heating to 1100 °C [SIL 09, SIL 12].

2.5.3. *Reactive ball milling*

Reactive ball milling is a technique starting from metallic material. The material is milled at room temperature in N_2 atmosphere. In absence of oxygen, nitride will form on the metallic surfaces with the N_2 in the milling atmosphere. Continuous formation of new metallic surfaces during the milling provides fresh surfaces to be nitrided. The milling ball to material ratio is quite high in the process and long milling times are required, making this a slow production procedure [SHE 00].

2.5.4. *Nitride formation from metal halides*

Uranium nitride can be produced starting from halides such as UCl_4 and UF_4 . Production of U_2N_3 followed by decomposition to UN from UF_4 can be accomplished by mixing UF_4 with Si and heating in N_2 atmosphere, to produce U_2N_3 and Si₄ [YOS 68]. Production from UCl_4 can be performed by mixing with aluminum powder and heating in N_2 atmosphere to form U_2N_3 and $AlCl_3$ [MIT 68].

2.5.5. *Carbothermal reduction*

Carbothermal reduction is a process starting from metal oxides. The material to be nitrided is mixed with elemental carbon and heated in N_2 or N_2/H_2 atmosphere. Production can be done by mixing powders that are either reacted as mixed powders or pressed into thin porous clinkers that are nitrided. By mixing carbon into the sol in sol gel processes, the method can also be adapted for nitride production from sol gel-derived materials. The process was developed for production of mainly uranium carbide fuels by heating the metal oxide/carbon mixtures in inert

atmosphere or vacuum [SMI 60, STR 67, BEČ 69]. The carbothermal technique was subsequently also developed for production of nitride materials from oxides, as well as reformation of UC to UN [LEI 70, GRE 73, WIL 76]. The main downside associated with carbothermal reduction is the risk of unwanted residual carbon and oxygen in the final product. Residual oxide in the material is generally a result of incomplete carbothermal reduction caused by either suboptimal thermal treatment or too inhomogeneous mixing of carbon and metal oxide. Oxygen impurities can be suppressed by addition of over-stoichiometric amounts of carbon. On the other hand this can increase the residual amounts of carbon in the system, making the ideal carbon addition during carbothermal reduction an important parameter for obtaining desired the result. An advantage of the carbothermal reduction process has been identified as being practically suitable for scaling up to pilot and industrial scale [BER 89]. The carbothermal reduction process is a nitride conversion method that is compatible with the internal gelation process. Nitride synthesis within this work has been performed using the carbothermal reduction method and the carbothermal synthesis route will be discussed in more depth in the theory part of this work.

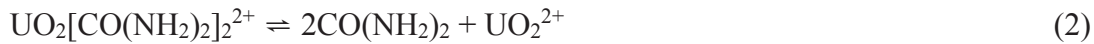
3. Theory

3.1. The internal gelation process

As stated in chapter 2, the internal gelation process is based on heat-induced gelation of an aqueous metal solution. In the process urea is added to the sol as a complexing agent to avoid premature gelation and HMTA is added as gelation agent. Cooling of the sol is important to be able to dissolve HMTA or add pre dissolved HMTA solution to the metal-containing sol. The element most studied in the internal gelation process is uranium, and the reactions in the gelation process are therefore illustrated by the case of gelation of uranium-based sols. In the case of uranium gelation the starting sol often consists of acid-deficient uranyl nitrate solution (ADUN). The ADUN solution is a uranyl nitrate solution that is sub-stoichiometric in nitrate content, having a $\text{NO}_3^-/\text{UO}_2^{2+}$ ratio of between 1.5 and 2 [VAI 87]. The reason for using an acid-deficient starting solution is that lower amounts of gelation chemicals are needed to perform the gelation.

The main steps of the internal gelation process have been determined to be [COL 87]:

Decomplexation of urea



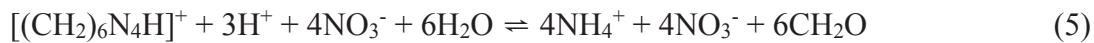
Hydrolysis of the uranyl ions



HMTA protonation



HMTA decomposition



The HMTA thus drives the reaction forward by scavenging the H^+ being released during the hydrolysis of the uranyl ions.

The formaldehyde formed in the degradation of HMTA can react further with the urea decomplexed from the metal ions by forming oligomeric reaction species by condensation reactions [JON 52].

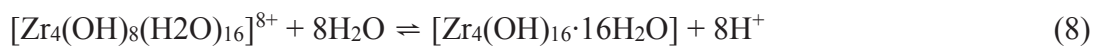


The formation of the monomer UO_2OH^+ , dimer $(\text{UO}_2)_2(\text{OH})_2^{2+}$ and trimer $(\text{UO}_2)_3(\text{OH})_5^+$ species of the hydrolyzed uranyl ion have also been reported during the hydrolysis reaction, indicating that this is at least partially a polymerization reaction and not just a precipitation. These oligomers are also present in the ADUN solution when the gelation chemicals have not

been added; when HMTA is used as the hydrolysis agent the predominantly formed oligomer is the trimer [KIN 90]. The formed microspheres also contain the protonated HMTA molecule $[(\text{CH}_2)_6\text{N}_4\text{H}]^+$ incorporated as intercalated cations in the gel [KIN 90].

When gelation of the sol has been performed the produced microspheres need to be washed. First the microspheres are washed in an organic diluent, such as CCl_4 or petroleum ether, to remove silicone oil from the microspheres. After washing in organic media the microspheres are washed in NH_4OH (aq) to remove residual chemicals like urea, unreacted HMTA and NH_4NO_3 . If the gelation chemicals are not removed the risk of microsphere cracking both during drying and thermal treatment increases due to gas formation in the microspheres [HUN 10]. The microspheres are also aged in NH_4OH (aq) in order to make sure that all metal in the microspheres has gelled/precipitated. During washing and ageing of the microspheres in NH_4OH the $[(\text{CH}_2)_6\text{N}_4\text{H}]^+$ ions are exchanged for ammonium ions and the structures present in the microspheres become $\text{UO}_3 \cdot 2\text{H}_2\text{O}$, $\text{UO}_3 \cdot 0.25\text{NH}_3 \cdot 1.75\text{H}_2\text{O}$ and $2\text{UO}_3 \cdot \text{NH}_3 \cdot 3\text{H}_2\text{O}$ [KIN 90, LLO 76].

Far less studies on the gelation behavior of Zr in the internal gelation process have been performed compared to U. It has however been suggested that the Zr solidifies as hydrated zirconium hydroxides formed from Zr tetramers present in the sol [HAG 04, TSU 99].



The data on the gelation of pure Pu-containing sols is scarcer than that of U in the literature. Several authors have published cogelation studies on U/Pu and Zr/Pu mixed sols or U/Ce and Zr/Ce surrogate studies. However, little consideration of any possible differences of the behavior of Pu compared to U or Zr has generally been discussed [IDE 03, SOO 10, GAN 93]. Little work on pure Pu-containing sols has been encountered in the literature. Gelation of pure plutonium sols have been performed at Oak Ridge National Laboratory using the ORNL water extraction process [LLO 78]. Regarding internal gelation the only attempt to perform sol gel on pure Pu sols was a single experiment on the side when producing U,Pu mixed gels at Jülich [FÖR 77]. There it was noticed that the pure Pu-gelled microspheres required longer washing times compared to U-microspheres to avoid microsphere cracking during thermal treatment. The explanation suggested was increased difficulty in removing nitrates during the washing compared to U-based microspheres.

During production of americium containing microspheres, precipitation of the americium is achieved in the gel during the ageing step in NH_4OH instead of together with the uranium and plutonium during the gelation [LED 96]. The coprecipitation behavior in Zirconia gels has not yet been investigated.

Sol Gel based processes can be used as the starting point for material preparation for production of both oxide, nitride and carbide fuel. In the case of preparation of nitrides or carbides, carbon needs to be added to the sol in order to have a reducing agent present in the subsequent carbothermal reduction process. The carbon is commonly added in the form of elemental carbon particles that are dispersed in the sol. The dispersion of carbon particles is normally assisted by addition of surfactant and/or block copolymer-based dispersion agents. A dispersion agent is a substance that enhances the lifetime of colloidal suspensions of solid particles in solution. If the particles consist of immiscible liquid droplets instead of solid particles the dispersion agent is commonly called an emulsifier instead. The two existing mechanisms for improving the

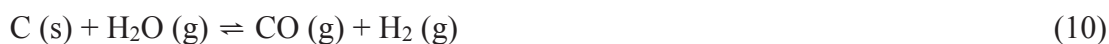
lifetime of a suspension are steric and electrostatic stabilization. Both stabilization mechanisms work by counteracting a decrease in entropy that occurs when the stabilizing ions or ethylene oxide chains on the dispersed particle surfaces approach each other [HOL 03]. When stabilizing particles in aqueous media containing high concentrations of ionic species it is generally favorable to opt for nonionic surfactants for steric stabilization, since ionic stabilization loses efficiency due to screening effects from the ions in the solution.

3.2. Carbothermal reduction and nitride formation

As in the case of internal gelation, carbothermal reduction for the production of nitride fuel has been most studied in the case of U. Reactions will thus be presented using U as the model element. It is however possible to produce all the transuranic actinides of interest for fuel applications, such as Np, Pu, Am and Cm by carbothermal reduction, even if optimal reaction conditions for each actinide may vary [TAK 01, TAK 08, OGA 95, NAK 98]. During the production of U-based microspheres in the internal gelation process the final material produced can approximately be represented by $UO_2(OH)_2$. The materials produced in internal gelation are generally hydroxides and need to be converted into oxides prior to carbothermal reduction. In the case of Pu or Zr the oxide formed upon heating and degradation of the hydroxide is the dioxide, but the case of U formation of UO_3 is also possible, requiring the material to be reduced to UO_2 prior to carbothermal reduction. This reduction can be performed in a hydrogen-containing reducing atmosphere [LED 92]:



When using hydrogen to reduce UO_3 to UO_2 some of the carbon blended into the microsphere is lost due to the formation of CO due to reactions between C and water vapor [MUK 93].



Some carbon can also be lost by methane formation.



An alternative to reducing The UO_3 using H_2 is to blend in extra carbon into the material, to use carbon as a reducing agent also for the UO_3 to UO_2 reduction [MUK 90, MUK 91].

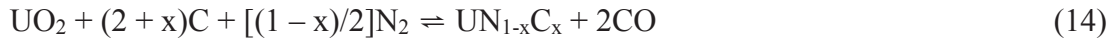


After the desired oxide has been prepared the subsequent carbothermal reduction can be performed using a variety of different reaction atmospheres, such as N_2 , N_2+H_2 or NH_3 [MUK 91, GAN 91, ALL 67, MUR 77].

When the reaction is performed in N_2 environments below about 1723 K it proceeds according to [MUK 91]



If the temperature exceeds about 1723 K a carbonitride material will preferentially form instead, according to the following reaction [MUK 91]



Continuation of the heat treatment eliminates the carbide by reformation of elemental carbon according to the following reaction



Reaction 15 will only proceed however if there is something present to remove the carbon that is formed, such as H_2 in the atmosphere or unreacted UO_2 .

If a carbonitride forms in the carbothermal reduction step the carbide can be eliminated by the presence of H_2 in the reaction atmosphere, removing the carbon as short chain alkanes, in this case illustrated by methane



Free elemental carbon can be removed in $\text{N}_2 + \text{H}_2$ mixed atmospheres by the formation of hydrogen cyanide [BAR 92]

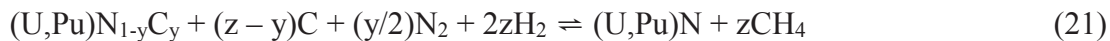


The HCN can in turn react further, forming cyanogen and cyanamide



Elemental carbon may thus be reformed according to reaction 19. It is however possible to lower the residual amounts of carbon in the final material by removal of the formed product gases, HCN, $(\text{CN})_2$ and CN_2H_2 from the system in the reaction gas flow.

Carbothermal nitridation studies have also been performed on mixed UO_2 , PuO_2 materials, and the reaction mechanisms that have been suggested show great similarities to those of nitridations of pure UO_2 [PAU 88].



The nitridation reaction can also proceed by direct reaction between metal oxide and hydrogen cyanide [BAR 92].



Production of ZrN from oxides by carbothermal reduction has been studied by Pialoux et al. [PIA 91] and several different temperature-dependent reactions have been proposed.

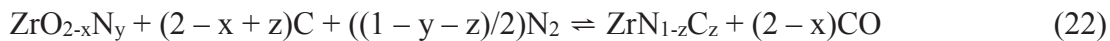
The first part of the reaction is the formation of oxynitride in the temperature range $1423 \leq T \leq 1883$ K by the reaction



The reaction can then proceed by direct nitride formation in the temperature range $1673 \leq T \leq 1783$ K if graphite carbon is used as the carbon source



If the temperature exceeds 1783 K there will instead be formation of carbonitride, according to the following reaction



3.3. Pellet formation and sintering

3.3.1. Mechanical pressing and sintering

Pellet pressing is a process that is based on mechanical compaction of originally free entities such as powders, microspheres, granules etcetera. There are several different techniques for producing cohesive mechanical bodies from free flowing material. Examples of such techniques are cold pressing, where the material is put in a pressing die and compacted; hot pressing, which is essentially cold pressing but at elevated temperature, and isostatic pressing. Isostatic pressing is a technique based on exerting simultaneous pressure on a bag-type pressing die from multiple directions [RIC 06]. What is commonly encountered during nuclear fabrication is uniaxial cold pressing of cylindrical pellets, meaning that the powder to be pressed is placed in a pressing die with a cylindrical profile and pressing is performed using top and bottom plungers along the axial direction of the pellet.

The aim is to expose the material to be compacted to a high enough pressure to force the individual grains close enough to each other that adhesive forces arise between the grains in the pressed body. In the case of pressing larger aggregates, such as microspheres or different kinds of granulates, some degree of disintegration of the input materials physical integrity into finer pieces is generally required in order to form a body with high enough cohesive strength to remain intact. A newly pressed body is generally of low theoretical density and low mechanical strength. Such a newly pressed body is referred to as a “green” body.

Several different kinds of additives can be used when pressing objects if needed. Examples of such are binder material that can be added to increase the mechanical strength of the newly pressed body, oil in the pressing die for lubrication purposes, or sintering agents to improve the sintering characteristics of the material.

When producing pellets or other mechanical bodies by cold pressing the green pellet formed possesses inadequate mechanical strength and density to be used in a nuclear reactor. In order to be useful the material has to be sintered. Sintering is a process that is based on heat induced densification of a material. In practice this refers to removal of pores in the pellet, and thus also shrinkage of the pellet [RIC 16]. The thermodynamic driving force for sintering phenomena is

minimization of surface free energy by consolidation of grain boundaries. Three driving mechanisms for sintering are [RAH 03]:

- Curvature of the particle surfaces
- Externally applied pressure
- Chemical reactions

These mechanisms are the reasons that cause sintering to occur, but the physical densification itself is facilitated by the movement of atoms within the material structure. In crystalline solids there are always defects present in the otherwise ordered structures, and it is through the defects that atomic transport mainly takes place. The equilibrium defect density in a crystalline material is dependent on the temperature of the material. Since the lowest possible energetic state in a crystal structure is a perfectly ordered one, the thermodynamic driving force for forming defects in a crystal is lowering of free energy by increase in entropy [SMA 05].

Crystalline materials normally contain different types of defects, which can be categorized as [RAH 03]:

- Point defects
- Line defects
- Planar defects

When spherical particles adjacent to each other sinter together, they do so by neck growth. In practice, this means that the particles sinter together at their respective contact points to one another, forming “necks”. There are several different kinds of mass transport mechanisms during this kind of neck growth, but only some of them lead to densification of the material.

The mass transport mechanisms are [RAH 03, RIE 11]:

- Surface diffusion
- Lattice diffusion from particle surface to the neck
- Vapor transport
- Grain boundary diffusion
- Lattice diffusion from the grain boundary
- Plastic flow

Of these mechanisms, the first three are non-densifying mechanisms. This means that they do lead to neck growth between grains but they do not transport material to pores forming between the neck growth areas of particle clusters. The grain boundary diffusion and lattice diffusion from the grain boundaries are mechanisms that do promote translation of material from the grain and neck boundary towards the pore. The plastic flow mechanism also leads to neck growth and densification during sintering but is more commonly observed during metallic sintering than ceramic [RAH 03]. Figure 1 illustrates schematically the six different material transport mechanisms possible when sintering spherical objects.

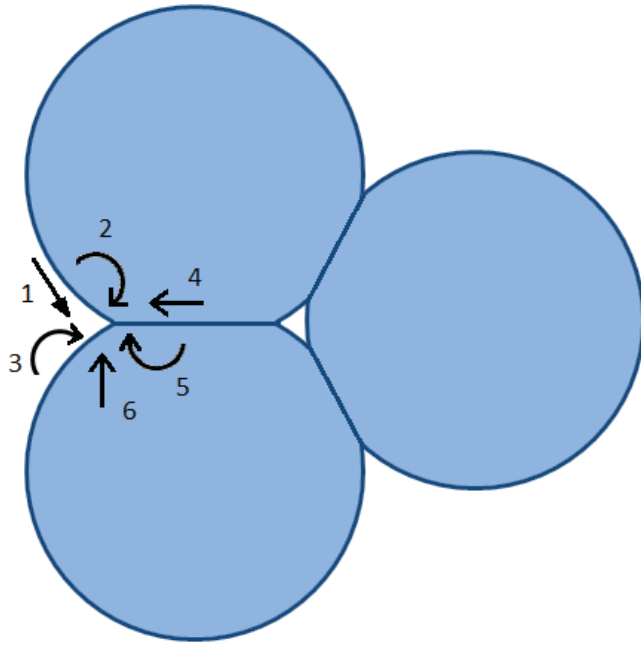


Figure 1. Schematic picture indicating the transport mechanisms occurring during sintering. The different arrows indicate 1 Surface diffusion, 2 Lattice diffusion from the surface, 3 Vapor transport, 4 Grain boundary diffusion, 5 Lattice diffusion from the grain boundary and 6 Plastic flow [RAH 03].

3.3.2. Spark plasma sintering

Spark Plasma Sintering (SPS) is a technique that is a combined pressing and sintering technique. In SPS no separate green pellet is formed but instead a graphite die is loaded with the material/powder that is to be pressed. The top and bottom plungers are inserted into the die and the entire entity is put into the instrument for simultaneous pressing sintering. Current is run through the graphite die and sample, thereby heating it up during pressing. The combination of pressing during heating allows for densification to occur at lower temperatures compared to what would be expected in traditional sintering. Localized temperatures at individual grain contact points may however be higher than that of the average temperature measured for the bulk of the system. In the cases where the sample to be sintered is a far poorer electrical conductor compared to the graphite die, most of the current will run through the die instead of the sample and the method becomes similar to hot pressing techniques.

3.4. Characterization techniques

3.4.1. Scanning Electron Microscopy

The SEM instrument used for imaging characterization in this work was a Hitachi TM 3000 tabletop microscope with a back scatter electron detector. The system can scan variably in the X-Y plane but is stationary in the Z direction, requiring the sample to be imaged to be adjusted to a proper height in the instrument prior to imaging in order to obtain a focused electron beam. During imaging of microspheres carbon adhesive tape was used to mount the samples properly on the aluminum sample holder while imaging of pellets was performed with pellets placed directly on the aluminum sample holder in order to keep the pellet surfaces free of adhesive.

Energy Dispersive X-ray Spectroscopy

The EDX application used for element mapping and quantification in the microscope system was a Quantax 70. Calibration of the EDX application was performed using Cu as a reference material. The detector was a silicon semiconductor detector.

3.4.2. X-ray diffraction

XRD was performed using a BRUKER D2 PHASER instrument. Both pellets, microspheres and powders were measured using XRD. In the cases of powder measurements a glass slide was used to height adjust the measurement sample to obtain the correct height level of the sample surface. Similarly a sample holder of variable depth was used to height adjust the surface of pellets during measurement to the desired level. In cases of XRD measurements of microspheres it was not possible to produce a flat, height-corrected surface, even when using adjustable sample holders, due to the inherent curvature of the microsphere surfaces. Ocular inspection was used to determine when the microsphere surfaces were on average at the correct sample height level. An advantage of diffraction measurements is that not only composition of a material can be estimated but the physical structure can also be determined. The inherent disadvantage of the technique is that amorphous phases can't be measured.

3.4.3. Elemental analysis based on inert gas fusion and/or combustion

The determinations of C/N/O data within the work performed were measured using measurement instruments from LECO. For measurement of C a LECO CS744 instrument was used and for N/O measurements a LECO TC-436DR instrument was used.

3.4.4. Computer X-ray tomography for density gradient evaluation

There are different techniques that can be used to measure density gradients. One such technique is X-ray tomography. X-ray tomography is a nondestructive measurement technique [PHI 97]. X-ray tomography is performed by placing the sample on a rotary stage located between a micro focus X-ray source and a digital flat panel detector (225 kV Nikon XTH 225 ST system). X-rays interact with the sample to form a 2D image of the X-ray attenuation pattern (shades of gray) on the detector.

The 3D volume of the measured sample can be produced from a series of 2D X-ray images that are collected while rotating the sample 360 degrees. This sequence is then reconstructed using dedicated software in order to create a 3D data set composed of elementary units called voxels. Each voxel is associated with a gray level value (in the range of 0 to 65536) that represents the attenuation of the X-rays at the voxel location depending on the density, atomic number and geometry of the specimen. The result is a grey scale image where lighter grey areas correspond to higher density and lower density corresponds to darker grey areas.

3.4.5. HPGe gamma spectrometry

The setup used for HPGe measurements was an Ortec DSPEC50 digital analyzer coupled to an Ortec GEM-15180-S co-axial detector system. ^{241}Am and ^{239}Pu were measured using gamma spectrometry and ^{241}Am was measured using the 125.3 keV gamma energy peak and ^{239}Pu was measured using the 129.3 keV peak.

3.5. Composition estimations of solid solutions

Mixed crystal systems containing two different crystalline species that are of the same crystal structure and have similar inter-atomic distances may produce diffraction peaks that are very close in angle. Such mixed systems, such as ZrN-ZrC, PuN-PuC or UN-UC may form solid solutions where, in these examples, the metal forms an FCC-NaCl structure and the N and C atoms randomly fill the octahedral holes in the structure. In such a material there would no longer exist two sets of diffraction peaks since there is only one crystal structure present in the system. Instead one set of diffraction peaks would be measured and the observed peaks would exist in between the positions of corresponding peaks for the pure phases. The chemical composition of such a system would influence how large the peak shift would be from that the peaks of the pure phases. For example, if PuN and PuC are present as a carbonitride solid solution PuCN, the diffraction peaks of PuC_{0.9}N_{0.1} would be closer to those of pure PuC than those of PuC_{0.7}N_{0.3} would be. Also the observed peaks would be more and more shifted towards those of pure PuN as the degree of nitride in the solid solution increased.

Cubic crystal systems are systems where the smallest repeating unit building up the crystal can be geometrically described as a cube. In such systems there is therefore no need to describe the unit cell size with three different unit cell lengths a, b and c as in several other crystal systems since all the sides are of identical length. Instead only one defined length is enough to describe all three physical dimensions of a cube and that length is commonly denoted by the letter a, and referred to as the lattice parameter, or the lattice constant. From diffraction data it is possible to calculate the lattice parameter of a cubic structure as a function of the constructive interference diffraction angles according to the following equation [SMA 05]

$$a^2 = (h^2 + k^2 + l^2) \cdot \lambda^2 / (4 \cdot \sin^2(\Theta)) \quad (\text{eq. 3.5.1})$$

where (hkl) is the Miller index of the reflecting plane in the crystal giving rise to the observed detected reflection in the diffractogram and λ denotes the wavelength of the X-rays used. If determining the lattice parameter using several different diffraction peaks for the same material it is possible to determine an average lattice parameter with standard deviation for the material.

The angle at which the diffraction peaks occur thus correlates to the lattice parameter of a structure. In the previous section it was concluded that in solid solutions the diffraction peak angles of a mix of, for example, A and B will generally be shifted to between those of the pure compounds. Since diffraction peak angle and lattice parameter is connected this means that the lattice parameter of the solid solution will shift depending on composition. By determining the lattice parameter of a solid solution it is therefore possible to make an estimate of the solid solution composition. Composition determinations in ternary solid solution cubic systems based on linear lattice parameter shift with composition is commonly known as Vegard's law.

Vegard's law was originally published in 1921 [VEG 21]. Vegard's law is based on measurement of the lattice parameter of a cubic compound and on linear interpolation between the lattice parameters of the pure phases, a_A and a_B . Estimation of the composition of the measured solid solution can mathematically be expressed as

$$a_{AB} = c_A a_A + c_B a_B = c_A a_A + (1 - c_A) a_B = a_B - c_A (a_B - a_A) \quad (\text{eq. 3.5.2})$$

where a_{AB} is the measured lattice parameter for the solid solution and c_A and c_B are the fractions of A and B in the solid solution.

Vegard's law is not a law in the traditional sense but rather an approximation. This is because there is no fundamental principle that states that the lattice parameters of solid solutions have to vary linearly with composition. In fact it can and has been shown that even if the solid solutions studied do behave as ideal solid solutions Vegard's law will only be an approximation and in the case of ideal solid solutions will underestimate the lattice parameter of a given composition compared to the true one [JAC 07]. Composition determinations using Vegard's law should thus be performed with the knowledge that the obtained result should be viewed as an approximate estimation and not as an absolute truth.

So far Vegard's law has been discussed for ternary solid solution systems, such as ZrCN or PuCN for example. If wanting to apply Vegard's law to a quaternary solid solution such as ZrPuCN Vegard's law has to be extended into an additional dimension by taking four different pure phases into consideration. Illustrated by the ZrPuCN system, the expression then becomes

$$\begin{aligned}
a_{\text{PuZrCN}} &= c_{\text{ZrCN}}a_{\text{ZrCN}} + c_{\text{PuCN}}a_{\text{PuCN}} \\
&= a_{\text{PuCN}} - x_{\text{Zr}}(a_{\text{PuCN}} - a_{\text{ZrCN}}) && \text{(eq. 3.5.3)} \\
&= (1 - x_{\text{Zr}})a_{\text{PuCN}} + x_{\text{Zr}}a_{\text{ZrCN}} \\
&= (1 - x_{\text{Zr}})[a_{\text{PuC}} - x_{\text{N}}(a_{\text{PuC}} - a_{\text{PuN}})] + [x_{\text{Zr}}a_{\text{ZrC}} - x_{\text{N}}(a_{\text{ZrC}} - a_{\text{ZrN}})] \\
&= [a_{\text{PuC}} - x_{\text{N}}(a_{\text{PuC}} - a_{\text{PuN}})] - x_{\text{Zr}}[a_{\text{PuC}} - x_{\text{N}}(a_{\text{PuC}} - a_{\text{PuN}})] + x_{\text{Zr}}[a_{\text{ZrC}} - x_{\text{N}}(a_{\text{ZrC}} - a_{\text{ZrN}})] \\
&= a_{\text{PuC}} - x_{\text{N}}(a_{\text{PuC}} - a_{\text{MeN}}) - x_{\text{Zr}}a_{\text{PuC}} + x_{\text{Zr}}x_{\text{N}}(a_{\text{PuC}} - a_{\text{PuN}}) + x_{\text{Zr}}a_{\text{ZrC}} - x_{\text{Zr}}x_{\text{N}}(a_{\text{ZrC}} - a_{\text{ZrN}}) \\
&= a_{\text{PuC}} - x_{\text{Zr}}(a_{\text{PuC}} - a_{\text{ZrC}}) - x_{\text{N}}(a_{\text{PuC}} - a_{\text{PuN}}) - x_{\text{Zr}}x_{\text{N}}(a_{\text{ZrC}} - a_{\text{ZrN}} - a_{\text{PuC}} + a_{\text{PuN}})
\end{aligned}$$

In such a quaternary system Vegard's law will geometrically describe a curved plane instead of a line, as in the ternary linear interpolation case. By knowing the input metallic composition of a solid solution it is thus possible to make an estimate of, in this case, the nitride purity from the lattice parameter also in quaternary solid solutions.

If a solid solution can be described to behave like an ideal solid solution there is no volume change during mixing of the pure phases. This means that ΔV_{mix} is equal to zero. This can also be expressed as

$$V_{AB} = c_A V_A + c_B V_B \quad \text{(eq. 3.5.4)}$$

By using this as starting point, equation 3.5.3 can be used by simply replacing lattice parameter a for lattice volume V to describe what the lattice volume would be in an ideal solid solution of ZrPuCN. This expression can in the end be stated as

$$V_{\text{ZrPuCN}} = V_{\text{PuC}} - x_{\text{Zr}}(V_{\text{PuC}} - V_{\text{ZrC}}) - x_{\text{N}}(V_{\text{PuC}} - V_{\text{PuN}}) - x_{\text{Zr}}x_{\text{N}}(V_{\text{ZrC}} - V_{\text{ZrN}} - V_{\text{PuC}} + V_{\text{PuN}}) \quad \text{(eq.3.5.5)}$$

Since the smallest repeating unit in the nitride solid solutions of interest is a cube, the lattice parameter of an ideal solid solution can be expressed as

$$a_{\text{PuZrCN}} = [V_{\text{PuC}} - x_{\text{Zr}}(V_{\text{PuC}} - V_{\text{ZrC}}) - x_{\text{N}}(V_{\text{PuC}} - V_{\text{PuN}}) - x_{\text{Zr}}x_{\text{N}}(V_{\text{ZrC}} - V_{\text{ZrN}} - V_{\text{PuC}} + V_{\text{PuN}})]^{1/3} \quad \text{(eq.3.5.6)}$$

It is thus possible to compare the behavior predicted by Vegard's law to what would be expected if the sample behaves like an ideal solid solution and also if measurement data shows positive or negative deviation from what would be expected of an ideal solid solution.

4. Methods and experimental procedures

4.1. Preparation of zirconium containing sols and microspheres

During preparation of zirconium based sols, zirconylchloride tetrahydrate ($\text{ZrOCl}_2 \cdot 4\text{H}_2\text{O}$, Alfa Products) was first dissolved in MQ water and HNO_3 (Sigma-Aldrich) was added to reach the desired NO_3^-/Zr ration. HNO_3 was added partly to make the system more similar to Pu-containing systems, which contain both high levels of H^+ and NO_3^- . It was observed that if NO_3^- addition was instead performed by NH_4NO_3 addition, to avoid the H^+ addition, the dispersion of carbon nanotubes was affected negatively. Addition of NO_3^- to the system was thus preferentially performed by HNO_3 addition. The final Zr concentration in the sol was varied between 0.6-0.9 M. Carbon material was added to the sol after dissolution of Zr to a C/Zr ratio of generally between 2-2.3. Different carbon sources have been tested and include carbon nanotubes (CNT, 5 μm length and 6-9 nm in outer diameter) from Aldrich, carbon nanopowder (CNP, Supelco, about 200 nm in diameter) and graphite powders from Acros Organics and Cabot. In order to increase the stability of dispersed material the nonionic surfactant Triton X-100 (t-octylphenoxypolyethoxyethanol, Sigma-Aldrich) was added to the system. There are ionic surfactants that are more effective in dispersing carbon nanotubes, such as sodium dodecylbenzene sulfonate [ISL 03], but due to the high concentrations of ionic species in the systems studied nonionic surfactants were considered a more effective dispersion option. The prepared sol was cooled to between 2-4 $^\circ\text{C}$ and mixed by magnetic stirring before adding urea (Sigma-Aldrich) to the system. Urea was added in a Urea/Zr ratio of between 1-2. After the urea had dissolved HMTA (Aldrich) was added to the system at a HMTA/Zr ratio of between 0.7-1.2. The HMTA was added slowly in small portions with stirring. Problems with premature gelation were not really observed at these temperatures if HMTA was added in an all-at-once fashion, but HMTA does however dissolve slowly in the system and if adding all of the gelation agent at once it formed a big ball, or rather a clump, which dissolved very slowly.

Gelation was performed by dripping the sol into silicone oil (Rhodorsil silicone oil 1000 cSt) heated to 90 $^\circ\text{C}$, either by producing droplets by hand using a Pasteur pipette or by semi-automated droplet generation using a syringe pump and nozzle. A permanent magnet vibrator was used for production of microspheres of variable size.

After gelation of the formed microspheres, the silicone oil was separated using a sieve to remove the major part of the “bulk oil”. The microspheres were then washed in petroleum ether (Fisher) to remove the residual silicone oil. Finally the microspheres were washed and aged in NH_4OH (aq). Washing was performed to remove the residual gelation chemicals and nitrates from the microspheres and ageing was performed to ensure complete gelation of the microspheres. The final aged microspheres were left to dry at room temperature in air.

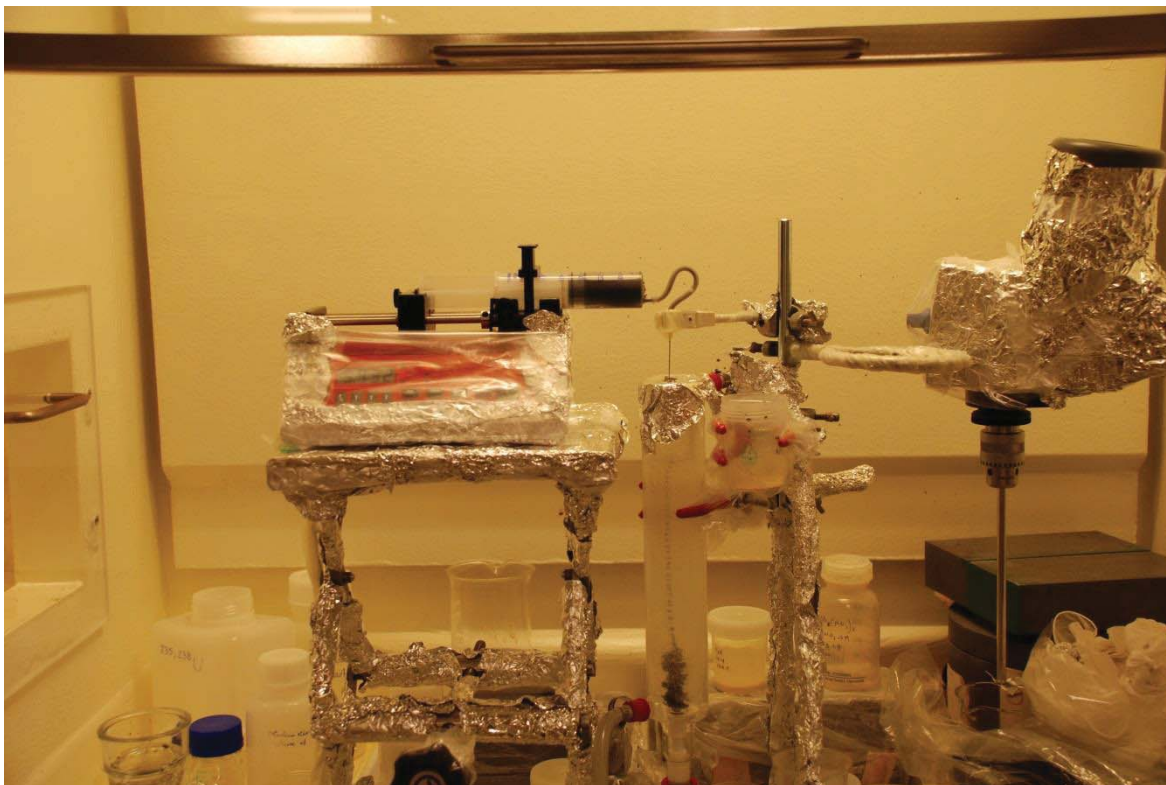


Figure 2. Sol gel instrumentation used for production of Zr-based microspheres. In the picture shown gelation was performed using a syringe pump but no vibrator for microsphere size reduction was used.

A single test was performed in order to establish if the addition of surfactant to the sol caused migration of water residing in surfactant micelles into the oil. A sol consisting of water, CNT and Triton X-100 was contacted with Rhodorsil silicone oil (1000 cSt), heated to 90 °C and mixed for a few minutes. The produced slurry was left to cool and phase separate. Samples of the silicone oil were collected and density was measured using a calibrated density probe (SIGMA, 701) and a microbalance. The density measured was then compared to that of pristine silicone oil the density of which had been measured using the same equipment. Free aqueous phase that was found in the bottom of the gelation column in connection with gelation was also collected and measured by ICP-OES (inductive coupled plasma-optical emission spectroscopy).

4.2. Preparation of Zr/Pu mixed sols and gelation of microspheres

The starting material for plutonium-containing material was PuO₂ powder that had to be dissolved prior to use in internal gelation. The Pu composition of the oxide powder used as starting material in all Pu work performed was 0.1% ²³⁸Pu, 84.7% ²³⁹Pu, 14.6% ²⁴⁰Pu, 0.2% ²⁴¹Pu and 0.4% ²⁴²Pu. Additionally the starting material contained in total about 1.5% ²⁴¹Am formed by ²⁴¹Pu decay. 0.75 M Pu solution was prepared by dissolving PuO₂ powder in 14.4 M HNO₃ (aq) (Sigma-Aldrich) containing 0.05 M HF (aq). To facilitate complete dissolution the powder the acid mixture was heated to 80 °C in a sealed glass container until no powder remained.

Based on the initial composition and age declaration of the PuO₂ material source used it was decided to remove the ²⁴¹Am content prior to use in gelation studies. The plutonium uranium redox extraction (PUREX) separation process was adopted to separate Pu from Am. The 0.75 M Pu stock solution was diluted with MQ and HNO₃ to a concentration of about 0.17 M Pu and 4 M HNO₃. The organic phase used during extraction was 30 vol% tri butyl phosphate (TBP, Aldrich) and 70 vol% solvent 70 (Statoil). During the extraction a 1:1 phase ratio was used between the aqueous and the organic phase. Back extraction of Pu from the organic phase was performed using MQ water as the aqueous phase. Mixing was performed by manual shaking during the extraction/back extraction steps and the contact time in every individual mixing step was 15 minutes.

The back extracted plutonium was too dilute to be used directly in the internal gelation process. The solution was therefore concentrated by boiling. The back extraction solution was boiled in three different batches of roughly equal volume. HCl was added during boiling to maintain a low pH and H₂O₂ was added to keep Pu in its +4 oxidation state [CON 49, MAI 01]. The final solutions were about 0.5 M Pu.



Figure 3. Plutonium stock solution for preparation of mixed Zr/Pu sols. From left to right: the initial Pu solution obtained from dissolution of PuO₂ powder, Pu solution after the first plutonium extraction step and lastly the plutonium solution after the second Pu extraction step.

Different methods for preparation of Zr/Pu mixed sols were tested. During preparation of sols for internal gelation the metal composition in the sol was however kept at 60% Zr and 40% Pu in all experiments and the total metal concentration was 0.6 M.

The initial step of sol preparation was addition of zirconium. Zr addition was tested using either ZrO(NO₃)₂ (Aldrich) or ZrOCl₂·4H₂O (Alfa products) as a Zr source. The ZrO(NO₃)₂ did not dissolve, possibly due to the high nitrate concentration in the solution. The ZrOCl₂·4H₂O dissolved, however, and was used in further experiments. Once the Zr-containing salt had been dissolved in the solution, the solution was cooled to 2 °C by putting the glass vial into a double-mantled cooling beaker with some water on the bottom to enhance heat transfer. Cooling of the sol was performed prior to the addition of base for pH adjustment or gelation chemicals.

The Pu and Zr-containing solution was then pH adjusted by addition of either 25 wt% aqueous ammonia (13.4 M, Fisher-Scientific) or 14 M NaOH (Sigma-Aldrich) (aq) to reach a low enough H^+ concentration for gelation by HMTA addition to be possible. Both NH_4OH (aq) and NaOH (aq) were tested for this decrease in H^+ concentration, but NH_4OH was considered to be the better method. NH_4OH (aq) was preferred over NaOH (aq), partly because NH_4OH (aq) is produced during the internal gelation process and is thus known to be compatible with the process, and partly because it was observed that precipitation was more likely to occur when H^+ concentration was adjusted using NaOH (aq). The concentration of Zr and Pu in the solution was adjusted by dilution using both aqueous ammonia and MQ water if needed.

Three different methods of adjusting the H^+ concentration using NH_4OH (aq) were investigated: one where NH_4OH (aq) was added and the gelation chemicals were added separately; one where urea (Sigma-Aldrich) had been dissolved in the NH_4OH (aq), and finally one where both urea and HMTA (Aldrich) were pre-dissolved in the NH_4OH (aq). The urea and HMTA/Me ratios were varied in order to find suitable gelation parameters. The urea/Me ratio investigated was either 1 or 2 and HMTA/Me ratio was varied between 0.7 and 1.2.

Triton X-100 (Sigma-Aldrich) was used as a dispersion agent for carbon black (Cabot, Mogul L). Both Triton X-100 and carbon was added separately to the sol after pH elevation had been completed and the gelation chemicals had been added. Carbon was added to a C/Me ratio of 2.1 and pure Triton X-100 was added as a single drop. Addition of Triton X-100 and carbon powder both prior to and after the addition of HMTA to the sol was also tested.

4.3. Preparation of Pu sol and gelation of microspheres

About 0.93 g unused PuN powder produced from carbothermal reduction of PuO_2 powder was used for solution preparation. Dissolution of the material in 3 ml 6 M HNO_3 containing 0.05 M HF was performed to produce the plutonium solution for internal gelation. Dissolution was observed immediately when the acid was added to the powder. Dissolution was performed in a closed glass vial that was periodically purged of formed NO_x compounds. The sample was left for a week to dissolve at room temperature, which only achieved partial dissolution of the powder. To increase the dissolution 0.5 ml 14.4 M HNO_3 containing 0.05 M HF was added and the sealed glass vial was heated to 353 K and left to dissolve for an additional week. The resulting solution still contained large quantities of undissolved material and filtration was performed. Some losses of liquid occurred during heated dissolution and filtration and after filtering about 2.4 ml of dark brown solution was obtained. The solution was determined to contain a concentration of 0.57 ± 0.03 M Pu. The use of HF during dissolution causes some degree of glass dissolution and silicate formation. Formed silicates and fluoride are however reported to be volatilized as SiF_4 and should therefore be removed simultaneously when the NO_x purging was performed [ISO 09]

The Pu solution was too acidic for direct application in the internal gelation process and needed to be partially neutralized by addition of NH_4OH (aq). Urea is not soluble under acidic conditions and was added before NH_4OH addition as an indicator of when sufficient base had been added to the sol. The general idea was that the urea would dissolve prior to the precipitation of Pu, indicating when the correct amount of NH_4OH had been added. This sol

preparation method was chosen because it had been successfully applied to acidified Zr-containing mock up solutions prior to the actual Pu experiments.

The sol for internal gelation was produced by addition of 0.14 g urea to 2 ml Pu solution. 1 ml of 25 wt% NH₄OH (13.4 M, Fisher-Scientific) was added in 25 µl batches. After the NH₄OH addition was completed, 3 droplets of Triton X-100 (Sigma-Aldrich) were added as a carbon dispersion agent. 0.031 g carbon powder (Mogul L, Cabot Carbon), equal to a C/Me ratio of 2.2, was added to the sol and mixed by manual shaking. Generally the carbon was found to have dispersed well by ocular inspection, however some larger residual agglomerates of carbon could not be avoided by this method. The sol was cooled to 275 K and 0.37 g HMTA (Aldrich) was added to the sol. The sol was gelled by manual dripping using a Pasteur pipette into silicone oil (Rhodorsil silicone oil 47) heated to 363 K. The gelled microspheres were washed 3 times, 20 minutes each time, in petroleum ether, followed by washing and aging for 3 times 20 minutes in 2.5 M NH₄OH. Finally the microspheres were washed once in 0.5 M NH₄OH for 20 minutes and left to dry in air at room temperature.

4.4. Nitridation of microspheres and powders

When nitriding microspheres, the dried microspheres were placed in a molybdenum metal crucible and placed in a furnace (Thermal Technology “1000-2560-FP20 High Temperature Graphite Furnace”) (Figure 4). This is a high temperature furnace with a graphite resistor heating element with a maximum operating temperature of 2500 °C. The furnace temperature regulation consisted of a molybdenum thermocouple up to 1300 °C, joint temperature measurements of the thermocouple and a two-color pyrometer between 1300-1450 °C. Above 1450 °C the molybdenum thermocouple was withdrawn and the pyrometer regulated the furnace alone. The furnace was placed in a glove box, and when the glove box was in operation and maintained a reasonably pure nitrogen environment (up to a maximum of around 10 000 ppm of oxygen) the furnace was evacuated and refilled three times, sequentially to ensure an oxygen-free environment in the furnace. When the atmosphere control of the box was turned off and the box atmosphere was air, the evacuation and refilling of the furnace was performed at least five times to ensure an oxygen-free atmosphere in the furnace.

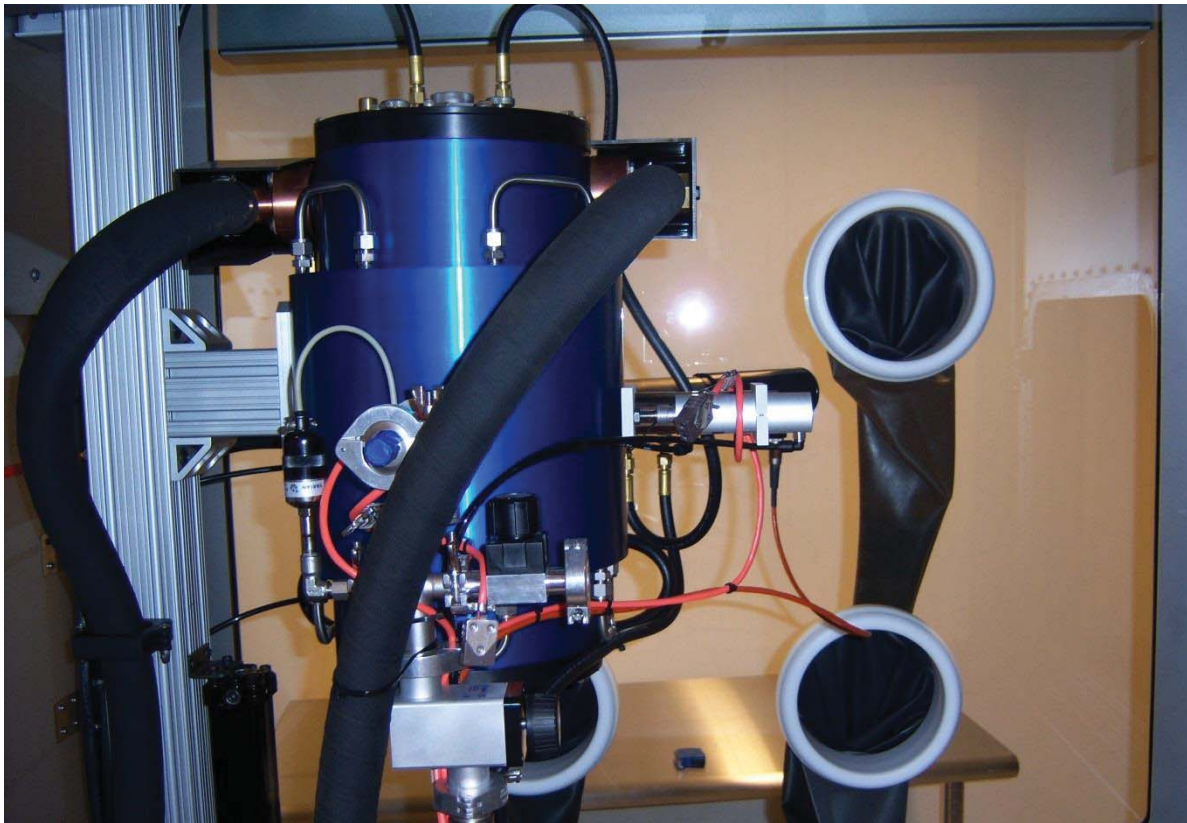


Figure 4. Thermal Technology “1000-2560-FP20 High Temperature Graphite Furnace”. This furnace equipment was used for both carbothermal reduction of materials and sintering of pellets.

The gases used for nitridation experiments were either nitrogen from the in-house nitrogen gas system (99.996% N₂, gas supplier AGA), High purity nitrogen (99.999%, Air Liquid) or nitrogen containing 5% hydrogen (Air Liquid, gas grade Blue). Generally the use of the in-house nitrogen was used as furnace gas until the installation on the high purity N₂ gas line had been finally installed.

4.4.1. Carbothermal reduction of Zr-based microspheres

The microspheres were generally first heated to 600 °C and held at that temperature for between 0.5-2 hours in order to evaporate/break down potential residues in the microspheres, such as urea, HMTA, water and NH₄NO₃. The NH₄NO₃ comes from the washing and ageing step of the microspheres where the NO₃⁻ containing microspheres are washed in NH₄OH (aq).

The microspheres were then heated to between 1400 and 1800 °C and nitriding was performed, either in a single step at a temperature in this interval or first at a temperature at the lower end of the range and then a second step at the higher end of the range. The point of, or idea behind, using two separate heating intervals is to first form the nitride at the lower temperature and burn off the residual carbon through formation of HCN and short-chain hydrocarbons such as CH₄ at the higher temperature step. The higher temperature step is sometimes referred to as the decarburization step. The heat treatment times for each separate heating step, when multiple steps have been used for carbothermal reduction and decarburization, varied from between 2 to 8 hours.

4.4.2. Carbothermal reduction of mixed Zr/Pu microspheres

Carbothermal reduction was performed in $N_2 + 5\% H_2$ gas. The microspheres were placed in a Molybdenum crucible and the sample was heated to 600 °C at a rate of 10 °C/minute and then held at 600 °C for 60 minutes. After removal of residual chemicals the sample was heated to 1400 °C at a rate of 20 °C/minute and held for 240 minutes for carbothermal reduction. Finally the sample was heated to 1650 °C at a rate of 20 °C/minute, dwelled for 240 minutes for decarburization, and cooled by 20 °C/minute to room temperature.

4.4.3. Preparation and carbothermal reduction of PuO_2 powders

Pure PuN was fabricated from PuO_2 powder by carbothermal reduction. The initial powder was mixed with carbon nanopowder by manual mixing using shaking. Ten minutes of vigorous shaking resulted in a mix that by ocular inspection was perceived as a dark green homogenous blend. No aggregates of either PuO_2 or C could be observed and the two powders generally appeared to mix well. Mixtures containing two different C/Pu ratios were produced; one set using a C/Pu molar ratio of 2.3 and one set using C/Pu molar ratio of 2.5.

Molybdenum crucibles were used as reaction vessels during carbothermal reduction. $N_2 + 5\% H_2$ gas was used throughout all heat treatments. The oxide batches was heated by a rate of 20 °C/minute to 1400 °C and reacted for 4 hours. After the carbothermal reduction step the samples were heated at a rate of 20 °C/minute to either 1600, 1650 or 1700 °C for decarburization. The reaction time used during decarburization was 2 hours. The samples were cooled to room temperature at a rate of 20 °C/minute.

4.4.4. Carbothermal reduction of Pu-based microspheres

Carbothermal reduction was performed in $N_2 + 5\% H_2$ atmosphere. The microspheres were heated 5 °C/min to 300 °C and held for 20 minutes. The sample was then heated by 10 °C/min to 600 °C and held for 20 minutes. The sample was then heated at a rate of 20 °C/min to 1400 °C and held for 4 hours. Decarburization was performed by heating 20 °C/min to 1650 °C and holding for 2 hours. The sample was cooled 20 °C/min to room temperature.

4.5. Pellet fabrication and sintering

4.5.1. Conventional cold pressing of pellets

Cold pressing of pellets was performed without addition of any additives such as lubricants, pore formers, binders or sintering agents. Pellets were pressed using pressing tools made of tungsten carbide. Pressing dies with internal diameters of either 4.5 or 9 mm were used for pellet fabrication. Mechanical compaction of the pellets was performed using pressures ranging from 600 MPa to 1200 MPa when pressing ZrN materials. Mixed Zr/Pu nitrides were pressed

using 1200 MPa compaction pressure. PuN powders were pressed using compaction pressures ranging from 1200 to 1800 MPa. PuN produced from the internal gelation process was pressed at 1800 MPa using a 4.5 mm diameter pressing die.

4.5.2. Sintering of pelletized compacts

Sintering was carried out with the pellet to be sintered placed on a molybdenum or tungsten plate. Heating rates of between 10 to 20 °C/minute were generally used during heating and cooling. Sintering of ZrN based pellets was performed in both Ar and N₂ environments. Sintering was performed at 1700 °C in Ar, while in the N₂ environment sintering temperatures varied between 1800-2000 °C and sintering was performed for 5 hours at maximum sintering temperature. Sintering of mixed Zr/Pu pellets was performed in both Ar and N₂ atmospheres at 1700 °C for 5 hours. Sintering of PuN pellets pressed from powder was performed in N₂ and Ar atmospheres at 1700 and 1800 °C and a sintering time of 4 hours. Sintering of PuN pellet from microspheres was performed at 1800 °C for 4 hours and the sintering atmosphere used was Ar. All sintering was performed using flowing gas conditions in the furnace.

4.5.3. Spark plasma sintering on nitrided Zr microspheres

Microspheres were weighed into a graphite pressing die and pre-compacted with a force of 0.5 kN. Diameters of the pressing dies used were 6 mm and, in one case, 10 mm, yielding pre-compaction pressures of 17.7 and 6.4 MPa, respectively. During SPS the compaction force used was 2.8 kN for the 6 mm diameter die and 7.8 kN for the 10 mm diameter die, corresponding to a pressure of 99 MPa in all sintering experiments. Samples were heated to 1700 °C at a heating rate of about 180-190 °C/min. Sintering times that were applied at 1700 °C were either 5 or 30 minutes and the atmosphere was varied between N₂ and Ar.

5. Results and discussion

5.1. Dispersion stabilization

Carbon nanotubes are hydrophobic if they are not surface treated and will settle quickly in aqueous systems if no dispersion agent is used. The same holds true for the carbon powders tested. Settling times of dispersed carbon materials were estimated by ocular inspection of the dispersions. In all cases it was determined that the aid of a dispersion agent was needed if dispersed powders would be used in the internal gelation process. The nonionic surfactant Triton X-100 was chosen as the preferred dispersion agent because the gelation systems studied contain high levels of ionic species. There are many other nonionic surfactants, but Triton X-100 was chosen due to the fact that it has previously shown the ability to disperse CNTs [RIG 00]. Figure 5 shows the result of leaving a CNT dispersion to settle without the addition of any surfactant; the settling time for the CNTs was estimated to be on the second scale, in the best case no more than half a minute. The same behavior was observed also in dispersion of all the carbon powder materials where settling times were estimated to be in the order of about a minute at most.

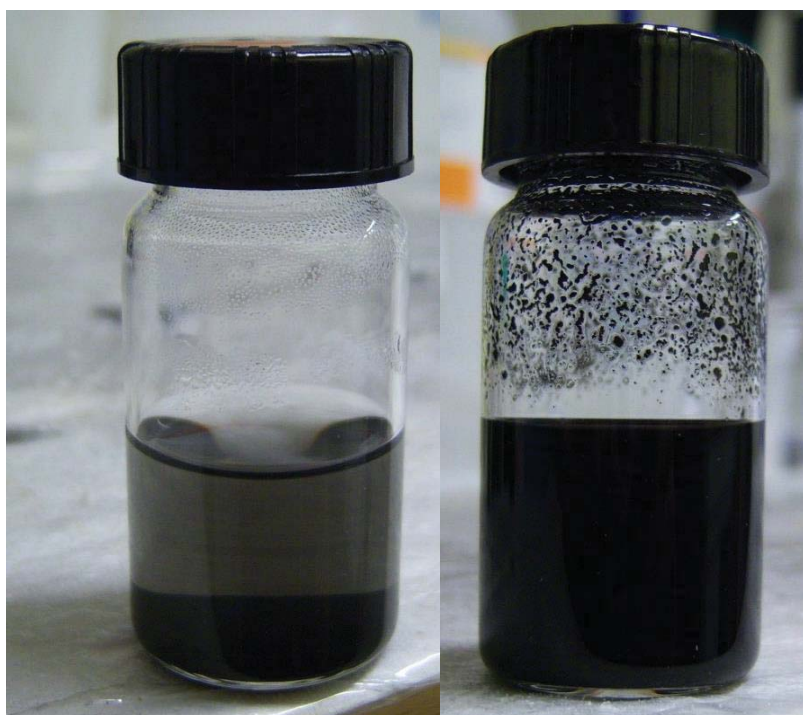


Figure 5. To the left: result of trying to disperse CNT in aqueous media without the addition of any surfactant. To the right: carbon nanotube suspension using Triton X-100 as a dispersion agent.

When Triton X-100 was added to the solution the dispersion stability was substantially increased for the fine powder CNT, Cabot powder and the CNP materials. For the coarser carbon powder, however, the stability increase was quite small. This is to be expected, since the settling time of a dispersion is inversely proportional to the square of the diameter of the

dispersed particles (solids or droplets) [HOL 03]. As the particles increase in size, the surface-to-volume ratio becomes too small for any dispersion agent to improve the dispersion stability to a significant degree.

Addition of 2 weight% Triton X-100 to the aqueous solution was sufficient to greatly increase the dispersion stability of the CNT, the Cabot powder, and the CNP dispersions.

With the use of Triton X-100 as a dispersion agent, the resulting particle suspensions showed a substantial increase in settling time, and Triton X-100 was regarded as being good enough for use for production of microspheres using the internal gelation process. It has been reported in the literature [RIG 00] that a 5% Triton X-100 solution can produce a good CNT suspension. The reason for using a lower amount of surfactant when producing the sol for the internal gelation process was to minimize the risk of leakage of water into the silicone oil during the gelation step by transfer of water within micelles formed by the surfactant.

In order to determine if water to any large extent was transferred into the silicone oil, a solution of CNT, water and Triton X-100 was prepared and shaken together with the silicone oil (Rhodorsil silicone oil 47). The mixture was left to settle and the silicone oil was separated from the aqueous phase and no trace of water emulsion or CNT could be detected in the oil by visual inspection. Density measurements were performed on the silicone oil that had been mixed with the CNT suspended aqueous phase and compared to density measurements of silicone oil taken directly from its container. The results are presented in Table 1.

Table 1. Density measurements for unused silicone oil compared to silicone oil that has been mixed and separated from aqueous solution containing water, Triton X-100 and CNT.

Density mixed silicone oil (g·cm ⁻³)	Density unused silicone oil (g·cm ⁻³)
0.968	0.971
0.968	0.972
0.969	0.973
0.971	0.978
0.969	0.985
Average	Average
0.969	0.9758
Standard deviation	Standard deviation
0.0012	0.0058

No significant differences in density could be detected. Combined with the visual inspection of the separated silicone oil this was interpreted as indicating that the leakage of aqueous medium into the silicone oil was insignificant from a gelation perspective. Additionally some aqueous phase was also collected during the gelation of zirconium-based sols from the aqueous solution that migrated from the microspheres into the silicone oil. This aqueous phase could be sampled after gelation had been completed and the cooled oil was decanted from the gelation column. ICP-OES analysis on the collected aqueous phase did not detect the presence of Zr, which strengthened the view that any potential Zr leakage out of the microspheres was small enough to be disregarded within the process. No corresponding measurements were performed on

aqueous leakage phase from mixed Zr/Pu sols. The reason for this was that sol batches of mixed Zr/Pu solutions were so small in volume that no migrated aqueous phase could be observed in the silicone oil post gelation and cooling of the oil.

5.2. *Microsphere production*

5.2.1. *Production of Zr based microspheres*

When no vibration of the nozzle was used during the fabrication of the microspheres containing only Zr, the produced microspheres were of a diameter of about 1 mm after washing and drying had been performed. General examples of the physical appearance of newly produced microspheres and dried microspheres, both containing carbon, are shown in Figure 6.



Figure 6. Zirconium based microspheres containing elemental carbon after washing has been completed is shown on the left. On the right side carbon-containing Zr microspheres after drying are shown.

The use of mechanical vibrations along the vertical axis of the gelation setup nozzle was tested to investigate the possibility of reducing the size of the droplets formed during gelation. Microspheres in a size range of about 50-100 μm in diameter could be produced in this fashion. It was however difficult to produce controlled narrow size distributions with the equipment used. It was observed that the problem was partly caused by slow build-up of larger droplets on the nozzle tip. By adjusting the sol flow through the nozzle this behavior could be affected but not entirely removed. It was also observed that coalescence of droplets into larger aggregates occurred when the droplets hit the silicone oil surface. Every drop requires a certain amount of time to sink through the silicone oil surface layer. If the droplets hit the surface of the oil too closely to each other they will merge and form larger droplets. This is one of the downsides in using an experimental set-up utilizing a stationary gelation column to produce the microspheres. Work that has been performed on the internal sol gel process elsewhere [POU 09] has solved this problem by dripping the sol into a laminar jet stream of silicone oil, followed by separation and recirculation of the silicone oil. This type of set-up may have benefits when it comes to

production speed capability but requires much more equipment and space for set-up than using a stationary gelation column.

Microspheres produced by use of the oscillating nozzle technique are shown in Figure 7.

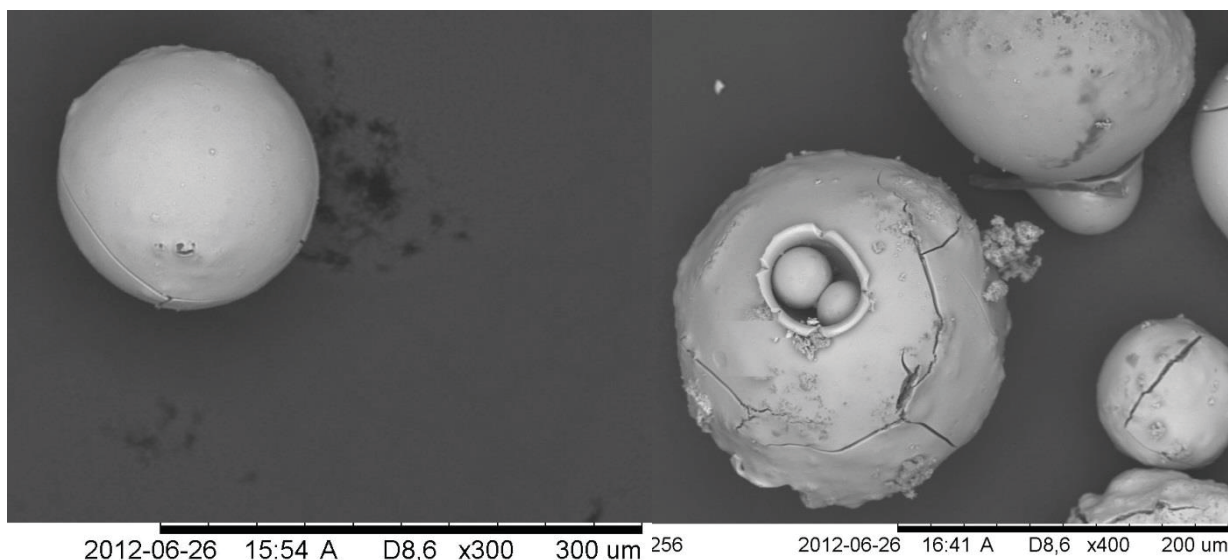


Figure 7. Microspheres produced by the oscillating nozzle technique. The microspheres were produced using carbon nanotubes as carbon source. No signs of formed agglomerates of carbon nanotubes could be observed in the microspheres using SEM. The batches of size-reduced microspheres produced contained a large variation in microsphere sizes formed.

When the coarser graphite carbon powder was used as the carbon addition, settling of the powder occurred both in the syringe in the gelation set up and in the droplets during gelation. The gelation result became microspheres that displayed an uneven distribution of carbon particles. As is shown in Figure 8, the uneven carbon distribution could be very clearly observed by SEM characterization of the microspheres produced.

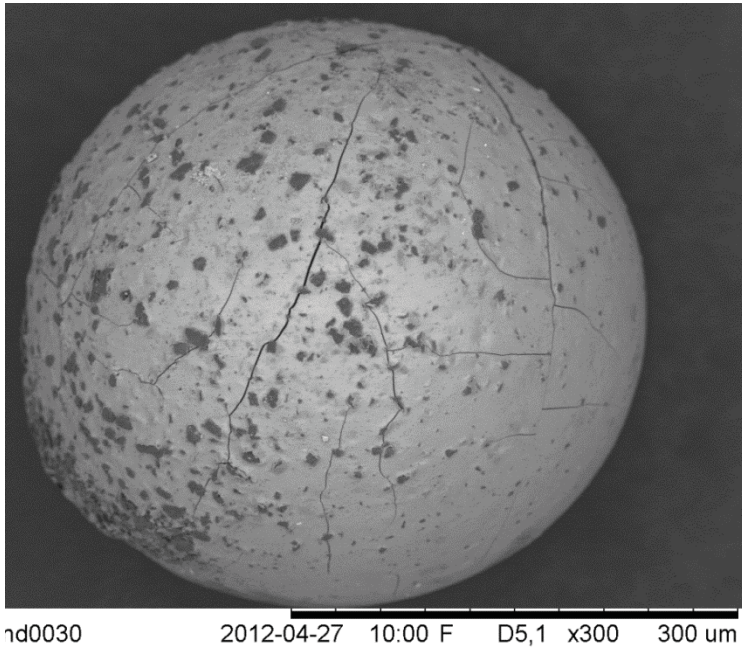


Figure 8. Zirconium-containing microsphere produced with a coarser graphite powder (about 10 μm size particles). The uneven carbon distribution makes the material impractical for carbothermal reduction.

This result indicated that the coarse graphite powder was not a suitable carbon additive for production of microspheres for carbothermal reduction. This is because materials with more homogeneous carbon distribution are more desirable when producing nitrides since more finely dispersed carbon decreases diffusion distances and lowers the probability for obtaining final materials containing residual clusters of unreacted carbon and oxide.

When CNT or CNP was used as the carbon source the resulting microspheres showed a much more homogeneous carbon distribution during SEM characterization, as can be seen in Figure 9.

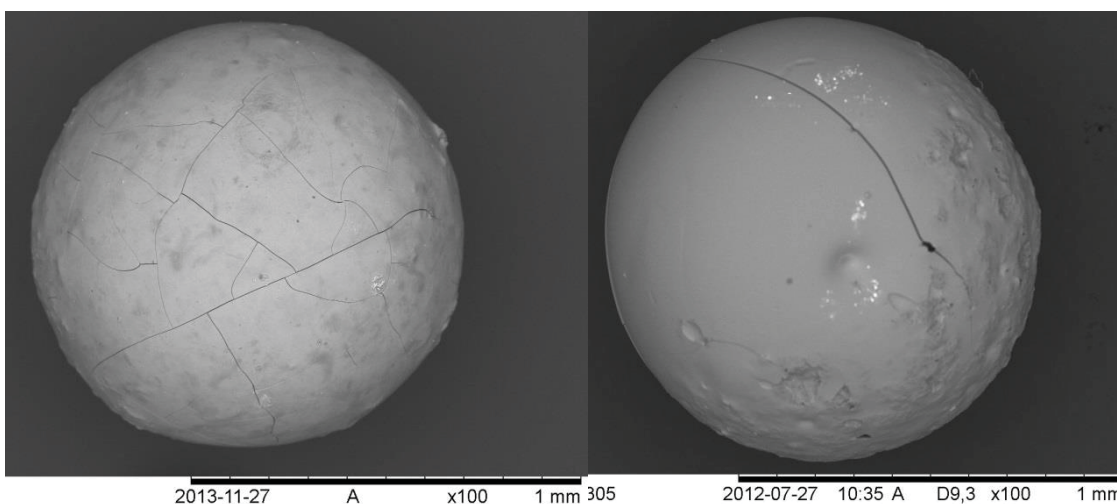


Figure 9. On the left: a microsphere containing CNT. On the right: a microsphere containing CNP as the carbon addition.

SEM characterization of microspheres performed after the carbothermal reduction step shows that significant amounts of cracking in the microsphere surfaces normally occurs during the

heat treatment. Figure 10 illustrates what the zirconium-based microspheres generally looked like after carbothermal reduction.

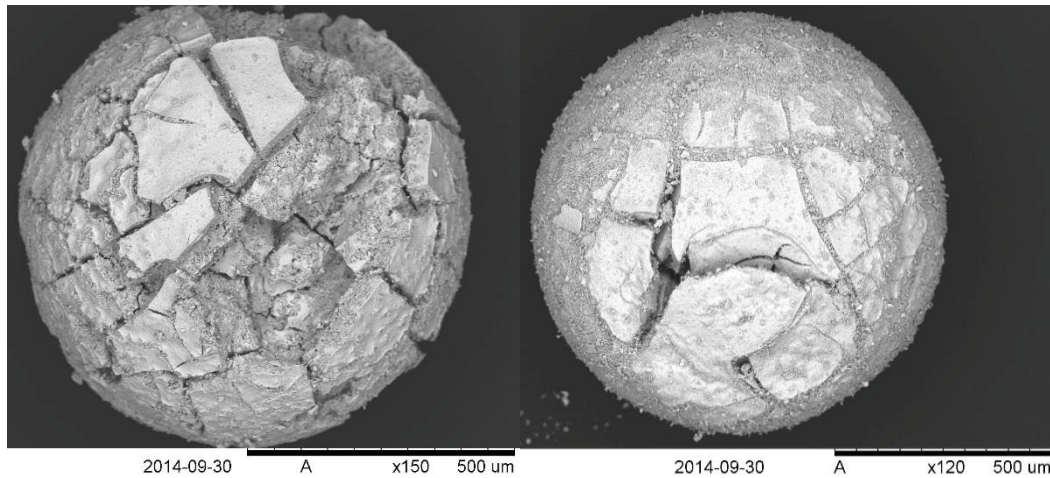


Figure 10. Zirconium-based microspheres post carbothermal reduction. The images represent the general appearance of greater and lesser degrees of fracturing observed in the microspheres [HED 16b].

The majority of the porosity and fracturing of the microspheres is believed to be formed during the initial heating stage of the microspheres when water and residual gelation chemicals are degraded and leave the microspheres. The heating ramp used was generally between 10-20 °C per minute, which probably causes the gasification of the residual chemicals to proceed fast enough to cause cracking of the microspheres. Since the purpose was production of fuel in the form of pellets and not sphere-pac fuel types, some degree of fracturing and porosity was not regarded to be a disadvantage, since crushing of microspheres during pressing would be easier to perform if the microspheres were not fully dense. The result of incomplete crushing of microspheres during pellet pressing can be that the formed pellet partially retains the structure of the microsphere feed material. This is known as blackberry structure. Blackberry structure is generally not desirable in the final pellet and incomplete crushing of microspheres also lowers the density of the green pellet compact.

5.2.2. Gelation of mixed Zr/Pu sols

During the production of mixed Zr/Pu microspheres it was found during the sol gel experiments that a reduction of the H^+ concentration in the sol was required to be able to perform any successful gelation from the sol. It was also decided that H^+ neutralization was preferably performed by addition of NH_4OH (aq), containing no urea or HMTA pre-dissolved in it. To be able to add HMTA without causing its premature decomposition the sol was required to be cold. This criteria could not be met if addition of NH_4OH (aq) was performed at the same time. The heat released during H^+ neutralization was too rapid for the sol to keep cool, even when performed during active cooling of the sol container. This was however a feature of the specific system studied and is not necessarily true if working with systems where larger batch volumes of sol are used. It was possible, but not convenient, to perform H^+ concentration adjustment with urea dissolved in the NH_4OH (aq). At higher acidities urea is not soluble, resulting in precipitation during the early stage of elevation of the H^+ concentration reduction. This made it difficult to judge if the H^+ concentration was decreased too much and precipitation of the metals

had occurred in the sol, or if there was undissolved urea in the sample. For these reasons the H^+ concentration adjustment was performed using NH_4OH (aq) without any additions and dissolution of urea and HMTA was performed separately once the addition of NH_4OH (aq) had been completed.

It was decided that addition of Triton X-100 and carbon was preferentially performed before HMTA was added to the system. It can sometimes be desirable to add carbon after the HMTA has been added to be able to see that all HMTA has dissolved before gelation is started. The reason for adding Triton X-100 and carbon before adding HMTA instead of after was that the carbon powder was dispersed by gentle manual shaking of the sol container. This method required removing the smaller sol container from the double-mantled cooling beaker and the small experiment volume used heated up too fast without active cooling for HMTA to be reliably added before carbon dispersion.

As a first estimate a urea/Me ratio of 2 and an HMTA/Me ratio of 0.7 was tested in the internal gelation process for mixed Zr/Pu sol. These ratios were chosen because of good results during the gelation of pure Zr-containing sols. The result was incomplete gelation. Microspheres started to form in the silicone oil but were deformed on the bottom of the column before gelation had been completed. When lowering the urea/Me ratio to 1 and increasing the HMTA/Me ratio to 1.2 the result instead became premature gelation when the sol was still in the cooling beaker. The use of a urea/Me ratio of 2 and HMTA/Me ratio of 0.9 could be used for the preparation of microspheres.

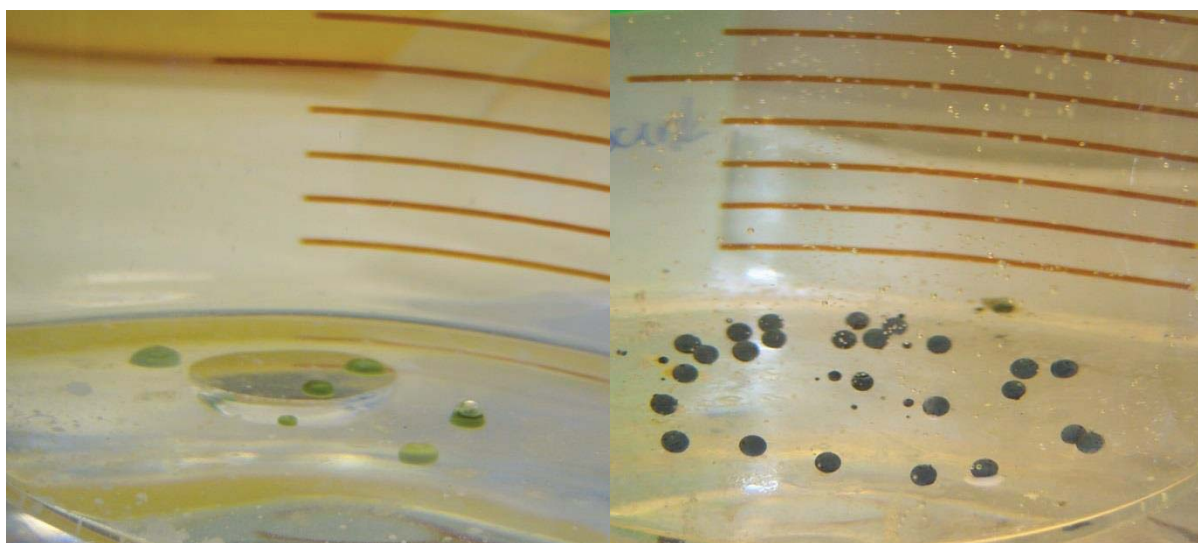


Figure 11. On the left: insufficiently gelled microspheres that have deformed on the bottom of the oil column. On the right: microspheres that have successfully gelled and retain their individual shape [HED 16a].

Imaging of produced microspheres using SEM was performed after the carbothermal reduction step and the pressed pellets were imaged after sintering.

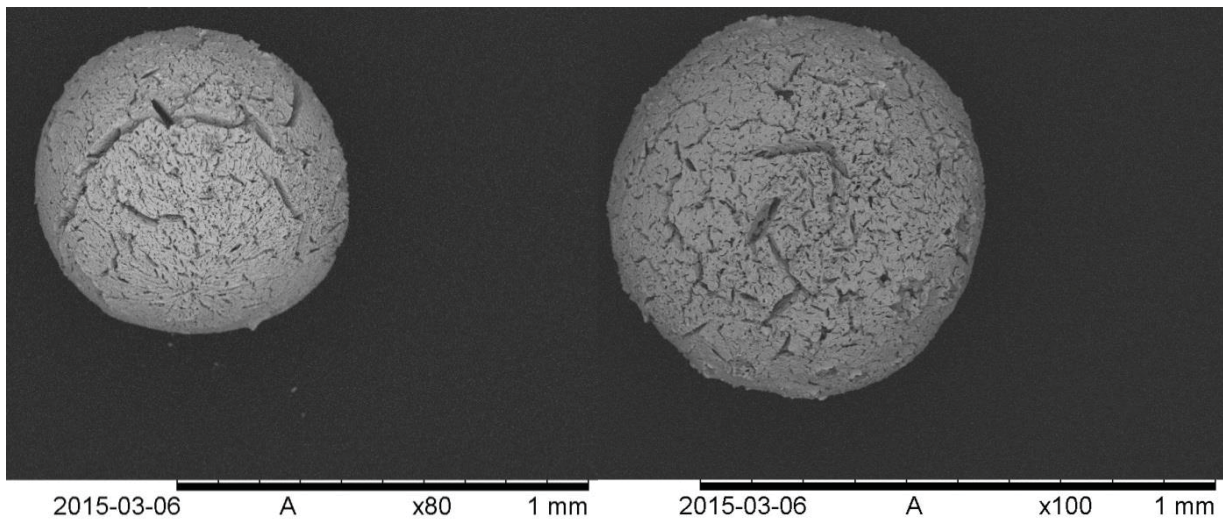


Figure 12. Microspheres after carbothermal nitridation has been performed [HED 16a].

The size of the nitrated microspheres was estimated to be in the range of 600 to 750 μm . The degree of surface fracturing in the nitrated microspheres is generally represented by the microsphere shown in Figure 12. The fracturing in the microspheres can also in this case likely be attributed to escaping gases during the initial heating of the sample.

By splitting a microsphere in half it was possible to study the porosity formed within the microsphere during carbothermal reduction. The cross section of a mixed Zr/Pu microsphere after carbothermal reduction is shown in Figure 13.

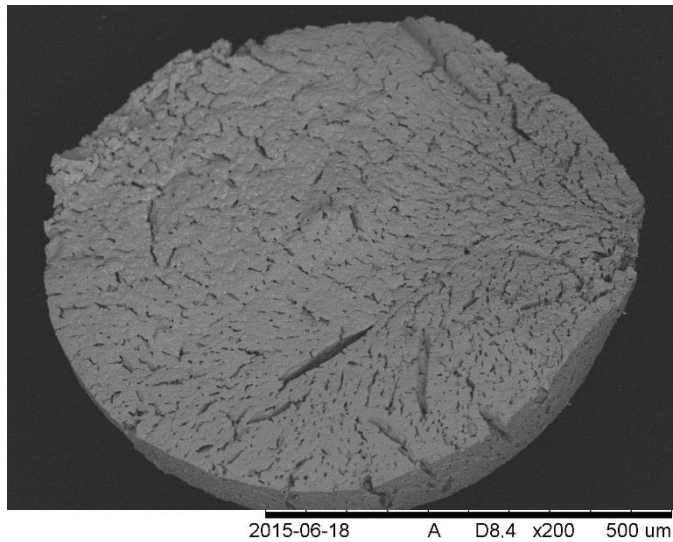


Figure 13. Cross section of a mixed Zr/Pu microsphere after carbothermal reduction has been performed [HED 16a].

Looking more closely, using higher magnification, two separate structures could be observed on the cross section surface of the microsphere. The structure of the microsphere surface is shown in Figure 14.

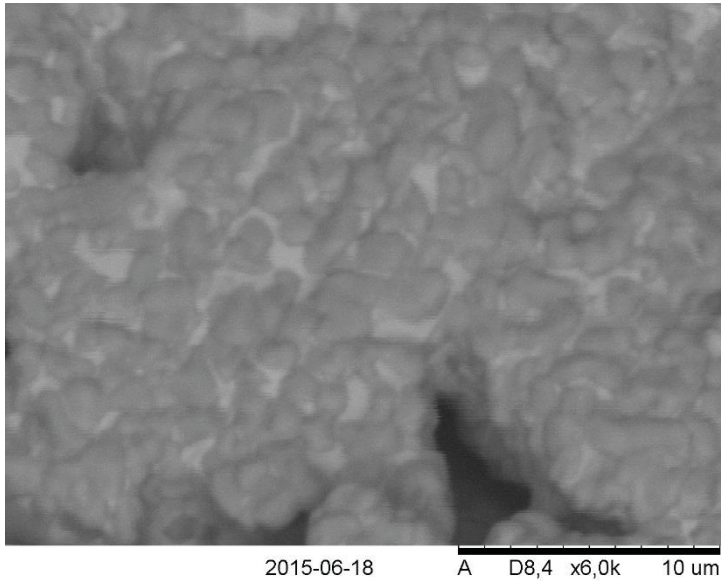


Figure 14. What seems to be a two phase structure could be observed during SEM imaging [HED 16a].

Since the SEM uses a back scattered electron detector it would be expected that areas containing separate structures of Pu and Zr would appear in different grey scale on the image produced. A potential explanation for this observation could be that no actual co-gelation of the metal ions occurred during the internal gelation step. If that is the case then the segregated structure would also have had to be at least partially retained in the microspheres during carbothermal reduction. By use of EDX mapping over the cross section surface it was possible to correlate the darker phase to Zr-rich material and the light phase to Pu-rich material, showing that this indeed seemed to be caused by separation of the metals at some point during the process.

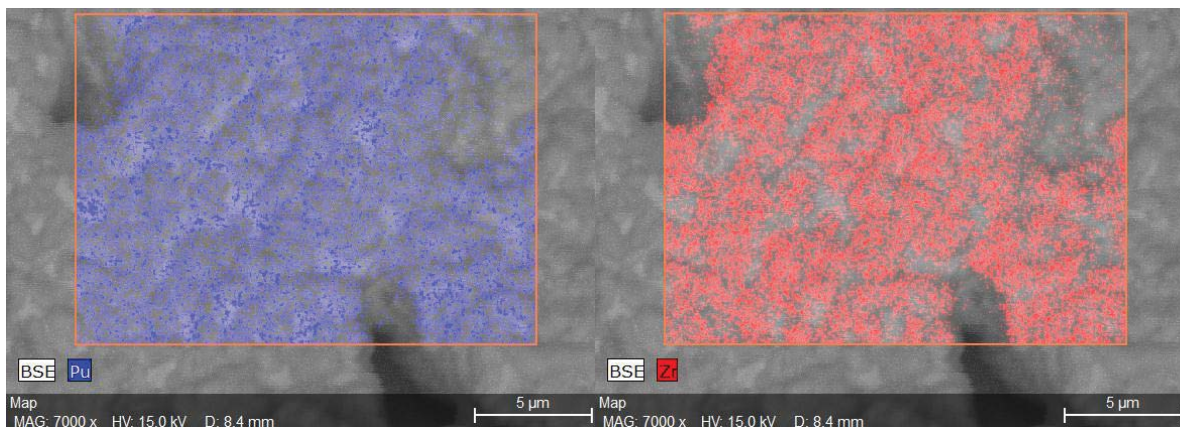


Figure 15. Elemental mapping of Pu (blue) and Zr (red) over the cross section surface. The Zr was found to be mostly distributed in the darker grains while the Pu was mainly found in the lighter, more continuously appearing phase [HED 16a].

The expectation before the experiments was that Pu(IV) and Zr(IV) would co-precipitate during the gelation step. The basis for this expectation is that the hydrolysis of Zr(IV) and Pu(IV) are similar. At first glance there are two viable ways in which the formed microspheres can phase separate, either in the gelation step or in the heat treatment. In the early stage of the carbothermal reduction the gelled hydroxide material is decomposed to oxides as water leaves the system. It

is possible that PuO_2 and ZrO_2 would prefer to form at least partially separate phases, since ZrO_2 crystallizes within the monoclinic and tetragonal structure [KLE 99] while PuO_2 crystallizes in the FCC- CaF_2 structure. The explanation of phase separation during thermal treatment was however considered less likely compared to separation of phases during gelation. This was based on two main arguments. The first reason was because the carbothermal reduction produces a nitride/carbide phase over the heat treatment cycle in which the Zr and Pu should form solid solution. There is therefore a reaction competing with and counteracting the driving force for phase separation. The second reason is based on the SEM observations. In Figure 15 it appears that the Zr-phase has formed grains while the Pu has not. This could be the case if Zr has hydrolyzed and precipitated before Pu and Pu has solidified in between the formed Zr grains. If the separate phase formation had been formed during heat treatment on the other hand, it would also be expected that Pu had formed some sort of grain structure rather than a bi-continuous structure in between the Zr grains.

One possible explanation could be that the Pu solution did not remain as Pu(IV) during the boiling step of the sol preparation. If a large enough proportion of the Pu present in solution changed in oxidation state from Pu(IV) and instead oxidized to Pu(VI), the overall hydrolysis behavior of the Pu-part of the sol may have been shifted enough to not co-gel with the Zr(IV). Based on the stability constants for the first hydrolysis step it can be seen that the hydrolysis of Zr(IV) and Pu(IV) occurs at about the same pH, while the hydrolysis of PuO_2^{2+} is shifted towards higher pH [BRO 15]. In Figure 15 it also appears that the Pu content is to some extent incorporated into the Zr-phase while the Zr-phase has a more pronounced preference for the darker appearing phase. This could be explained either by that some Pu(IV) did co-gel during internal gelation, or if several Pu oxidation states were present in the final gel, this could also be a result of the higher average metal mobility of the Pu compared to Zr during the thermal treatment, and therefore does not necessarily originate from gelation behavior.

A final potential explanation could be extensive carbide formation during some stage of the carbothermal reduction. PuN and ZrN form solid solution over the entire composition region [KLE 99] but PuC and ZrC do not. If the PuC concentration exceeds about 25% a multi-phase structure is formed instead [HOL 69]. In this case there would not be a driving force against a solid solution during at least parts of the reaction and a phase-separated material could be the result. It is still strange, however, that no grain formation or agglomeration of Pu seem to have occurred, which could still be expected if the material has phase-separated during heat treatment.

After nitridation some microspheres were dissolved in $\text{HNO}_3 + \text{HF}$ and the metal composition was determined by inductively coupled plasma mass spectrometry (ICP-MS). The metal composition determined by ICP-MS of the dissolved microspheres was 40.75 ± 3.3 mol% Pu and 59.25 ± 3.1 mol% Zr. Since the microspheres had not formed solid solution and ZrN and PuN separately would have had to volatilize in proportional amounts during heat treatment to keep the initial metal composition ratio, the composition measurement was interpreted as no significant losses of either Zr or Pu occur during gelation or carbothermal reduction.

5.2.3. *Production of Pu based microspheres*

Production of Pu based microspheres could be successfully performed by the internal gelation technique. Significant amounts of surface cracking could however be observed after drying. Due to what probably was a result of incomplete carbon dispersion during sol preparation, carbon agglomerates of up to about 50 μm in characteristic length could be observed on the microspheres surfaces after drying. This was likely caused by that no proper mixing or shear forces could be applied during the carbon dispersion step. An example of a microsphere is shown in Figure 16.

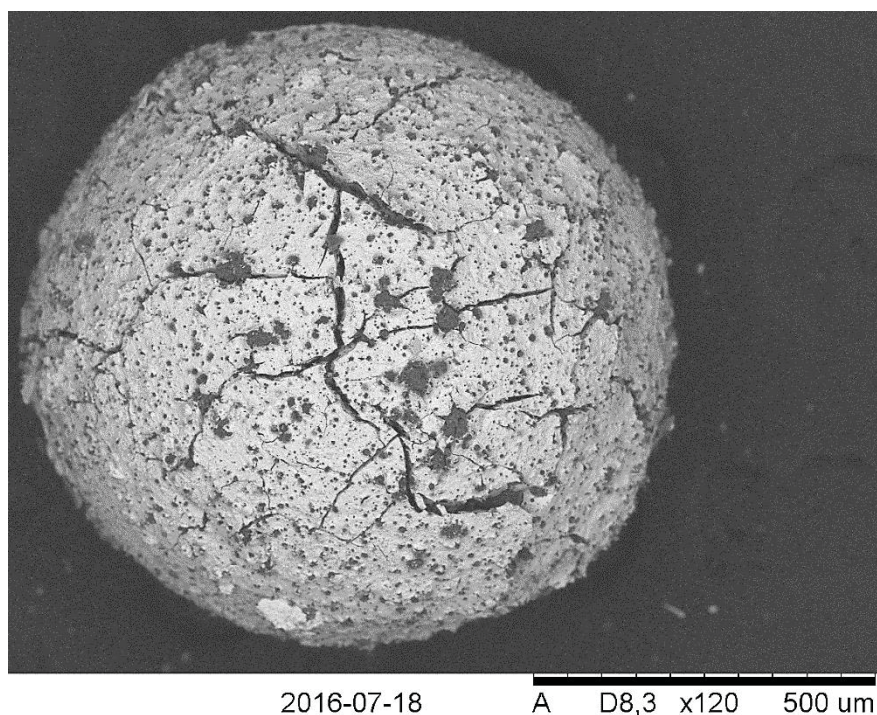


Figure 16. Non heat-treated Pu microsphere after being dried in air [HED 16d].

The degree of fracturing observable in Figure 16 is formed during the drying procedure. Low concentration of Pu during the internal gelation caused significant shrinkage of the microspheres during drying. This shrinkage likely contributed to partial fracturing of the microspheres.

The mechanical integrity of the microspheres was not retained during carbothermal reduction. The microspheres generally fractured into a coarse powder, as indicated in Figure 17.

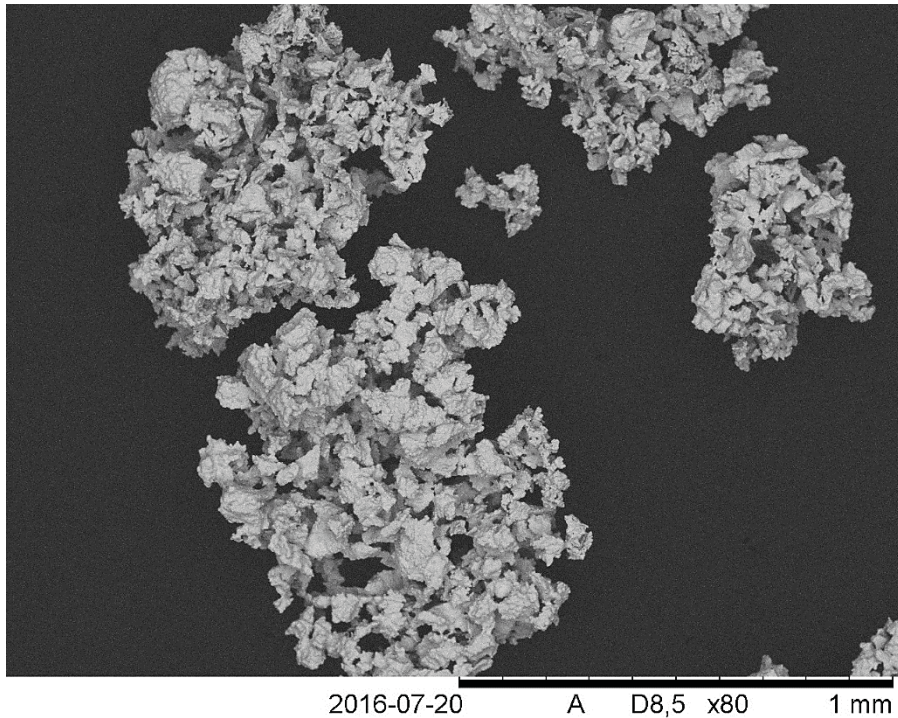


Figure 17. Fragments of semi-sintered powder produced during carbothermal reduction of the Pu microspheres [HED 16d].

The tendency to pulverize during thermal treatment could be a result of incomplete removal of residual gelation chemicals during the washing steps. The fracturing during heat treatment was not expected based on previous experience in production and carbothermal reduction of Zr and Zr,Pu-based microspheres. The greater than expected fracturing behavior of the microspheres could be caused by the low concentration of Pu used during gelation. Causing the formed microspheres to be mechanically more fragile than anticipated.

5.3. *Light element quantification by EDX*

Energy dispersive X-ray spectroscopy (EDX) was used to investigate the elemental composition of the surface of several Zr-based nitride materials. Examples of the results are presented in Table 2.

Table 2. Results of EDX measurements performed on the first batch of nitride material produced and two sintered pellets. The pellets have been produced from separate microsphere batches and none of them from the batch presented in the table.

Sample Name	Zirconium (at%)	Carbon (at%)	Nitrogen (at%)	Oxygen (at%)
Microsphere batch	24.3 ± 3.1	51.4 ± 3.5	19.0 ± 1.9	5.2 ± 0.7
Pellet sintered in N₂ 1800 °C	40.0 ± 3.4	23.1 ± 2.0	36.9 ± 1.2	Not detected
Pellet sintered in N₂ 2000 °C	39.7 ± 3.3	25.9 ± 1.2	34.4 ± 1.8	Not detected

The results in Table 2 illustrate what the results of the EDX measurements on ZrN materials commonly looked like. These results were interpreted as being very strange. According to Table 2 too much N and C is present compared to zirconium to be able to explain the data as the existence of only ZrCN material. This could possibly be explained by a surface covering of the microspheres and pellets with extra carbon transported there by reactions 15-19 from the graphite heating element. This would mean that the surface analysis provided by EDX would produce measurements that do not represent the composition of the bulk material. Measuring on cross sections of samples did not provide reasonable results either, indicating that the use of EDX simply gives erroneous results. EDX is known to be less efficient when it comes to quantifying light elements such as carbon, nitrogen and oxygen compared to when measuring heavier elements; for optimal results measurements should also be done on flat smooth surfaces. EDX measurements performed on both non heat treated microspheres and nitride materials and the results produced by the measurements indicates that EDX is an unsuitable technique for producing reliable estimates of elemental composition of light element atoms. For example the oxygen content measured in several different nitride samples appeared to be strongly dependent on measurement time used. Initially the measurements showed no presence of oxygen in the material. If the measurement time was prolonged for sufficient amount of time a threshold level was encountered where estimated oxygen levels suddenly increased from nothing to about 3 atomic percent. The observation of such irregular behaviors on several occasions strongly indicated that EDX was a sub-optimal technique for light element quantifications.

5.4. Light element quantification and XRD measurements

To be able to make more precise measurements of the elemental composition in the produced nitrides, samples of two different nitridation experiments were taken to an external lab for analysis using high temperature LECO elemental analyzers. The instruments used were of LECO type and worked by the same principle as the instrument models described in the theory section, with the exception that the N/O instrument also could measure H by IR measurements of formed H₂O during heating. One sample of microspheres using CNT as the carbon source and one sample containing CNP was taken for analysis and the results are presented in Table 3. The uncertainties in Table 3 are presented as ± 2σ.

Table 3. Results from measurements performed to analyze chemical composition.

Sample	Element (weight fraction)				
	O	N	C	H	Zr
Zr + CNT Microspheres	0.356 %	10.5 %	2.96 %	90 ppm	86.2 %
Zr + CNP Microspheres	0.22 ± 0.02%	9.34 ± 0.02%	3.67 %	73 ± 6.4 ppm	86.8 %

It should be noted that uncertainty is only given for N, O and H content in the Zr + CNP sample. This is because insufficient material was present to perform triplicate measurements on the Zr + CNT sample. Sufficient material was only present for the Zr + CNP sample to allow duplicate measurement when measuring carbon content. Therefore no standard deviation could be calculated, but it showed that the measurement data obtained was not totally arbitrary. There was also insufficient material to produce triplicate measurements for the carbon composition in the Zr + CNT sample.

By adopting the assumption that N, O and H are only present in the material as bonded to zirconium and that carbon can be present both as carbide and as free amorphous carbon, an approximate chemical composition is obtained of $Zr(N_{0.79}C_{0.17}O_{0.024}H_{0.009})$ for the nitride produced by carbothermal reduction with CNT and $Zr(N_{0.70}C_{0.28}O_{0.014}H_{0.008})$ when CNP was used. These results are considered to be much more credible than the results provided by EDX measurements due to the fact that this type of analysis measures the bulk of the material and not only just the surface, which may not be representative of the sample.

Composition determination for the Zr + CNT sample in Table 3 by use of Vegard's law on XRD measurement data was also performed.

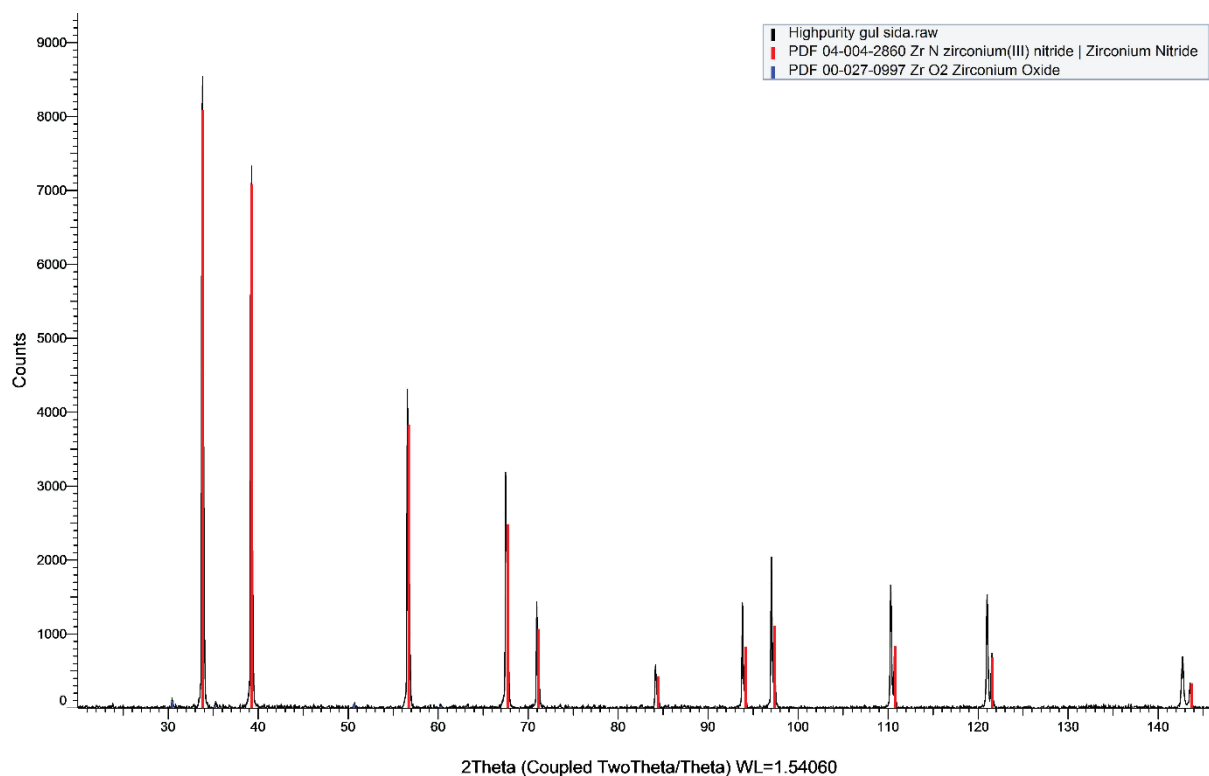


Figure 18. XRD measurement on sintered pellet pressed from the Zr + CNT material batch in Table 3.

The structure estimated by Vegard's law was $\text{ZrN}_{0.82}\text{C}_{0.18}$, which corresponds approximately to the $\text{ZrN}_{0.79}\text{C}_{0.17}\text{O}_{0.024}\text{H}_{0.009}$ structure suggested by the elemental analysis. XRD and elemental analysis therefore appeared to be useful complementary techniques for determining the structure and composition of the nitride materials produced, while EDX was retained as a complementary technique with utilization mostly connected to quantification estimates and mapping of metallic species, such as the data presented in Figure 15.

5.5. Composition determinations by Vegard's law and mixed nitride influence on lattice parameter

5.5.1. Ternary ZrCN materials

By compilation of data for mixed ZrCN materials produced and characterized at Chalmers and at Paul Scherrer Institute (PSI) in Switzerland a more in depth analysis of the influence of carbide determinations by lattice parameter measurements could be performed. The data used in the evaluation was collected for samples produced both at Chalmers and PSI, and some commercial ZrN samples were also included in the evaluation. The input data was divided into three different sets; in one set both C and N/O measurements were performed on the samples, in one set only C was measured and in one set only N/O was measured. The reason for not measuring all elements in all samples was that not all analysis equipment was available at each point in time. All data used is presented in the tables in paper III [HED 16c].

By plotting the lattice parameter of ZrCN materials with varying composition as a function of the nitride fraction in the materials a regression line describing the data points could be calculated and compared to the predictions of Vegard's law. The results are presented in Figure 19. The data in Figure 19 is plotted using different colors for the three different subsets.

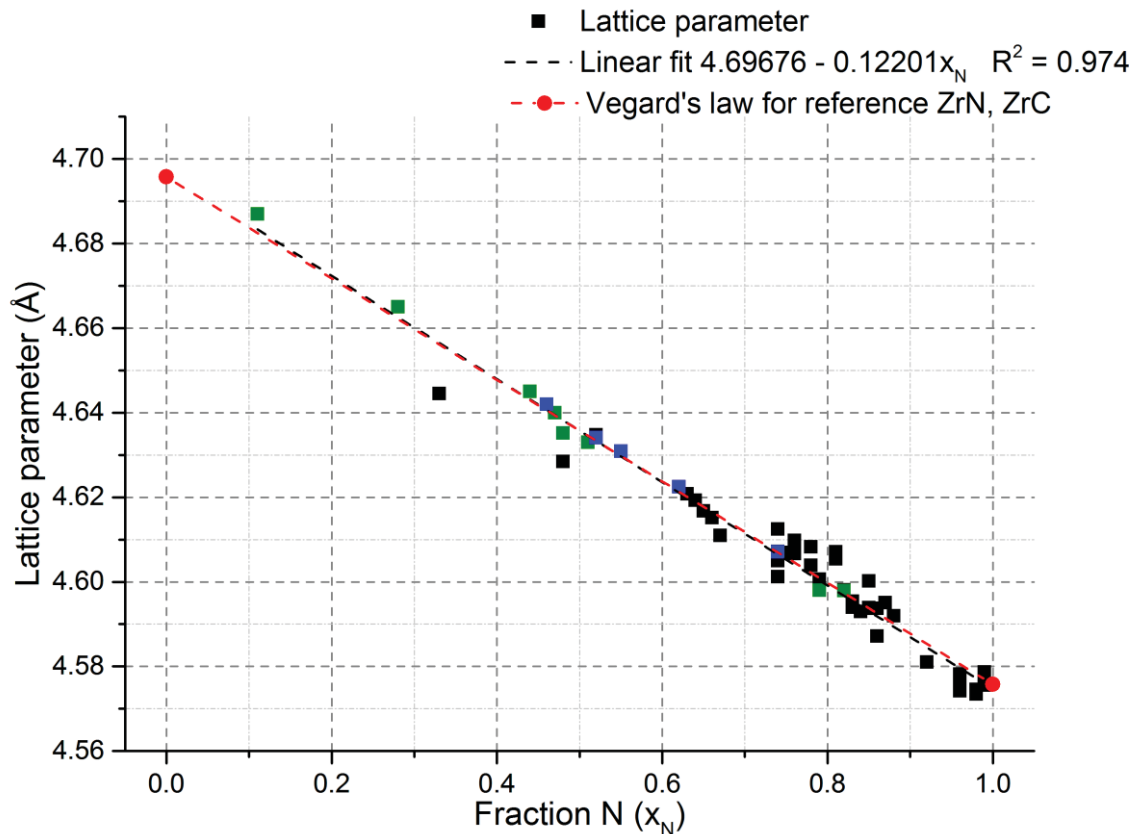


Figure 19. Lattice parameter variation as a function of nitride fraction in ZrCN material. The linear regression of the experimental data shows good agreement to Vegard's law. Note that the black dashed regression line is based on all three (black, blue and green) colored data sets [HED 16c].

From Figure 19 it seems that the predictions made by Vegard's law are in good agreement with the measurement data. This implies that Vegard's law is a good approximation for composition determination of mixed ZrCN materials. From the data in Figure 19 it also appears that the data points where only C or N/O content has been measured do not introduce any strong errors or biases into the regression model.

5.5.2. Quaternary ZrPuCN materials

An analysis was also performed on mixed ZrPuCN materials produced at PSI. The metal composition of the input data was 20, 25 and 30% Pu. During the evaluation it was observed that the application of a 3-D Vegard's law from Equation (3) in the theory section continuously overestimated the lattice parameter compared to the measurement data. On average Vegard's law overestimated the lattice parameter by 0.42%. In Figure 20 it can be seen that in all cases, except for two, Vegard's law overestimated the lattice parameter compared to the measured data. All data used is presented in the tables in paper III [HED 16c].

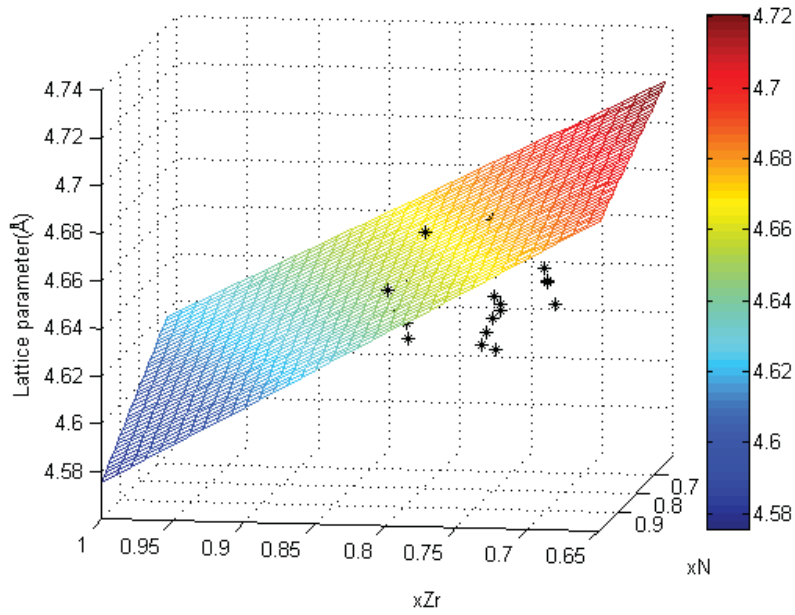


Figure 20. Plane describing 3-D Vegard's law estimations for ZrPuCN and measured data points for ZrPuCN samples. In all cases but two Vegard's law overestimates the lattice parameter compared to the measured samples [HED 16c].

By subtracting the lattice parameter predicted by 3-D Vegard's law from that predicted by an ideal solid solution model a residual is obtained, which is presented in Figure 21.

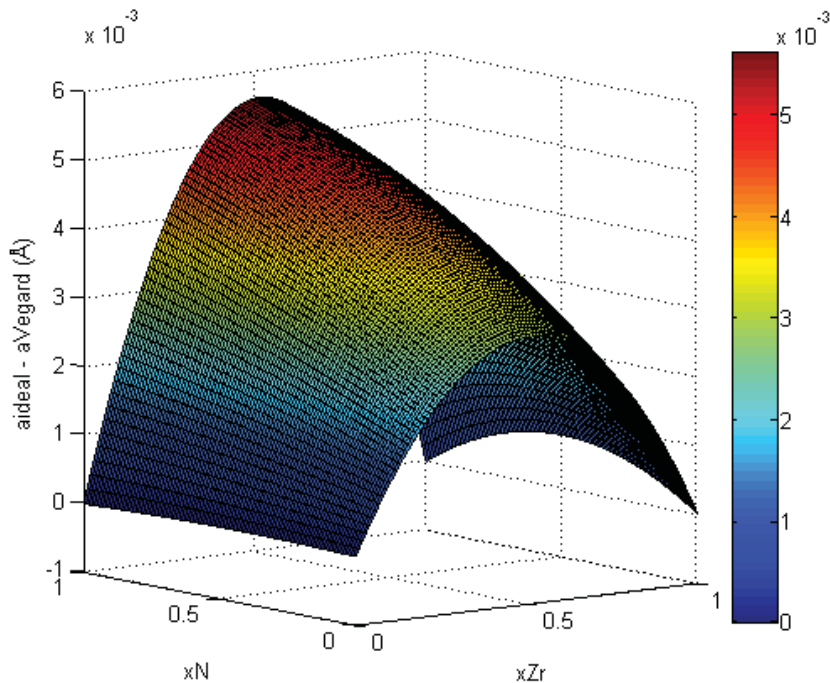


Figure 21. Surface plot of the residual lattice parameter between hypothetical ideal quaternary solid solution of ZrPuCN and 3-D Vegard's law [HED 16c].

From Figure 21 it can be observed that the residual between the hypothetical ideal solid solution of ZrPuCN and 3-D Vegard's law is a positive value for every mixed data point over the entire

composition range. By connecting Figures 20 and 21 the result becomes that 3-D Vegard's law overestimates the lattice parameter compared to actual data measurements and underestimates lattice parameters compared to ideal solid solution. Therefore it is reasonable to draw the conclusion that the actual measured materials have a smaller lattice parameter than would be expected from an ideal solid solution. Mixed ZrPuCN materials can therefore not be considered to be as well described as materials behaving like ideal solid solutions.

If trying to use 3-D Vegard's law to determine nitride content from measured lattice parameters of ZrPuCN materials one finds that the predicted nitride content is higher than the actually measured one. This is not unexpected since it has already been seen that Vegard's law overestimated the lattice parameter compared to the measurements in the data investigated. If a lattice parameter smaller than the value that would be expected by Vegard's law is used as input to calculate nitride composition, Vegard's law will overestimate the presence of the component that has the lower lattice parameter in the mix. Since metallic composition is known in the samples analyzed, the result will be overestimation of nitride because PuN and ZrN have smaller lattice parameters than PuC and ZrC. The averaged overestimate in percent of the nitride content is presented in Table 4. The table presents the data as a percent of the measured nitride content and not as percentage points, i.e. if the measured nitride content is 20% Vegard's law estimates about 25% and not 45%, for example.

Table 4. Averaged overestimate by Vegard's law in percent of measured nitride content.

Material matrix	Average overestimate (%)	Standard deviation (%)	Number of data points
ZrPuCN	24.4	22.9	32
ZrPuCN data points with O < 1 wt% content	11.7	11.9	10
ZrPuCN data points with O < 1 wt% content and Pu fraction = 0.2	5.3	3.1	6
ZrPuCN data points with O < 1 wt% content and Pu fraction = 0.3	27.6	8.1	3

The standard deviation of the entire dataset for ZrPuCN measurements becomes very large. Further analysis can be performed by removing data points where the oxygen content is above 1 wt%. The results indicate that the 3-Vegard's law estimates are much closer to the measurement data. It therefore appears that any residual oxygen in the quaternary ZrPuCN system has a stronger effect compared to the ternary ZrCN system. If further narrowing down the data set to the 20% and 30% plutonium fraction and O < 1 wt% samples the average overestimate is 5.3% and 27.6%, respectively. A similar approach for the $Zr_{0.75}Pu_{0.25}CN$ is however futile since the dataset becomes reduced to a single data point when the data points containing O > 1 wt% have been filtered out. Due to the small sets of data it is difficult to draw any certain conclusions about the magnitude of the effect of increasing Pu content in the material, but there seems to be an effect on the quality of estimates by Vegard's law when the fraction of Pu in the material increases that cannot be neglected.

5.6. Pellet formation and sintering

5.6.1. Conventional pressing and sintering of Zr-based microspheres

When using compaction pressures up to 1200 MPa, green pellets could be produced, both with and without blackberry structure. Why any certain compaction resulted with or without blackberry structure was not completely clear. The formation of blackberry structure is probably strongly connected to the thermal treatment cycle, but there could be different outcomes regarding presence of blackberry structure during pressing even in nitrided microspheres where no clear difference in surface fracturing could be observed.

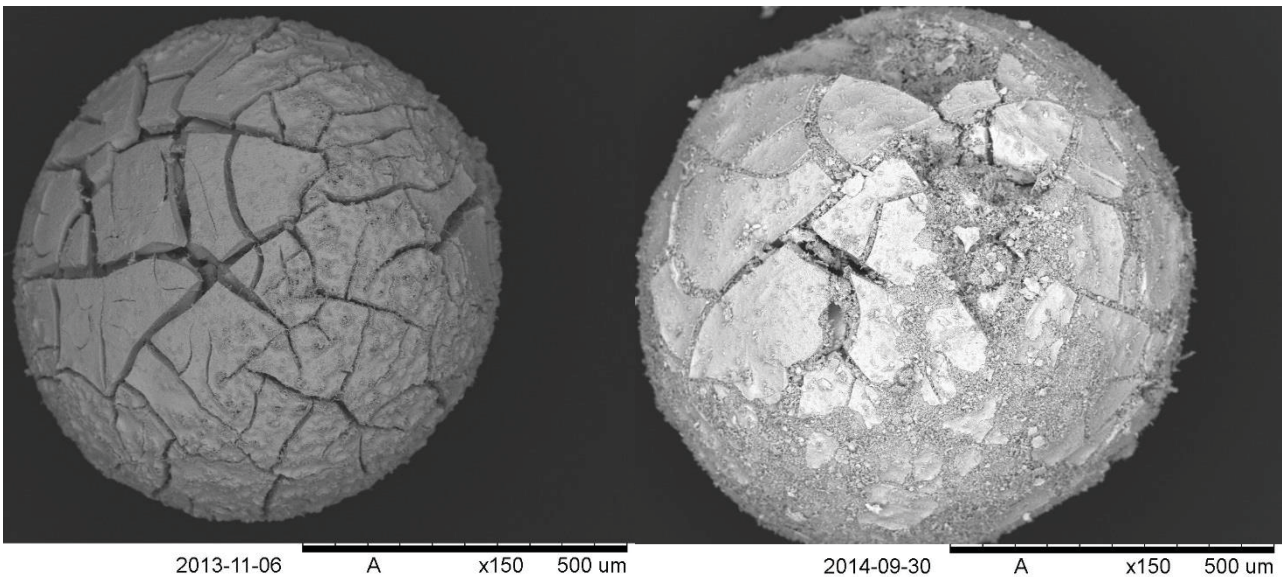


Figure 22. On the left: a microsphere from a batch with blackberry structure in the pellet when compacting using a pressure of 1200 MPa. On the right: a microsphere from a batch that formed a pellet without presence of blackberry structure when compacted using a pressure of 600 MPa. Both microspheres were judged to be roughly representative of the microspheres present in the respective batch.

The main difference between the materials was that the reaction time during carbothermal reduction and decarburization was different. The batch represented by the microsphere on the left was thermally treated at 1400 °C for 8 hours during carbothermal reduction, followed by decarburization at 1700 °C for 8 hours. The image on the right is from a microsphere batch that was heat treated at 1400 °C for 4 hours and at 1700 °C for 4 hours. It is thus reasonable to believe that the difference in compaction behavior is a result of a larger degree of internal sintering in the microspheres heat treated for a longer time. If the intention is to press pellets of the nitride microspheres it is therefore desirable to be able to minimize the time and/or temperature during the decarburization step.

Sintering performed in N₂ gas resulted in a more or less strong discoloration of the surface of the pellets exposed towards the furnace atmosphere during the sintering process.

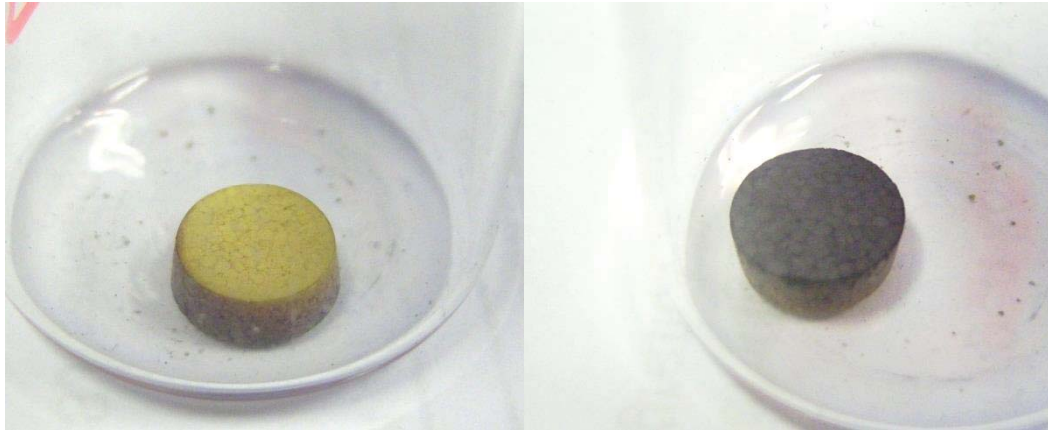


Figure 23. ZrN pellet sintered in N₂ gas at 2000 °C for 5 hours.

Sintering at 2000 °C produced a discoloration on the top surface that was very dark red, almost approaching black. When lowering the sintering temperature by 200 °C the discoloration did not disappear but was strongly reduced. The sintering of the pellet was strongly influenced.

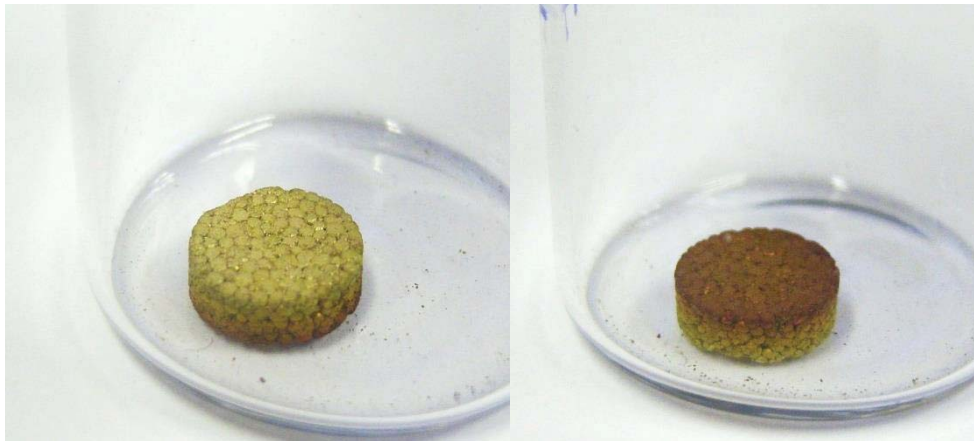


Figure 24. ZrN pellet sintered in N₂ gas at 1800 °C for 5 hours.

As can be seen in Figure 24 the blackberry structure of the pellet is very pronounced, even after sintering, compared to the pellet in Figure 23 where the blackberry structure is only just observable by eye. It was believed that this discoloration was caused by transportation of carbon material from the graphite heating element onto the top surface, potentially promoting carbide formation on the exposed surface. XRD measurements on both sides of the pellet in Figure 23 and application of Vegard's law estimated that the yellowish side of the pellet had a composition of Zr(N_{0.82}C_{0.18}) while the reddish side was estimated to be Zr(N_{0.45}C_{0.55}), and so the carbon transport theory seemed credible.

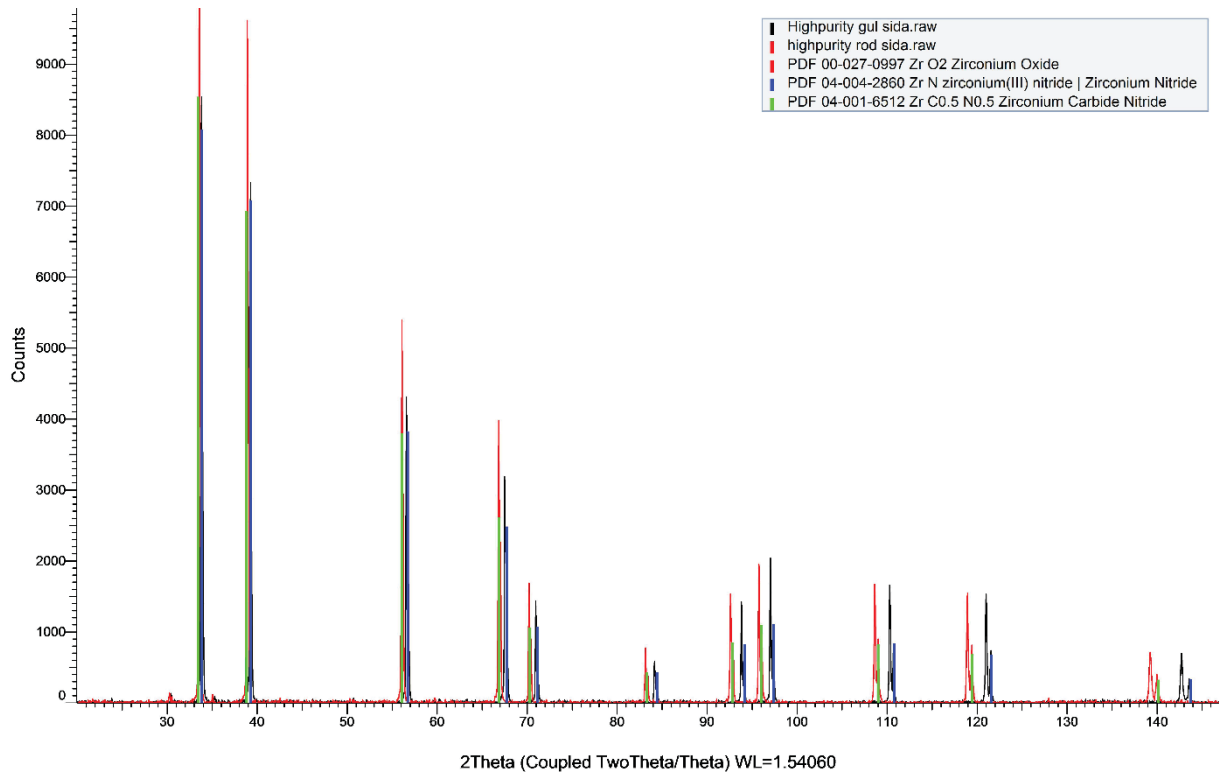


Figure 25. Evaluated XRD spectra of both sides of the pellet sintered in N_2 at 2000 °C. The black diffraction peaks are from the yellowish side of the pellet and the red diffraction peaks are from measurement of the reddish pellet side.

Splitting the pellets along the axial direction allowed investigation of how far the reddish phase had propagated into the pellets.

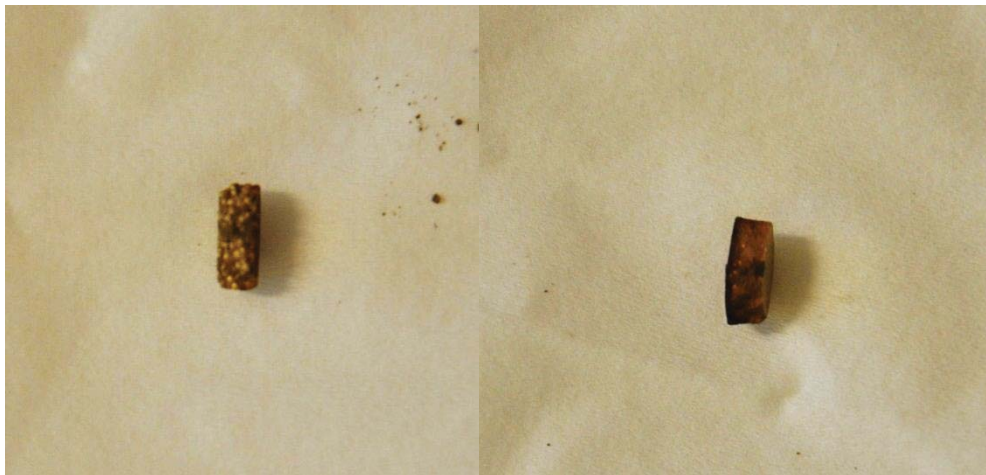


Figure 26. Pictures of cross sections of the pellets sintered at 1800 and 2000 °C.

The reddish phase had penetrated further into the pellet in the case of sintering at 2000 °C and the layer was estimated to be a little less than one mm thick. The reason for observing the propagation of the reddish phase by the naked eye instead of by SEM was that no differences between the phases could be observed using SEM characterization.

Three conventionally pressed and sintered pellets are presented for illustration of sintering behavior of ZrN microspheres. The pelletization characteristics for the three pellets are presented in Table 5.

Table 5. Pelletization characteristics of conventionally sintered pellets.

Sample	Compaction pressure (MPa)	Sintering temperature (°C)	Sintering atmosphere
Sintered 2000 °C	1200	2000	N ₂
Sintered 1800 °C	1200	1800	N ₂
Sintered 1700 °C	600	1700	Ar

SEM characterization was performed and revealed that there was still a considerable amount of blackberry structure observable at the pellet surface of the pellet sintered at 2000 °C.

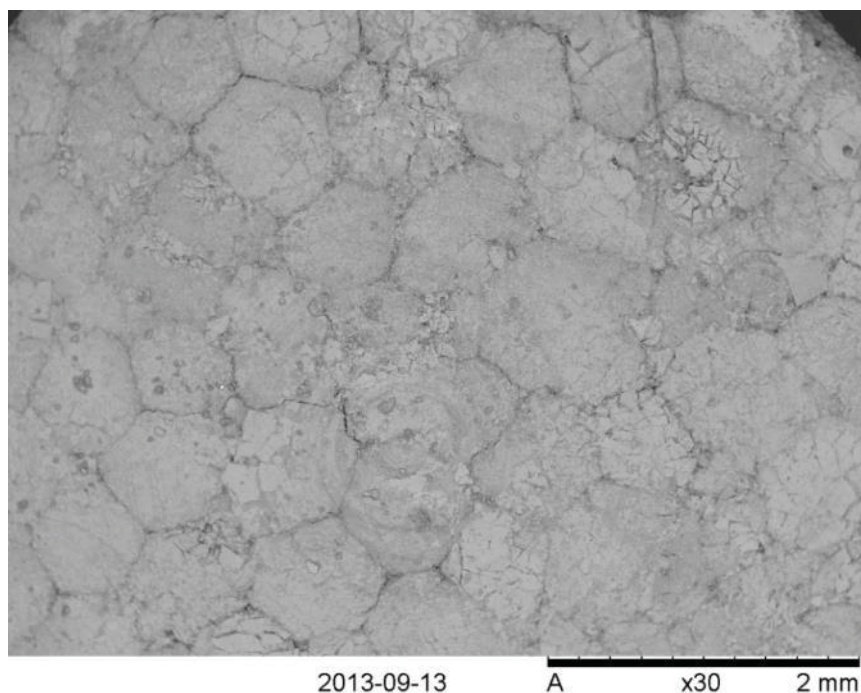
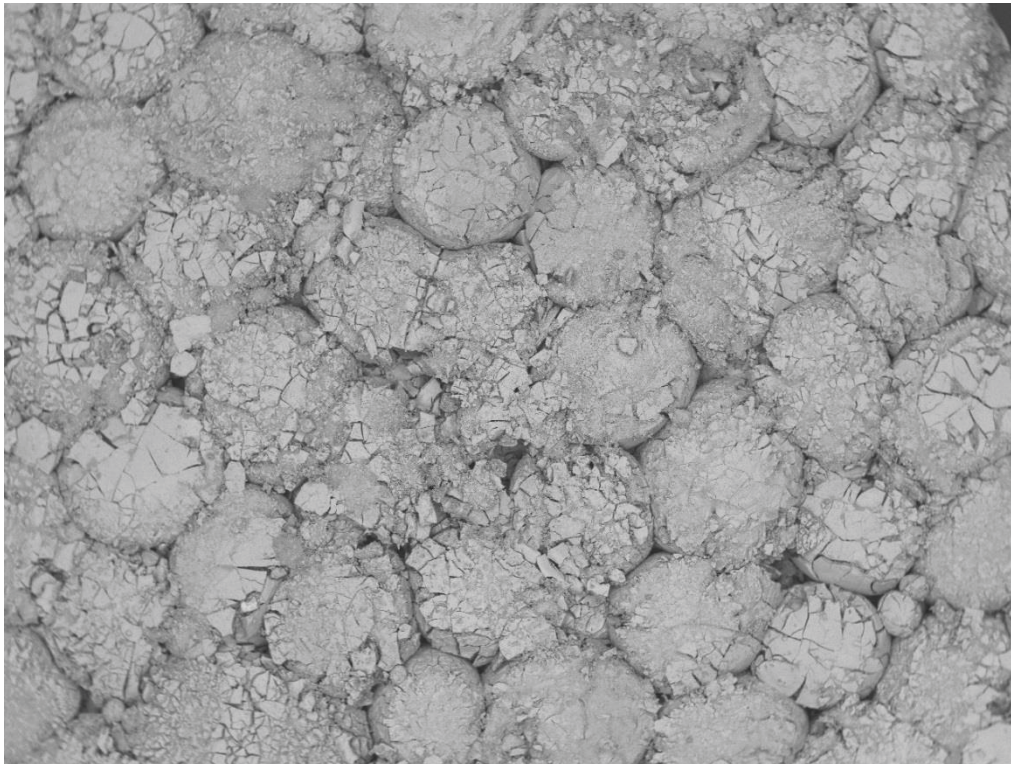


Figure 27. SEM image of the surface of the pellet sintered at 2000 °C.

From Figure 27 it can be seen that neck growth has occurred between the microspheres, showing that sintering has indeed occurred but an apparent blackberry structure still remains.

In the sample sintered at 1800 °C very little sintering occurred.



2014-01-14 A x30 2 mm

Figure 28. SEM image of the surface sintered at 1800 °C.

At some spots where there has been contact between the microspheres some degree of necking has occurred but generally the sample can't really be thought of as having sintered to any larger degree during heat treatment.

The pellets were also characterized using SEM after being split to study their cross sections.



2016-05-30 A D9,1 x30 2 mm 2016-05-30 A SD8,4 x30 2 mm

Figure 29. SEM images of cross sections of the pellets sintered at 1800 and 2000 °C, respectively.

In the pellet sintered at 1800 °C it could again be observed that the microspheres did not disintegrate properly during pressing and retained their individual shape also after sintering. In the pellet sintered at 2000 °C no clear traces of blackberry structure could be observed on the inside of the pellet. This could be attributed to more extensive crushing of the microspheres in this pellet since no unsintered pellets were examined using SEM. From the appearance of the surfaces, however, it seems unlikely that complete disintegration of microspheres would have occurred inside the pellet. It therefore seems that the additional 200 °C had a strong impact on the sintering behavior. From Figure 29 it also can be seen that it was not possible to distinguish between the different colored phases using SEM.

Pellets where no blackberry structure could be detected were also produced. Microspheres from batches that were heat treated for 5 hours at 1700 °C during decarburization could be pressed into pellets where the microspheres seemed to be completely crushed during pressing.

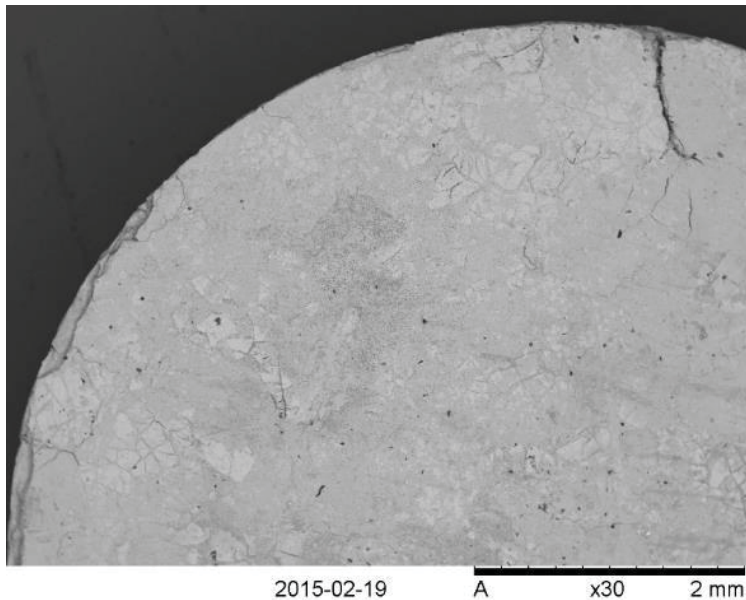


Figure 30. SEM image of a pellet produced by 600 MPa compaction pressure after being sintered in Ar atmosphere for 4 hours at 1700 °C [HED 16b].

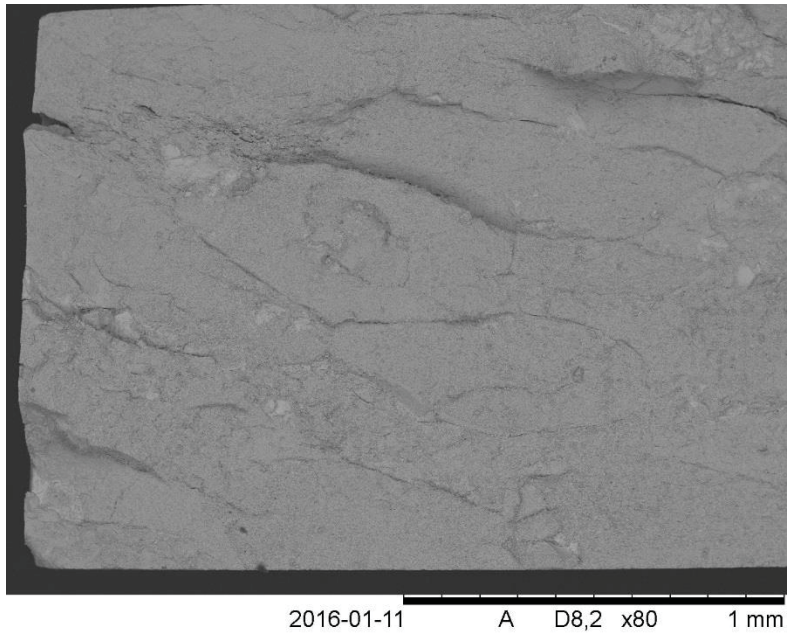


Figure 31. Cross section of the pellet sintered at 1700 °C in Ar atmosphere.

Neither on the surface of the produced pellet nor in the cross section could any remains of uncrushed microspheres be detected in the sintered pellet. Also no direct discoloration of the pellet surface could be detected. This was believed to be a result of further lowering the sintering temperature rather than the change of reaction atmosphere since no surface discoloration was observed on the surface of microspheres during heat treatment at 1700 °C in an environment containing N₂.

The grain structure of the conventionally sintered pellets was also investigated by SEM. In general, as expected, the overall grain size seemed to increase with increasing sintering temperature, but all pellets contained fairly large amounts of open porosity. The pores observed in the pellets ranged from small cracks down to pores on the μm scale.

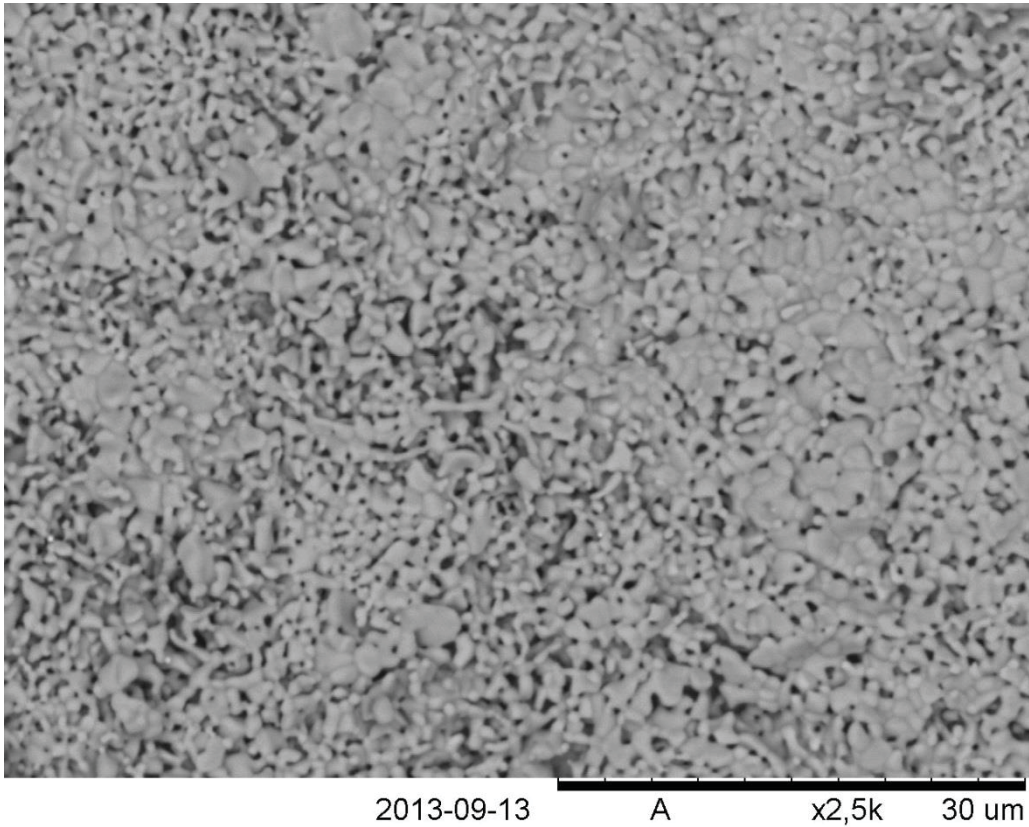


Figure 32. Microstructure of the pellet sintered at 2000 °C.

Sintering at 2000 °C seemed, as would generally be expected, to result in the largest grains. There was however no large difference in grain size between sintering at 2000 °C compared to 1800 °C. For sintering at 2000 °C the final grains ranged from about 1 μm up to about 3 μm in size, while for sintering at 1800 °C the final grain size was predominantly about 1 μm in size with far fewer grains in the 2-3 μm size region.

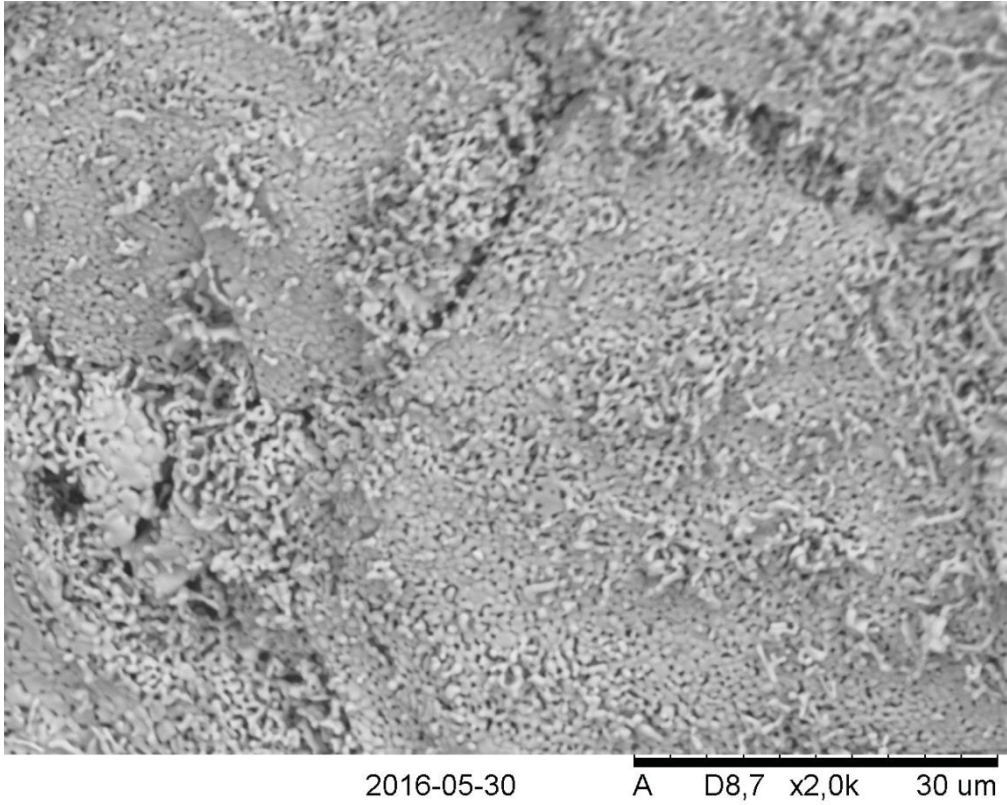


Figure 33. Microstructure of a pellet sintered at 1800 °C.

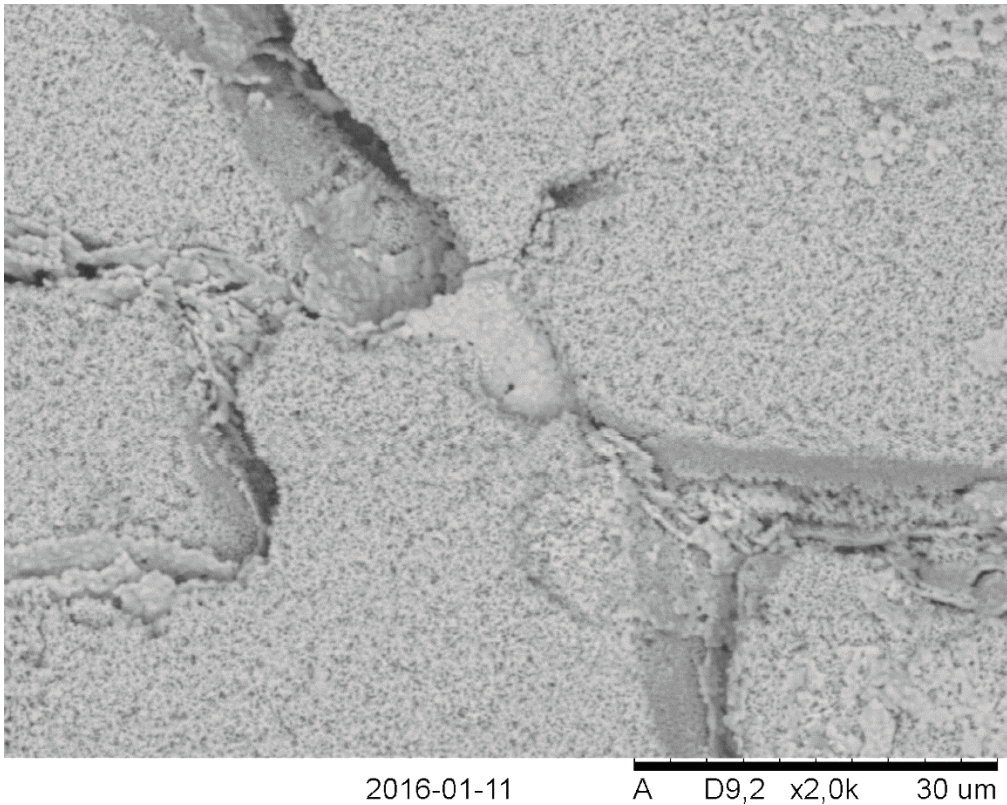


Figure 34. Microstructure of a pellet sintered at 1700 °C.

Sintering at 1700 °C resulted in the smallest grain sizes in the observed pellets. This is not really surprising, since this pellet was sintered at lower temperature than the other pellets investigated.

Measured densities in the pellets after sintering are presented in Table 6.

Table 6. Estimated compositions and final densities of the investigated pellets.

Sample	Lattice parameter (Å) (s.d)	Estimated composition	Density (g/cm ³)	% of theoretical density
Sintered at 2000 °C	4.598 (± 0.0005)	Zr(N _{0.82} C _{0.18})	3.88	54.2
Sintered at 1800 °C	4.592 (±0.011)	Zr(N _{0.86} C _{0.14})	2.33	32.5
Sintered at 1700 °C	4.622 (±0.003)	Zr(N _{0.62} C _{0.38})	3.69	52.5

An interesting observation is that sintering in 1700 °C in Ar produces a final pellet that is about equally dense as the pellet sintered in N₂ at 2000 °C. Sintering in Ar may increase the atomic mobility in the pellet by the formation of slightly sub-stoichiometric zirconium nitride, making the sintering more effective. The more likely explanation for obtaining similar densities despite the large temperature difference during sintering could instead be the ability to effectively crush the microspheres when pressing the pellet sintered at 1700 °C. The pellet sintered at 2000 °C possessed very pronounced blackberry structure before sintering, indicating that the pressing step produced a green pellet of low density, while the newly pressed pellet that was sintered at 1700 °C did not show any trace of blackberry structure at all, indicating better crushed microspheres and higher green pellet density. Actual density measurements of the green pellets was however not performed due to what seemed to be low mechanical cohesive strength. Regardless of which of the presented pellets is considered the final density reached is however quite low. To be able to sinter ZrN-based compacts from microspheres by conventional sintering it seems that both very high pressures and sintering temperatures would be required. Sintering in Ar may be more efficient compared to sintering in N₂ but there can be practical difficulties regarding equipment when using Ar as the sintering atmosphere at too high temperatures, since Ar may start to ionize when temperatures start to approach around 2000 °C. An alternative to Ar may be sintering in a vacuum, which should also promote the formation of sub-stoichiometric nitride. When producing actual nuclear fuel it can however be desirable to keep the sintering temperature as low as possible, since the actinide nitrides have higher vapor pressures compared to ZrN. Sintering additives could be considered, but one difficulty when working with gelation-based processes is that the sintering aid must be added before gelation of the microspheres if it is to be well dispersed in the material when sintering. This also requires the sintering additive to remain in the microspheres during nitride formation, while at the same time not sintering the microspheres during decarburization, as that diminishes the possibilities of crushing the microspheres during pellet compaction. Another potential solution to increase final densities would be to choose another pellet fabrication route than cold pressing and sintering.

5.6.2. Spark plasma sintering of Zr-based microspheres

Spark plasma sintering was performed to investigate if it was possible to press cohesive pellets directly from nitride microspheres. SPS was performed at 1700 °C and the pellet was conventionally pressed and sintered at 1700 °C as already described and was used as a reference for conventional sintering at the same temperature. The composition of both the microspheres

and the final pellets were estimated using X-ray diffraction and the total carbon content in the final pellets was measured by combustion in O₂. The results of the composition analyses are summarized in Table 7.

Table 7. Lattice parameter and carbon content measured in the microspheres and pellets produced. The - annotation indicates not measured.

Sample	Lattice parameter (Å)	Standard deviation (Å)	Carbon content (wt%)	Standard deviation (wt%)
Microsphere batch 1	4.637	$3.37 \cdot 10^{-3}$	-	-
Microsphere batch 2	4.635	$6.68 \cdot 10^{-4}$	-	-
Microsphere batch 3	4.631	$4.33 \cdot 10^{-3}$	-	-
Microsphere batch 4	4.608	$4.07 \cdot 10^{-3}$	-	-
SPS1	4.634	$1.23 \cdot 10^{-3}$	6.05	0.31
SPS2	4.631	$5.88 \cdot 10^{-3}$	6.14	0.09
SPS3	4.638	$4.83 \cdot 10^{-3}$	9.68	1.05
SPS4	4.643	$3.97 \cdot 10^{-3}$	9.22	1.42
SPS5	4.642	$1.83 \cdot 10^{-3}$	4.32	0.17
SPS6	4.607	$3.18 \cdot 10^{-3}$	2.09	0.17
Conventionally sintered	4.622	$2.54 \cdot 10^{-3}$	4.39	0.13

Vegard's law was used for estimating the composition as solid solution carbonitride for both microspheres and final produced pellets. For the sintered pellets carbide content was also calculated using the assumption that all carbon detected was present as carbide (Table 8).

Table 8. Sample composition estimated by Vegard's law and carbon measurements. In microsphere batches 3 and 4 a molybdenum lid partially covering the molybdenum crucible was used during carbothermal reduction.

Sample designation	Composition Vegard's law	Composition by carbon content	Used for pellet
Microsphere batch 1	Zr(N _{0.49} C _{0.51})	-	SPS1, SPS2
Microsphere batch 2	Zr(N _{0.51} C _{0.49})	-	SPS3, SPS4
Microsphere batch 3	Zr(N _{0.55} C _{0.45})	-	SPS5, Conventionally sintered
Microsphere batch 4	Zr(N _{0.83} C _{0.27})	-	SPS6
SPS1	Zr(N _{0.52} C _{0.48})	Zr(N _{0.47} C _{0.53})	-
SPS2	Zr(N _{0.55} C _{0.45})	Zr(N _{0.47} C _{0.53})	-
SPS3	Zr(N _{0.49} C _{0.51})	Zr(N _{0.17} C _{0.83})	-
SPS4	Zr(N _{0.45} C _{0.55})	Zr(N _{0.20} C _{0.80})	-
SPS5	Zr(N _{0.46} C _{0.54})	Zr(N _{0.62} C _{0.38})	-
SPS6	Zr(N _{0.74} C _{0.26})	Zr(N _{0.82} C _{0.18})	-
Conventionally sintered	Zr(N _{0.62} C _{0.38})	Zr(N _{0.62} C _{0.38})	-

Overall the composition estimated by the different methods agrees fairly well. There is however some deviance between Vegard's law and carbon content measurements in pellets SPS3 and SPS4. Both of these pellets were produced from the same microsphere batch and the carbon measurements indicate a higher presence of carbide than Vegard's law does. This is potentially caused by residual elemental carbon in the microsphere batch causing the carbon measurement method to overestimate the carbide content.

In all cases of pellet production by SPS it was possible to form a cohesive pellet from the microspheres. During SPS the pressing force, sintering temperature and densification behavior was recorded. Figure 35 shows a comparison of the densification properties between one sintering experiment in Ar atmosphere (SPS6) and the sintering performed in N₂ atmosphere (SPS2).

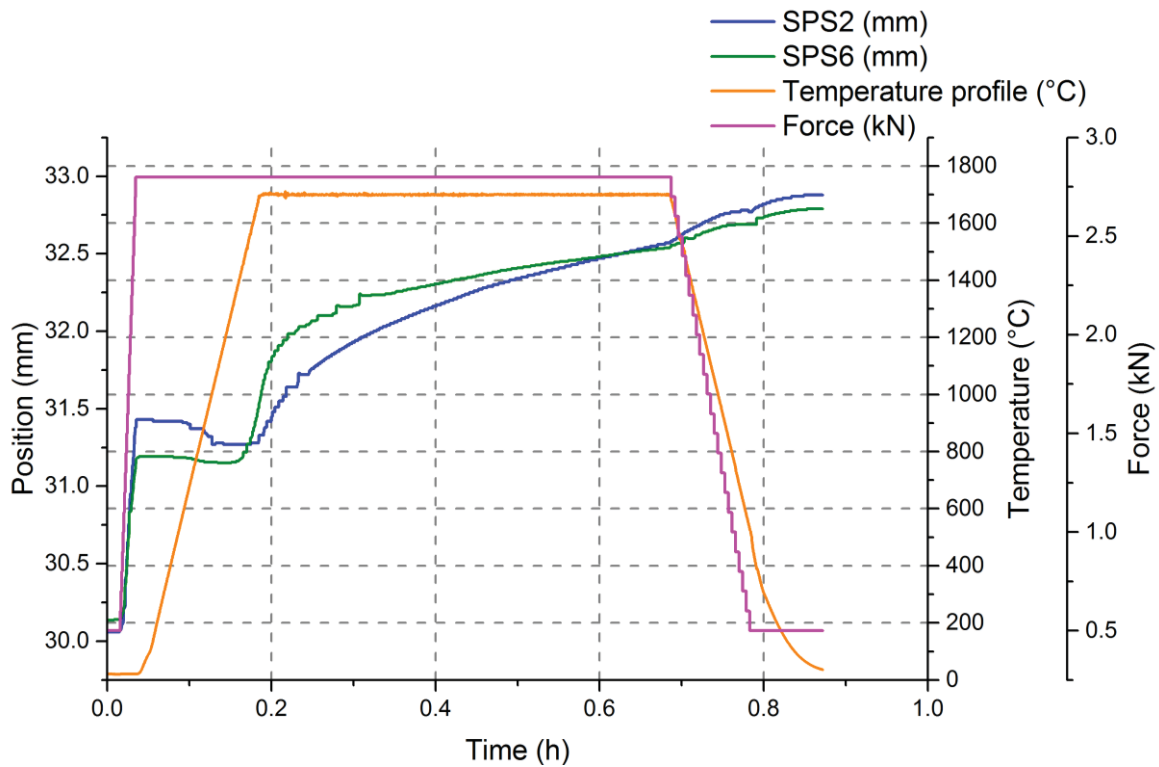


Figure 35. Densification behavior during spark plasma sintering. The plots compare the compaction behavior between sample SPS2 sintered in N_2 and sample SPS6 sintered in Ar, together with the applied temperature and compaction force profiles during sintering [HED 16b].

The same compaction pressure and temperature profile was used during both sintering experiments. The densification behavior during SPS starts with mechanical compaction at room temperature of the sample. In Figure 35 this part of the process can be observed as a steep increase in the position measurements. Densification of the sample is therefore measured by an increase in position measurement. The initial material compaction is followed by a decrease in the measured position. This is caused by swelling of the sample due to thermal expansion. The point where sintering starts to be observed is when the slope of the sintering profiles in Figure 35 equal 0. At this point the densification due to sintering equals the thermal swelling caused by the temperature increase. When the slope of the position measurements become positive the sintering is progressing faster than thermal swelling and when the set sintering temperature is reached all position change is caused by sintering, since no thermal swelling occurs once the temperature of the system becomes constant. Sintering became observable at about 1100-1200°C when using Ar as the sintering atmosphere, while sintering in N_2 became observable at about 1600°C. Table 9 presents the densities achieved in the produced pellets.

Table 9. Sintering data and density of the pellets produced. The X-ray diffraction data was used for composition, and thus estimation, of theoretical density.

Pellet designation	Pellet diameter (mm)	Composition pellets	Sintering atmosphere	Dwell time (min)	Density (g/cm³)	% of TD
SPS1	6	Zr(N _{0.52} C _{0.48})	Ar	5	3.59	51.5
SPS2	6	Zr(N _{0.55} C _{0.45})	N ₂	30	3.72	53.3
SPS3	6	Zr(N _{0.49} C _{0.51})	Ar	30	4.14	59.6
SPS4	10	Zr(N _{0.45} C _{0.55})	Ar	30	4.32	62.6
SPS5	6	Zr(N _{0.46} C _{0.54})	Ar	30	5.74	82.9
SPS6	6	Zr(N _{0.74} C _{0.26})	Ar	30	6.20	87.2
Conventionally sintered	9	Zr(N _{0.62} C _{0.38})	Ar	300	3.69	52.5

In all cases where SPS has been performed for 30 minutes the final densities are closer to their theoretical densities compared to the pellet conventionally sintered, even if there was very little difference between SPS in N₂ atmosphere and conventional sintering. It is notable that the sample sintered in N₂ has significantly lower density compared to the other pellets sintered for 30 minutes by SPS. Even 5 minutes of spark plasma sintering in Ar produced pellets of comparable density to sintering in N₂ for 30 minutes. As in the case of conventional sintering in either N₂ or Ar the formation of a slightly sub-stoichiometric ZrN_{1-x-y}C_x carbonitride was observed, where y denotes the nitrogen vacancies, with enhanced atomic mobility due to the vacancies formed in the structure. This possibility is also a reasonable explanation for why the sample SPS6, which contained the highest nitride content, was the sample that was sintered to the highest density.

A discrete uneven surface discoloration, looking like a blackberry structure could be observed on the pellets produced by SPS by visual inspection. SEM characterization of the sintered pellets did however not show any signs of blackberry structure when performed on the surface of unpolished pellets. After polishing had been performed faint tendencies to blackberry structure could be observed on most pellets using SEM.

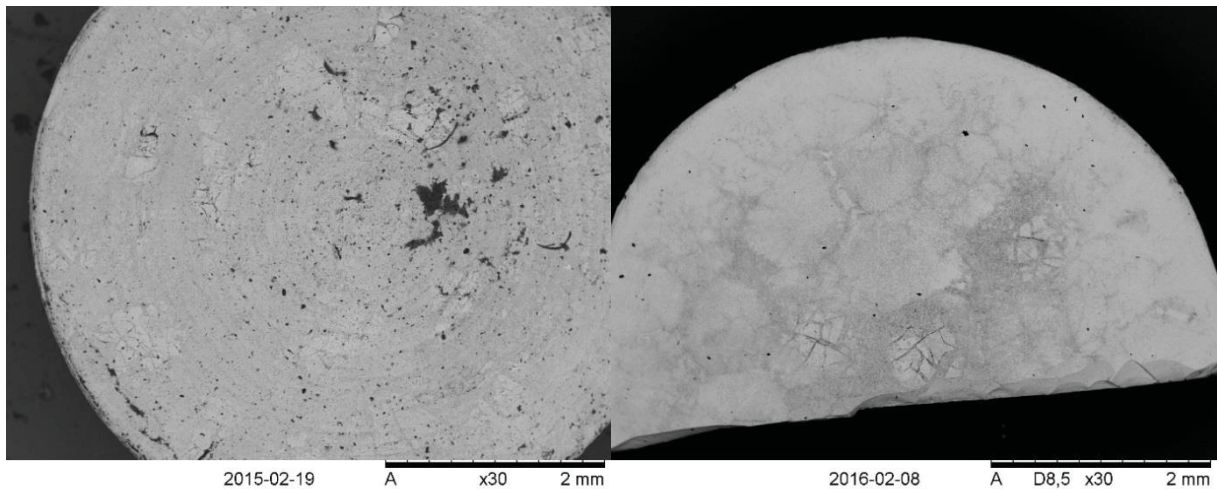


Figure 36. SEM images of two of the SPS-produced pellets. On the left an unpolished pellet where no blackberry structure could be observed by SEM. On the right the same pellet after polishing, where a faint circular pattern could be observed during imaging [HED 16b].

SEM characterization of pellets sintered by the SPS technique revealed that no appreciable degree of grain growth occurred during sintering, as shown in Figure 37. This was expected, since the short sintering times used in SPS should not allow extensive grain growth to be able to occur.

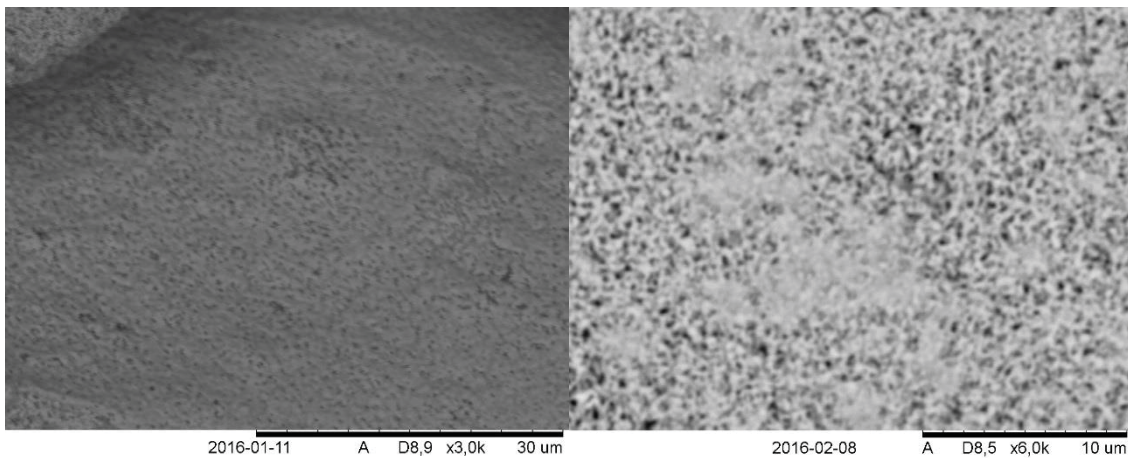


Figure 37. SEM imaging of the spark plasma sintered pellets SPS1 and SPS6 after polishing. The grains making up the structure are generally less than 1 μm in size. The same was true for all other pellets sintered by SPS [HED 16b].

Computer tomography was used to try to detect macropores and density gradients in the produced pellets. Blackberry structure could be detected in several pellets by computer tomography. No strong tendency for density gradients could be observed over the radial direction in any of the pellets. The computer tomography could not detect any pores in the material, however, suggesting that all porosity present in the pellets was below a size of about 50 μm , which was the detectable pore size limit in the tomography measurements.

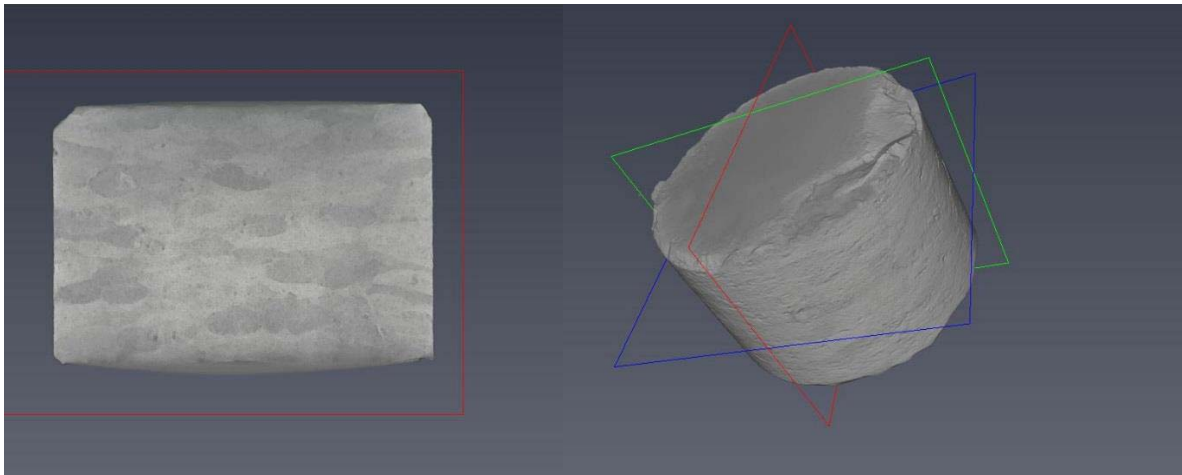


Figure 38. Tomography imaging of pellet SPS1. The remains of deformed microspheres can be observed in the image on the left [HED 16b].

As shown in Figure 38, residual structure of the microspheres could be detected by computer tomography in the pellets as faint structures of partially deformed microspheres.

By studying histograms of the gray level distribution in measured pellets, indications of density gradients in the samples can be evaluated. The histogram is computed by counting the frequency of occurrence of voxels within a specific gray level range. If a pellet possess uniform density distribution down to the size of the voxels used for producing the tomography image, the histogram of the pellet would be expected to have the shape of a single peak. The presence of two distinctly different density areas would on the other hand be expected to show double peaks in the histogram. Noise is always present and manifests itself as tails on both sides of the peak. These tails could be interpreted as slight density variations or, in extreme cases, could mask the contribution of a second peak. In order to minimize the noise contribution the 3D data set was filtered with a 3x3 median filter. An additional software correction was then carried out in order to minimize the beam hardening effect caused by the higher attenuation of low energy photons as they travel through the sample. Beam hardening results in apparent higher density regions at the sample edges and must be corrected for or minimized.

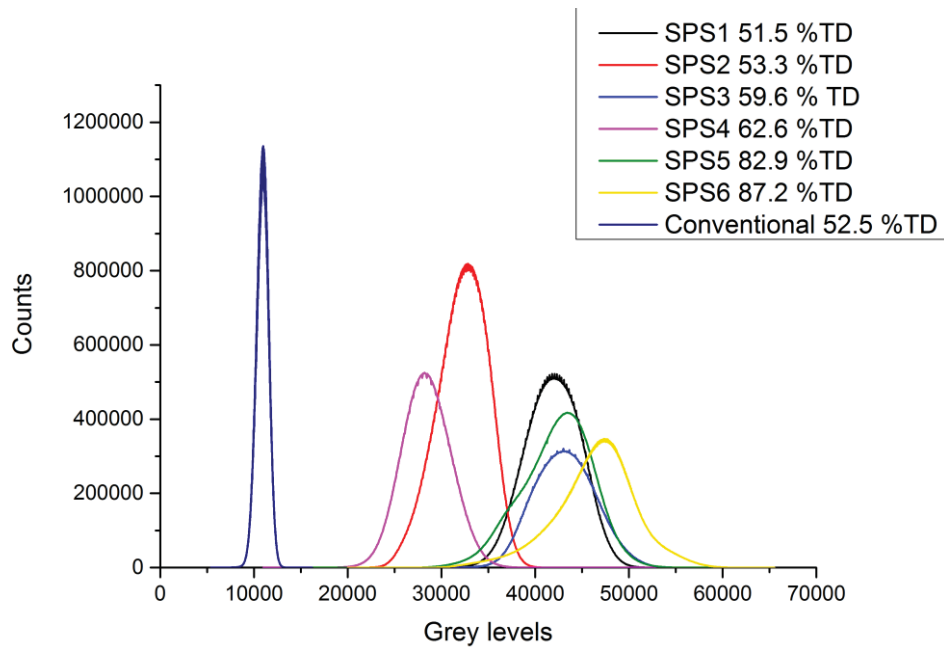


Figure 39. Grey level distribution within the produced pellets [HED 16b].

Figure 39 shows the gray level distribution for all of the 7 samples; 6 SPS samples and the conventionally sintered reference. When looking at Figure 39 it can be observed that the conventionally sintered pellet showed by far the narrowest grey level distribution. This could be expected, as the conventionally sintered pellet was pressed by applying the highest pressure, most likely resulting in a more effective crushing of microspheres compared to the SPS pellets before sintering. In pellets SPS5 and SPS6 wider distribution profiles can be observed compared to the other SPS-produced pellets. These are also the densest pellets. The likely explanation for this is that higher density causes a larger degree of beam hardening during measurement. Quantification of the noise and beam hardening contributions is difficult without a homogenous standard of the same composition for each pellet. The resulting single peak distributions, however, provide a strong indication for relatively homogenous samples with minimum density gradients.

5.6.3. Pellet formation of mixed Zr/Pu microspheres

The pressed and sintered pellets were surface characterized using SEM. No residual microsphere structure could be observed in the pellets. Again these were microsphere treated for decarburization for 4 hours, but the temperature used in this case was 1650 °C. The result was microspheres that could readily be crushed during pellet fabrication, indicating that shorter decarburization times are beneficial for the pelletization properties of the microspheres.

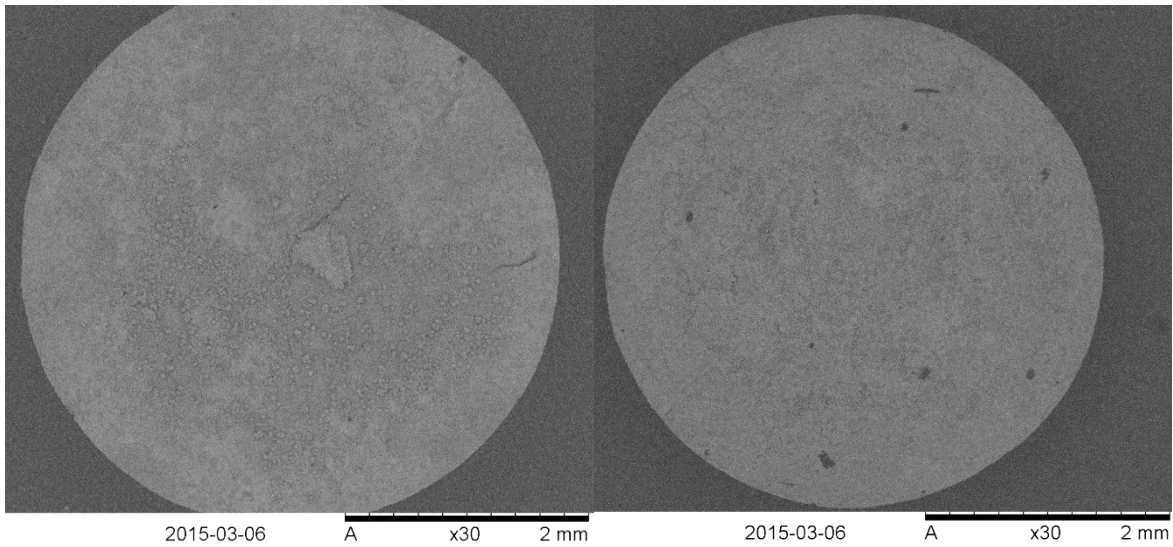


Figure 40. On the left: SEM image of a pellet sintered in N₂ atmosphere. On the right: SEM image of a pellet sintered in Ar atmosphere [HED 16a].

The plutonium present in the material caused a strong disturbance of the signal obtained from the SEM, making it difficult to obtain high resolution images of the microstructures of the pellets. In the case of the pellet sintered in N₂ it was not possible to obtain a focused image clear enough for any determination of the grain size to be made. This was however possible when imaging the pellet sintered in Ar and it was observed that the grain size of the pellets making up the structure was about 2-3 μm .

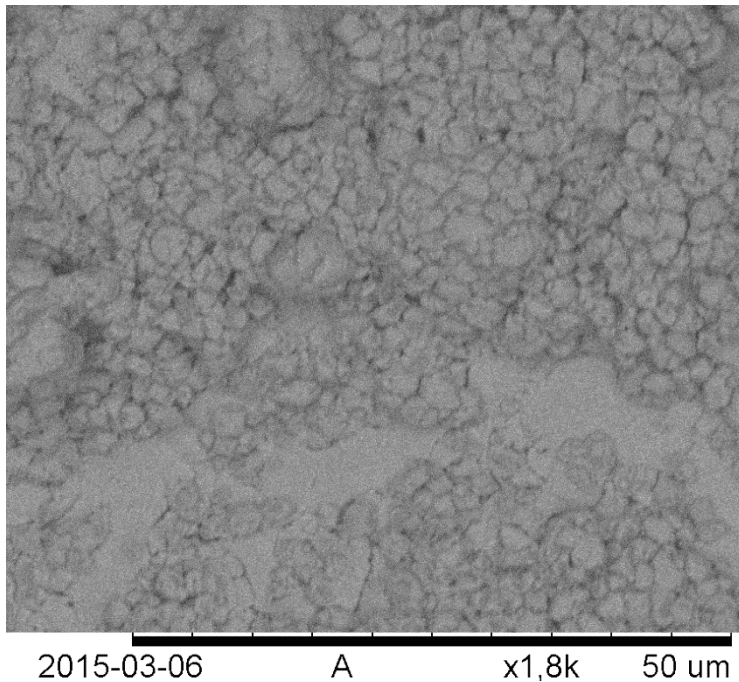


Figure 41. Image of the microstructure in the pellet sintered in Ar. Some larger grains can be observed but on average the overall predominant grain size in the material was estimated to be characteristically around 2-3 μm [HED 16a].

EDX was performed on the pellet surfaces and it was observed that the pellet sintered in N₂ contained areas with increased amounts of Pu on the surface. The increase in Pu at the pellet surface could be an explanation for why imaging of the pellet sintered in N₂ was subjected to larger noise in the signal compared to the pellet sintered in Ar. In the EDX measurements only Zr and Pu were taken into account during the measurements.

Table 10. EDX data sampled on pellet surfaces sintered in Ar/N₂. The number index indicates measurements on arbitrarily chosen points of the sample surfaces. The line notation (-) in the uncertainty column indicates that no uncertainty could be estimated by the EDX software.

Sample	Zr (at %)	Pu (at %)	Uncertainty Zr/Pu (%)
Sintered Ar 1	53.9	46.1	1.1 / 2
Sintered Ar 2	68.8	35.2	1.2 / 1.4
Sintered Ar 3	67.7	32.3	1.3 / 1.4
Sintered Ar 4	69.0	31.0	1.3 / 1.3
Sintered N ₂ 1	0.01	99.99	- / 0.6
Sintered N ₂ 2	34.4	65.6	0.2 / 0.6
Sintered N ₂ 3	0.02	99.98	- / 0.5
Sintered N ₂ 4	0.01	99.99	- / 0.3

Increased levels of Pu on the pellet surface could potentially be explained by the higher vapor pressure and mobility of PuN compared to ZrN [OLS 64, ERO 76], resulting in increased plutonium amounts on the pellet surface.

Formation of solid solution in the sintered pellets was measured using X-ray diffraction.

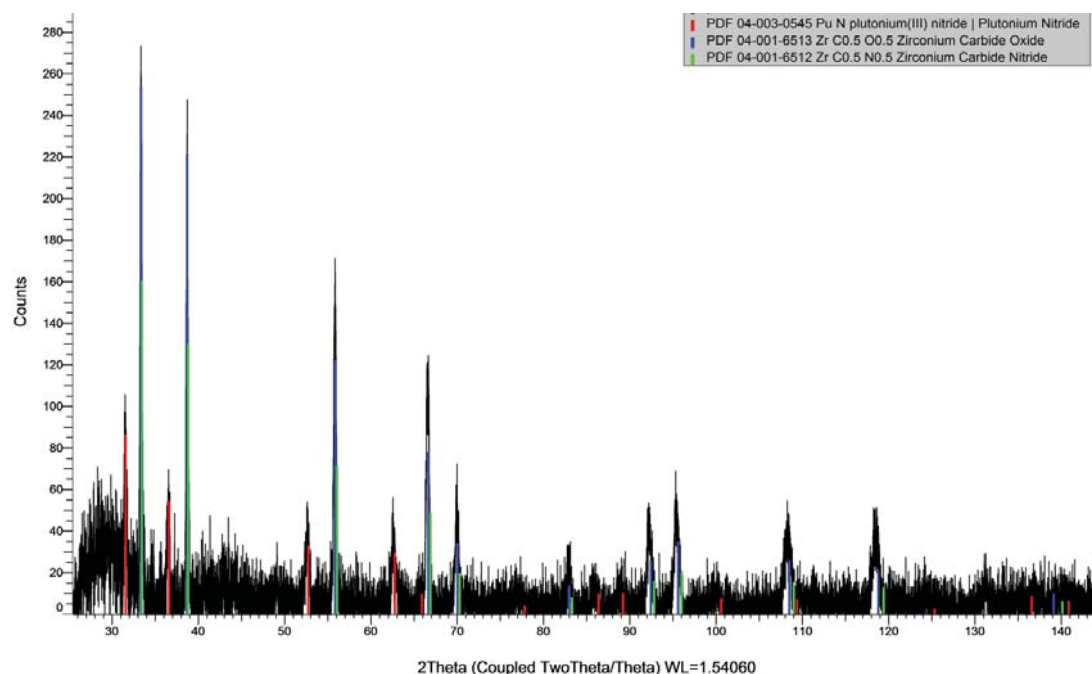


Figure 42. X-ray diffraction spectrum of the pellet sintered in Ar. Two distinctly different structures could be identified in the pellet [HED 16a].

Sintering in Ar atmosphere did not produce solid solution. Instead two different structures, both of the FCC-NaCl type, could be identified within the pellet, which is what would be expected to observe in a phase separated PuN/ZrN material no matter the carbide level present in any of

the nitride phases. Exact determination of the different phase compositions was not possible from the XRD data since PuN, PuC, ZrN and ZrC all crystallize in the same structure and several varying material compositions of type $\text{Pu}_w\text{Zr}_x\text{N}_y\text{C}_z$ can exist that produces identical or close to identical diffraction spectra. Due to this the possibility of inter-diffusion of Pu and Zr between the different phases to some degree cannot be excluded from the diffraction data. By using the assumption that Zr and Pu are mainly distributed into separate phases it is possible to match the data against database references. The limited sample size make several expected high angle peaks indistinguishable from the background noise, it does however seem like one set of peaks can be matched against PuN or PuC. The peak positions of pure PuN and PuC are very close at low angles, making it uncertain to draw any conclusions regarding purity, but PuN seems the better fit of the two, although a mixed Pu(N,C) solid solution is a more probable estimation. The second set of diffraction peaks can be roughly explained by $\text{Zr}(\text{N}_{0.5}\text{C}_{0.5})$ or $\text{Zr}(\text{C}_{0.5}\text{O}_{0.5})$. The use of hyper-stoichiometric amounts of carbon compared to the theoretical requirements for nitride production and the absence of any peaks from residual oxide in the diffraction data suggests that $\text{Zr}(\text{N}_{0.5}\text{C}_{0.5})$ is the more probable composition of the second phase.

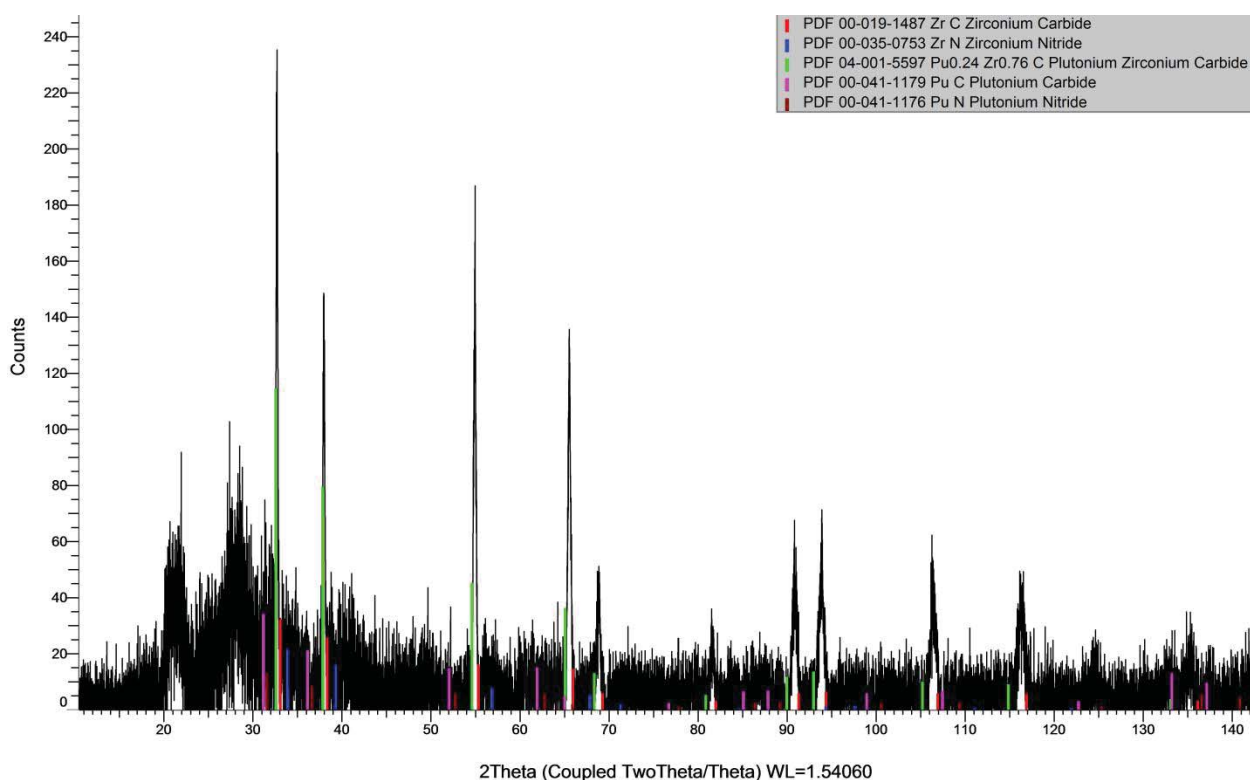


Figure 43. X-ray diffraction spectrum of the pellet sintered in N_2 . Only one FCC-NaCl structure is observable in the diffractogram [HED 16a].

In the pellet sintered in N_2 only one crystalline phase could be detected by X-ray diffraction. The shift of the diffraction peaks in Figure 43 are such that the diffraction pattern cannot be explained by any ZrN-ZrC solid solution and neither by any PuN-PuC solid solution. The observed diffraction pattern can however be explained as a mixed solid solution of both Pu(N,C) and Zr(N,C). The lattice parameter was determined to 4.717 \AA with a standard deviation of about $4 \cdot 10^{-3} \text{ \AA}$. By assuming that the metal composition in the sintered pellet is equivalent to the ICP-MS analysis of the produced microspheres and that the structure contains insignificant levels of oxide Vegard's law estimates the the pellet composition to be

$Zr_{0.6}Pu_{0.4}N_{0.87}C_{0.13}$. It should however be noted from the data of evaluating the PSI ZrPuCN materials in section 5.5 that there is likely to be somewhat of an overestimate of the nitride content using Vegard's law and, if making a rough estimate correction using the suggested 24.4% overestimate from Table 4, the composition of the material should be $ZrPuN_{0.7}C_{0.3}$. This is naturally an estimate correction with large uncertainty since there is no knowledge about the O content of the material and the oxygen level clearly influences the precision of the estimate of Vegard's law.

The densities achieved in the produced pellets were $6.9 \pm 0.2 \text{ g/cm}^3$ when sintering in N_2 and $7.6 \pm 0.2 \text{ g/cm}^3$ when sintering in Ar. Due to solid solution formation it was possible to estimate the density of the pellet sintered in N_2 to be $66 \pm 2\%$ of the theoretical density. Similar determination was not possible for the pellet sintered in Ar since no theoretical density could be determined, but using the theoretical density of the pellet sintered in N_2 as an approximation of the density allowed an estimation of the pellet sintered in Ar to be about $73 \pm 2\%$ of TD. Given the unknown magnitude of the error introduced by using the theoretical density of the N_2 sintered pellet it is difficult to compare the theoretical densities. Comparison of the actual measured pellet densities do however show that the pellet sintered in Ar reached higher density. Reaching higher density during sintering in Ar given a large enough nitride content is to be expected, as the absence of N_2 partial pressure ought to promote the formation of sub-stoichiometry in the material, consequently promoting atomic mobility. Therefore it does not seem that the lack of atomic mobility during sintering in Ar compared to N_2 was the reason for not forming solid solution. An alternative explanation could be that the material composition of the phases in the pellet do not form solid solution under the sintering conditions applied. Sintering in N_2 may however have resulted in solid solution due to further propagating the nitride formation. The reason for additional nitride formation may be the redistribution of residual carbide/oxide phases that occur during crushing of the microspheres during pellet pressing. This strengthens the theory that the separate phases observed in Figure 14 were caused by the fact that the compositions in the phases did not favor the formation of solid solution. If solid solution would have been favored in the material composition of the microspheres then solid solution should have been observed during sintering in Ar as well as in N_2 , as the limiting factor did not appear to be atomic mobility based on the achieved densities.

5.6.4. PuN pellets produced from powders and internal gelation

The purity of the PuN powders produced by carbothermal reduction was estimated from XRD data by use of Vegard's law.

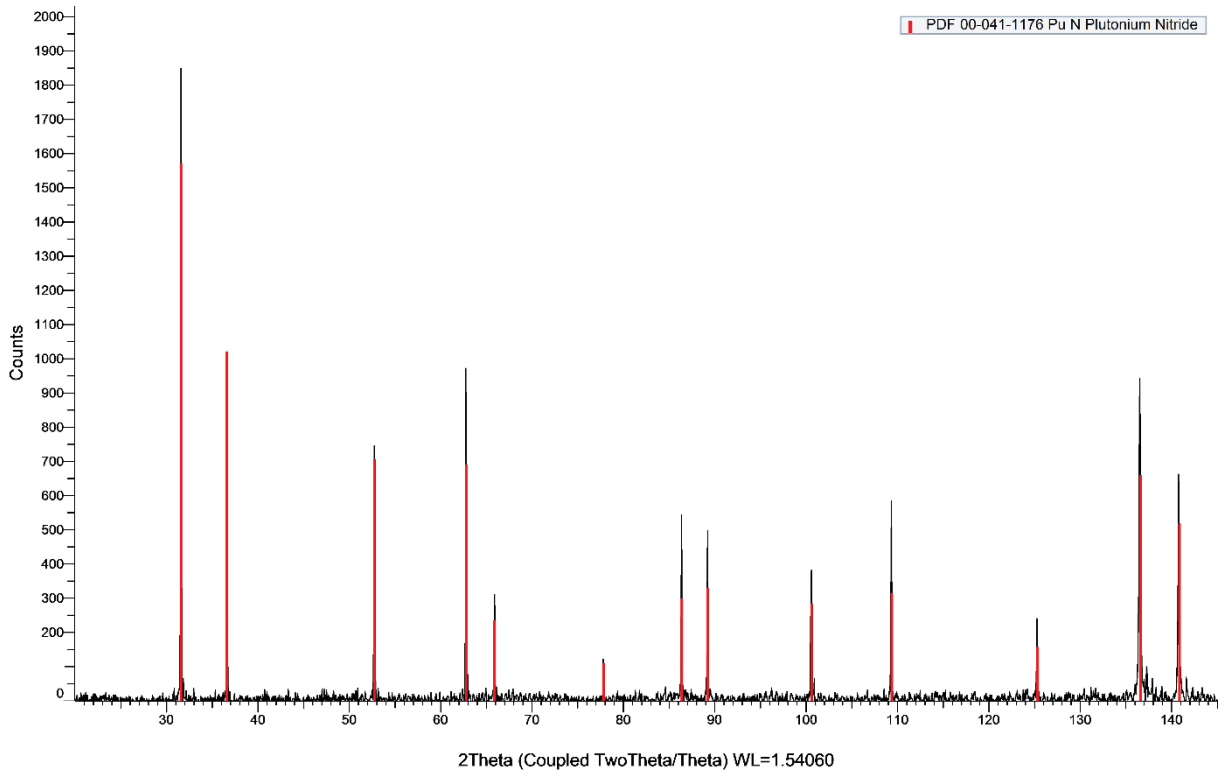


Figure 44. X-ray diffraction spectrum measured on one of the produced PuN batches matched against a data base spectrum of PuN. The spectrum presented was measured for production batch P-2-3-4.

The materials produced were in good agreement with the literature data. Only one FCC-NaCl structure could be observed in the material batches and no remainder of any PuO₂-phase could be observed in any of the samples. Vegard's law was applied to estimate the carbide and nitride content of the samples produced.

Table 11. Estimated composition of the nitride powders produced. The first three points are produced using a C/Me ratio of 2.3 and the three last Pu-containing points using a C/Me ratio of 2.5. The last point in the table is added for comparison with the purity reached in ZrN produced by carbothermal reduction on pulverized microspheres produced by sol gel technique.

Sample	Lattice parameter (Å)	Standard deviation (Å)	Composition	Carbon content (ppm)	Standard deviation (ppm)
P-2-3-1	4.9072	$3.44 \cdot 10^{-4}$	Pu(N _{0.96} C _{0.04})	1740	270
P-2-3-2	4.9068	$4.74 \cdot 10^{-4}$	Pu(N _{0.97} C _{0.03})	1390	380
P-2-3-3	4.9089	$1.17 \cdot 10^{-3}$	Pu(N _{0.93} C _{0.07})	3100	920
P-2-3-4	4.9058	$6.15 \cdot 10^{-4}$	Pu(N _{0.99} C _{0.01})	600	490
P-2-3-5	4.9085	$1.11 \cdot 10^{-3}$	Pu(N _{0.94} C _{0.06})	2740	880
P-2-3-6	4.9061	$7.05 \cdot 10^{-4}$	Pu(N _{0.98} C _{0.02})	890	560
PuN from microspheres	4.910	$3.0 \cdot 10^{-3}$	Pu(N _{0.91} C _{0.09})	4150	1550
Zr powder	4.5943	$2.96 \cdot 10^{-3}$	Zr(N _{0.85} C _{0.15})	17600	2780

Due to the relatively close match between the PuN samples produced and the reference material in the diffraction data base Vegard's law was believed to work as a good estimation of the

nitride purity The purity in the ZrN reference is, as presented previously, representative of the highest nitride purities achieved during production of ZrN. As estimated by Vegard's law the purity of the PuN materials formed generally seems to be around or in excess of 95% nitride purity. A possible reason for the much higher carbon value measured in P-2-3-5 compared to the other two samples (P-2-3-4 and P-2-3-6) where a C/Me ratio of 2.5 was used is that during the nitrification process of P-2-3-5 the graphite heating element broke down and was replaced and the heat treatment was restarted on the P-2-3-5 powder batch.

The density of the sintered pellets was measured by geometric measurements of the pellet volumes. In the case of batch P-2-3-3 the pellet was fractured into two parts after pressing and sintered as two pellets. Due to the irregular size of both pellets formed, density measurements for these pellets were omitted.

Table 12. Compaction pressures and sintering parameters when preparing PuN pellets from powder.

Sample	Compaction pressure (MPa)	Sintering Temperature (°C)	Sintering atmosphere
P-2-3-1	1200	1700	N ₂ + 5% H ₂
P-2-3-2	1800	1800	N ₂ + 5% H ₂
P-2-3-4	1200	1800	N ₂ + 5% H ₂
P-2-3-5	1200	1800	Ar
Microspheres	1800	1800	Ar

Table 13. Physical dimensions and densities determined for the PuN pellets produced.

Sample	Height (mm)	Diameter (mm)	Weight (mg)	Density (g/cm ³)	% of theoretical density
P-2-3-1	1.27	4.51	182.9	9.02	63.4
P-2-3-2	1.93	4.52	349	11.58	79.3
P-2-3-4	2.84	4.52	460.9	10.11	71.1
P-2-3-5	3.29	4.33	501.2	10.35	72.8
Microspheres	0.80	4.60	113.8	8.60	60.7

70-80% of theoretical density was reached by the conventional pressing and sintering procedure used. Density requirements of the fuel varies depending on reactor concept but densities reaching about 80-85% of TD are of interest in fast reactor concepts where a small gap width in the cladding tube is desired [ARA 12]. The pellet pressed from microsphere residues and sintered in Ar resulted in unexpectedly low density compared to densities reached in the other samples when sintering at 1800 °C. During SEM characterization it was concluded that this was caused by irregularities formed in the microsphere-based pellet, causing geometrical measurements to incorrectly describe actual pellet geometry.

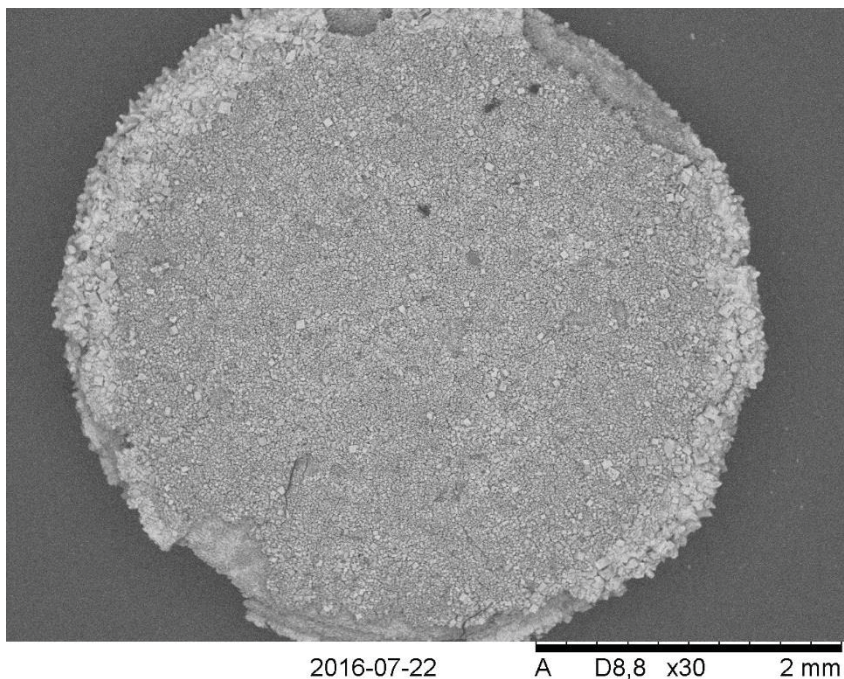


Figure 45. SEM image of a sintered pellet pressed from the microsphere-derived material [HED 16d].

Geometrical measurements of the pellet resulted in an overestimation of the pellet volume due to partial radial swelling of the top surface of the pellet. This implies that the actual pellet density should be somewhat larger compared to the measured density. Closer investigation of the pellet topside revealed the formation of crystals.

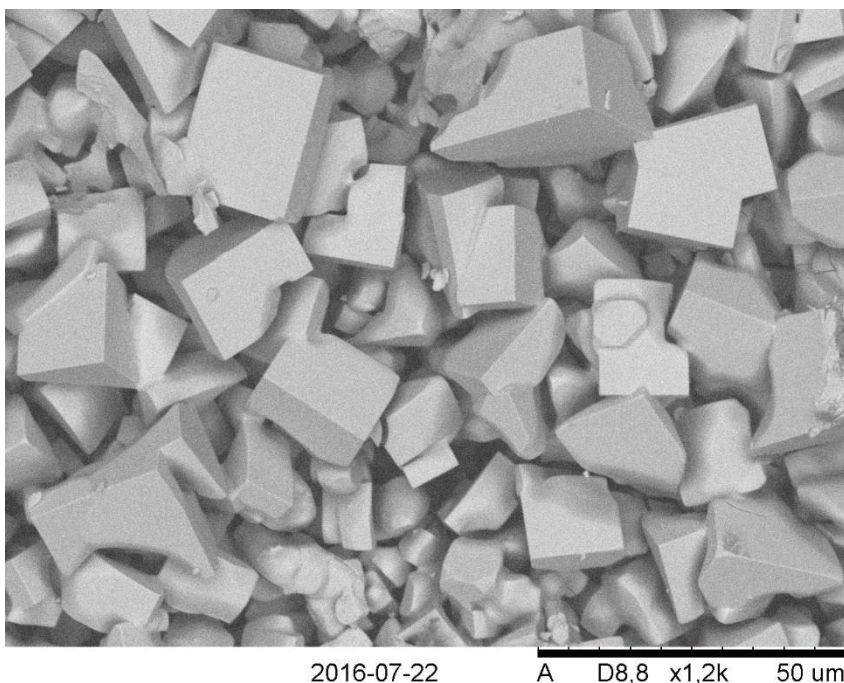


Figure 46. Crystal formation on the surface facing the atmosphere during sintering [HED 16d].

The crystals formed on top of the pellet were identified as a slightly distorted Pu_4O_7 phase (Figure 47) by X-ray diffraction. The distortion could possibly be caused by residues of N or C in the oxide structure. This implies that the sintering environment suffered from at least a partial

ingress leakage of O₂ during the sintering. Formation of an oxide phase on the top part of the pellet explains the radial swelling of the pellet top part since the density of plutonium nitride is higher than the density of plutonium oxide. Diffraction measurements of the bottom side of the pellet did not reveal any oxide layer formation but instead retained a Pu(N,C) structure. Similar phenomena has not been encountered during sintering any of the other pellets.

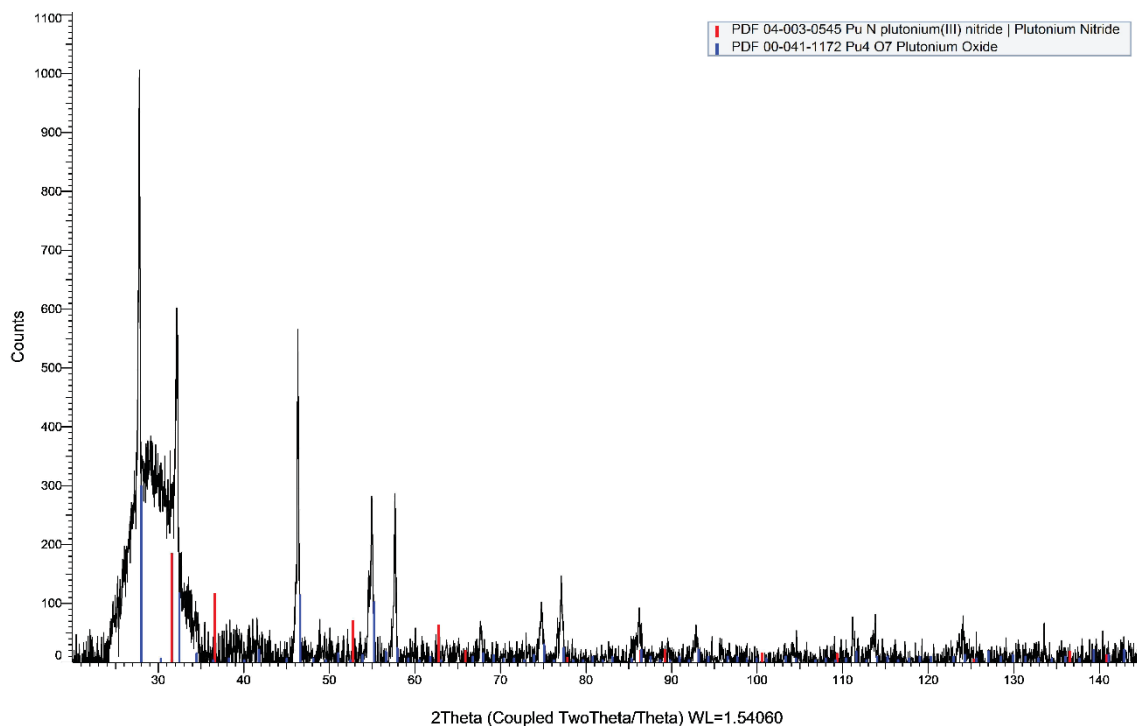


Figure 47. XRD spectrum of the Pu₄O₇ side of the microsphere material pellet. The absence of the PuN (200) peak (the second red line), suggests that the second spectrum peak originates from an oxide reflection and not the PuN (111) reflection. The material was thus interpreted as a slightly distorted Pu₄O₇ phase [HED 16d].

Higher densities could, as would normally be expected, be achieved in the pellets by increasing compaction pressure and sintering temperature. Using equivalent compaction pressure and sintering temperature, similar final densities were achieved during sintering in Ar and N₂ + 5% H₂ atmosphere. This is not totally unexpected since PuN has a narrow homogeneity range [KLE 99, MAT 87] and low promotion of sintering would be expected if no, or only little, sub-stoichiometry formed in PuN during sintering in Ar. If comparing the radial shrinkage of the produced pellets it can be observed that the pellets sintered in N₂ + 5% H₂ atmosphere did not shrink at all during the sintering process. The final diameter of the pellets sintered in N₂ + 5% H₂ atmosphere was somewhat larger than the 4.5 mm target diameter for the pressing tool. The deviations are within the tolerance of the pressing tool however so it is not considered that any swelling of the pellets occurred during sintering. Sintering of pellet P-2-3-5 in Ar produced a radial shrinkage of about 3.8% in the pellet. There is therefore an observable effect of sintering in a non-N₂-containing inert atmosphere even if this is limited in magnitude. The swelling of the microsphere pellets, caused by partial oxidation of the material due to oxygen ingress into the furnace during sintering, makes the density measurements of the pellet non-descriptive of the actual sintering behavior in Ar and no reliable comparison can be made with pellet P-2-3-2, which was similarly produced but sintered in N₂ + 5% H₂ instead of Ar.

5.7. Am volatilization in PuN matrix pellets

HPGe gamma spectroscopic measurements were performed on the powder batches produced, as well as on the starting PuO₂ powder and one of the dissolved sintered pellets, to examine the degree of americium losses from the material during carbothermal reduction and sintering. The ratio between ²⁴¹Am and ²³⁹Pu was determined in every sample and normalized against the Am/Pu in the stock PuO₂ material. The evaluation of the ²⁴¹Am presence during HPGe measurements was performed using the 125.3 keV peak and ²³⁹Pu was evaluated using the 129.3 keV peak.

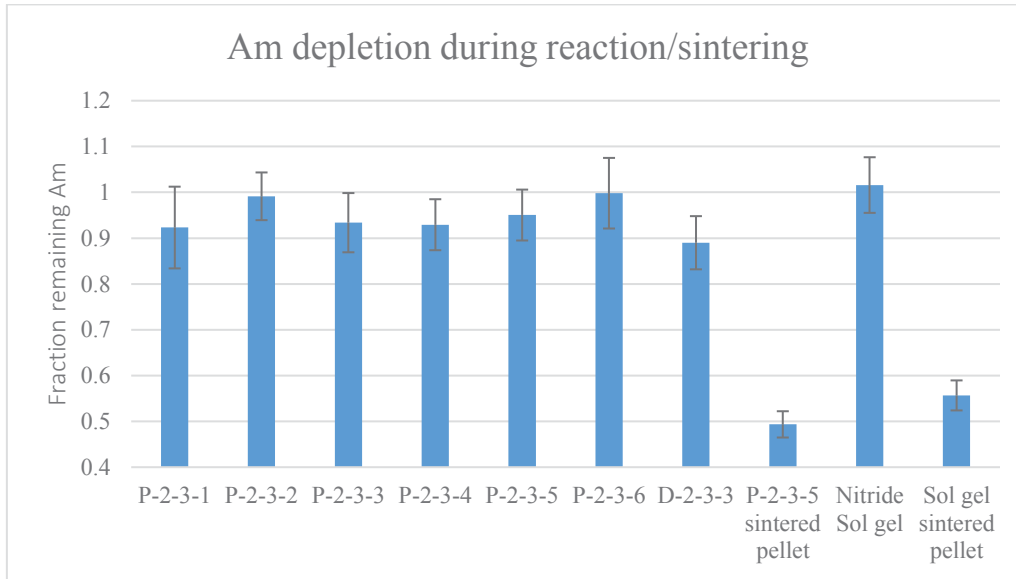


Figure 48. Am/Pu ratios in the different samples normalized against the Am/Pu ratio in the stock PuO₂ powder used. The sample named D-2-3-3 is a measurement performed on one of the fully dissolved pellets from P-2-3-3 [HED 16d].

The uncertainty in Figure 48 is plotted as a 95% confidence interval and the uncertainties presented are errors propagated from the ²⁴¹Am/²³⁹Pu measured in each individual sample. The uncertainty of the measurement of the ²⁴¹Am/²³⁹Pu ratio in the PuO₂ stock material is therefore also taken into consideration, even if this is not inherently obvious from Figure 48 itself. Since the Am/Pu ratio measured in every sample is normalized against the Am/Pu ratio in the stock material used, a resulting value of 1 is expected if no depletion of Am has occurred during heat treatment. From Figure 50 it can be observed that the Am/Pu ratio differs from the Pu stock material on a significant level in only one sample of the nitridation experiments (sample P-2-3-4). Given the uncertainty levels in the measurements it is however not possible to determine if there actually are any differences between any of the nitride sample batches. The measurement method used therefore seems suboptimal for accurately determining low levels of Am depletion in PuN matrixes. Bearing this in mind, taking an overall average of all nitridation measurements, about $96.3 \pm 6.6\%$ of the Am content is retained during carbothermal reduction. The losses were larger in the dissolved sintered pellet compared to the nitrided materials and suggests that in total about 11% of the Am is lost during the entire production cycle of the fuel pellet. A substantial increase in Am losses were observed when sintering the atmosphere was changed from N₂ containing atmosphere to inert Ar atmosphere. The absence of an N₂ partial pressure suppressing nitride dissociation resulted in increasing Am volatilization. Sintering at

1800 °C for 4 hours resulted in losses of about 50% and 45% Am, respectively, in the two (P-2-3-5 and Sol gel) pellets. The pellet produced from microsphere-based material lost a bit less Am compared to pellet P-2-3-5 during sintering. This may be the result of oxygen ingress during sintering, decreasing the Am volatilization due to surface oxide formation. Oxide formation may also have increased Pu volatilization compared to Am due to the formation of gaseous PuO [OHM 85].

6. Summary and Conclusions

In this work the production of ZrN, (Zr,Pu)N and PuN has been studied. Production of Zr and mixed Zr,Pu microspheres has been performed and the formation of nitrides via the carbothermal reduction process has been investigated. In the production of ZrN and (Zr,Pu)N low oxygen-containing products have been obtained but significant carbide content on the order of 15-20% has been found to be present in the material. Formation of PuN from PuO₂ by carbothermal reduction was produced more readily and low carbide content could be achieved. It therefore appears that ZrC formed during carbothermal reduction is more difficult to remove from the nitride matrix compared to PuC. This was also observed in the dual phase mixed Zr,Pu pellet sintered in Ar, where one phase seemed to describe PuN while the second phase showed more resemblance to Zr(C_{0.5}N_{0.5}) than to ZrN. Ideally these findings should be verified using a reaction system that is not based on graphite heating element technology. The reaction system used seemed compatible with PuN production, but ZrC equilibration by heating element reaction interferences may be an issue.

Pellet fabrication by conventional sintering should be performed using microspheres of good crushability. Pressing at 1200 MPa and sintering at 2000 °C of low crushable microspheres produced final densities similar to 600 MPa pressure and 1700 °C sintering when the microspheres were readily crushed using pressure. Generally speaking however, all conventional sintering performed yielded low final densities. Addition of sintering additives becomes complicated when pressing microspheres, but may be required for obtaining high density pellets. Spark plasma sintering produced higher density material compared to conventional sintering. Sintering propagated more easily in Ar than in N₂ atmospheres, suggesting that formation of hypo-stoichiometric nitride promoted sintering. In addition, nitrides with less carbide content also sintered to higher final densities. Densities approaching 90% of theoretical density were achieved, making SPS a reasonable option for pellet production even if more data on microsphere sintering characteristics is required.

It was shown that Zr(N,C) material compositions could be reliably quantified from X-ray diffraction data and the application of Vegard's law. In the quaternary (Zr,Pu)(N,C) system Vegard's law produced far less accurate composition estimations and uncertainties of the estimations were quite large. It was observed that residual oxygen in the carbonitride structure had a strong influence on the lattice parameter and affected the composition estimates.

Contradictory to what is generally believed, no large losses of americium were observed during fabrication of PuN through carbothermal reduction or during pellet sintering. Most synthesis samples did not show any statistically significant loss of ²⁴¹Am, but an average of the synthesis data indicated about 4% Am losses during fabrication. The total losses during fabrication and sintering were about 11%. It thus seems that, with some process optimization, production of low level Am-containing nitrides should be possible without unacceptably high losses of Am.

7. Future Work

Studies regarding preparation of nitride-based nuclear fuel are nowhere near being completed and there are several questions that remain unanswered.

Regarding fabrication of dense nitride pellets from sol gel-derived microspheres there are several possibilities of interest left to explore. In conventional sintering it appears that the addition of a sintering aid is required to facilitate reasonable sintering of the green pellets. The challenge is to find a sintering agent that can be homogeneously mixed with the microspheres without requiring a separate milling step. A solution could be to find an appropriate dopant to add to the sol and incorporate into the gelation step. The dopant has to survive the carbothermal reduction step, however, without volatilizing or sintering the microspheres too densely so that pressing becomes an issue.

In conventional sintering, as well as in spark plasma sintering, investigations of the influence of microsphere size and mixed size fractions would be of interest for producing pellets of controlled density.

Further studies of Am volatilization during fuel production using different Am levels in the fuel matrix could be of importance, together with behavior when present with inert matrix. The behavior of Am may differ depending on its perceived environment, both with regard to metal composition in the nitride and the level of carbide phase present.

Continuation of Zr-Pu co-gelation in the internal gelation process and studies regarding the gelation behavior as a function of Pu content is of interest. Clarification regarding if the observed dual phase formation in nitride microspheres is actually attributed to the gelation step or a result of incomplete carbothermal reduction is also of interest.

Production of low carbon impurity nitrides by carbothermal reduction needs to be continued. Some materials, such as PuN, seem to be producible with reasonable levels of impurities while the formation of ZrN needs to be refined. If carbothermal reduction of ZrO₂ proves to be a non-viable method for ZrN fabrication one option could be investigation of ZrN powder production by cyclic hydriding/nitriding. Production of ZrN powders, coupled with mixing and pellet pressing with PuN microspheres and sintering could be one way to achieve lower carbide contents while avoiding processes based on fine radioactive powders.

8. Acknowledgements

During years filled of toil and of troubled despair
Life seemed at its darkest but now I am there
By ink upon paper on which you now stare
My words have been sculptured and my thanks I will share

To Christian Ekberg, who travels indeed
Yet e-mail he answers at ludicrous speed
Go forth build the fuel lab, such was the decree
I'm happy and honored you trusted in me

To examiner Gunnar, both cunning and kind
No matter the problem the answer he find
I hope you're enjoying your German retreat
And that work's been exchanged for fine beer and good meat

Emma and Elin, then Aneta of course
Such excellent roommates I truly endorse
It's been a real pleasure from start and along
Though one girl is missing but it shan't be for long

She came to my office and talked without end
My ears almost shattered but then we befriend
Sharing of knowledge and gossip and such
Jenny you showed me one can't speak too much

We started together, we traveled around
She learned when I'm hungry I won't make a sound
Thank you Lovisa it's really been fun
Even at those times you forced me to run

To all at the workplace, both present and past
I can't name you all cause the list grows to vast
In skills and in talents you all are unique
For better co-workers one would have to seek

To all members of ASGARD I direct my thanks
For all help and friendship within our ranks
Both meetings and evenings have always been good
And everyone helped out whenever they could

To my parents and siblings, I gratitude send
Whatever my trouble, on you I can depend
Through progress and hardships you've all stood by me
On this five year long travel towards my PhD

The last is to Emma, which with home I share
In computerized gaming from her beware
In strategy games you're both skillful and smart
But in real life you managed to conquer my heart

The research leading to these results was performed within the ASGARD project and has received funding from the European Atomic Energy Community's Seventh Framework Programme FP7/2007-2011 under grant agreement n°295825.

9. References

- [ADA 85] Adamson, M.G., Aitken, E.A., Caputi, R.W., *Experimental and thermodynamic evaluation of the melting behavior of irradiated oxide fuels*, 1985, Journal of Nuclear Materials 130, pp. 349-365
- [AKH 67] Akhachinskii, V.V., Bashlykov, S.N., *Systems of Uranium and Plutonium with Carbon, Oxygen and Nitrogen: Phase Diagrams and Methods of Production*, 1969, Translated from Atomnaya Énergiya 27 (6), pp. 524-532
- [ALL 67] Allbutt, M., Dell, R.M., *Chemical aspects of nitride, phosphide and sulphide fuels*, 1967, Journal of Nuclear Materials 24, pp. 1-20
- [APA 12] Aparicio, M., Jitianu, A., Klein, L.C., *Sol-Gel Processing for Conventional and Alternative Energy*, pp. 341 – 373, New York, Springer Science + Business media, 2012
- [ARA 92] Arai, Y., Suzuki, Y., Iwai, T., Ohmichi, T., *Dependence of the thermal conductivity of (U,Pu)N on porosity and plutonium content*, 1992, Journal of Nuclear Materials 195, pp. 37-43
- [ARA 98] Arai, Y., Nakajima, K., Suzuki, Y., *Thermal conductivity of actinide mononitride solid solutions*, 1998, Journal of Alloys and Compounds, pp. 602-605
- [ARA 12] Arai, Y., *Comprehensive Nuclear materials - Nitride Fuel*, Elsevier, 2012
- [ARO 66] Aronson, S., Auskern, A.B., *Vapor Pressure Measurements on Thorium Nitride*, 1966, Journal of Physical Chemistry 70 (12), pp. 3937-3941
- [BAK 13] Baker, M.P., King, J.C., Gorman, B.P., Marshall, D.W., *Selection and properties of alternative forming fluids for TRISO fuel kernel production*, 2013, Journal of Nuclear Materials 432, pp. 395-406
- [BAN 12] Banerjee, S., Govindan Kutty, T.R., *Functional Materials: Preparation, Processing and Applications*, London, Elsevier, 2012
- [BAR 92] Bardelle, P., Warin, D., *Mechanism and kinetics of the uranium-plutonium mononitride synthesis*, 1992, Journal of Nuclear Materials 188, pp. 36-42
- [BAR 08] Bart, G., Botta, F.B., Hoth C.W., Ledergerber, G., Mason, R.E., Stratton, R.W., *AC-3-irradiation test of sphere – pac and pellet (U,Pu)C fuel in the US Fast Flux Test Facility*, 2008, Journal of Nuclear Materials 376, pp. 47-59
- [BEČ 69] Bečvář, J., *The preparation of Uranium Monocarbide*, 1969, Journal of Nuclear Materials 32, pp. 156-160
- [BEG 90] Begun, G.M., Haire, R.G., *Raman spectra of some actinide dioxides and of EuF₂*, 1990, Journal of the Less-Common Materials 162, pp. 129-133
- [BEN 08] Benay, G., Hubert, F., Modolo, G., *Preparation of yttria-stabilized zirconia-ceria kernels as fuel precursors using internal gelation*, 2008, Radiochimica Acta 96, pp. 285-291

- [BEN 70] Benz, R., Hutchinson, W.B., *U + N₂ reaction layer growths*, 1970, Journal of Nuclear Materials 36 (2), pp. 135-146,
- [BER 89] Bernard, H., *Advanced fuel fabrication*, 1989, Journal of Nuclear Materials 166, pp. 105-111
- [BLA 88] Blank, H., *Specification and Characterization of Dense Fuels for Liquid Metal Cooled Fast Breeder Reactors*, 1988, Journal of Nuclear Materials 153, pp. 171-177
- [BLA 89] Blank, H., Richter, K., Coquerelle, M., Matzke, H., Campana, M., Sari, C., Ray, I.L.F., *Dense fuels in Europe*, 1989, Journal of Nuclear Materials 166, pp. 95-104
- [BON 75] Bond, W.D., Leuze, R.E., *Removal of actinides from high-level wastes generated in the reprocessing of commercial fuels*, International transplutonium elements symposium, Baden-Baden Germany, 1975, Report number CONF-750913-9
- [BRA 70] Brambilla, G., Gerontopulos, P., Neri, D., *The SNAM process for the preparation of ceramic nuclear fuel microspheres: laboratory studies*, 1970, Energia Nucleare 17, pp. 217-224
- [BRO 55] Brown, F., Ockenden, H.M., Welch, G.A., *The Preparation and Properties of Some Plutonium Compounds. Part II. Plutonium Nitride*, 1955, Journal of the Chemical Society (resumed), pp. 4196-4201
- [BRU 70] Bruggen v.d, F.W., Noothout, A.J., Hermans, M.E.A., Kanij., J.B.W., Votocek, O., *a U(VI) – process for microsphere production*, 1970, Symposium on sol-gel processes and reactor fuel cycles. Gatlinburg, Tennessee, CONF – 700502, pp. 253-263
- [BRY 14] Brykala, M., Deptula, A., Rogowski, M., Lada, W., Olczak, T., Wawaczak, D., Smolinski, T., Wojtowicz, P., Modolo, G., *Synthesis of microspheres of triuranium octaoxide by simultaneous water and nitrate extraction from ascorbate-uranyl sols*, 2014, Journal of Radioanalytical Nuclear Chemistry, pp. 651-655
- [BRY 15] Brykala, M., Deptula A., Rogowski, M., Lada, W., *Modification of IChTJ Sol Gel Process for Preparation of Medium Sized Ceramic Spheres ($\varphi < 100\mu\text{m}$)*, Ceramics International 41, pp. 13025-13033
- [BUG 64] Bugl, J., Bauer, A.A., *Phase Relations in the System Uranium-Nitrogen*, 1964, Journal of American Ceramic Society 47, pp. 425-429
- [BUR 01] Burghartz, M., Ledergerber, G., Hein, H., Laan v.d, R.R., Konings, R.J.M., *Some aspects of the use of ZrN as an inert matrix for actinide fuels*, 2001, Journal of Nuclear Materials 288, pp. 233-236
- [BYK 15] Bykov, D.M., Raison, P.E., Konings, R.J.M., Apostolidis, C., Orlova, M., *Synthesis and crystal structure investigations of ternary oxides in the Na-Pu-O system*, 2015, Journal of Nuclear Materials 457, 99. 54-62
- [CAR 14] Carvajal Nuñez, U., *Synthesis and Characterization of Advanced Nuclear Fuels*, Doctoral thesis, Technische Universiteit Delft, 2014
- [CHA 98] Chase, M.W., *NIST-JANAF thermochemical tables 4th edition*, 1998

- [CHA 99] Chauvin, N., Konings, R.J.M., Matzke, H.J., *Optimisation of inert matrix fuel concepts for americium transmutation*, 1999, Journal of Nuclear Materials 274, pp. 105-111
- [CHA 06] Charollais, F., Fonquernie, S., Perrais, C., Perez, M., Dugne, O., Cellier, F., Harbonnier, G., Vitali, M-P., *CEA and AREVA R&D on HTR fuel fabrication and presentation of the CAPRI experimental manufacturing line*, 2006, Nuclear Engineering and Design 236, pp. 534-542
- [CHA 08] Charollais, F., Perrais, C., Moulinier, D., Perez, M., Vitali, M.P., *Latest achievements of CEA and AREVA NP on HTR fuel fabrication*, 2008, Nuclear Engineering and Design 238, pp. 2854-2860
- [CHO 02] Choppin, G., Liljenzin, J.O., Rydberg, J., *Radiochemistry and nuclear chemistry, Third edition*, Woburn (U.S), Butterworth-Heinemann, 2002
- [COL 87] Collins, J.L., Lloyd, M.H., Fellows, R.L., *The Basic Chemistry Involved in the Internal-Gelation Method of Precipitating Uranium as Determined by pH Measurements*, 1987, Radiochimica Acta 42, pp. 121-134
- [CON 49] Connick, R.E., McVey, W.H., *The Peroxy Complexes of Plutonium(IV)*, 1949, Journal of the American Chemical Society 71, pp. 1534-1542
- [DAU 97] Daumas, S., *Etude et réalisation de support-matrices inertes par le procédé sol-gel pour l'incinération des actinides mineures*, doctoral thesis, Marseille, 1997
- [DEP 92] Deptula, A., Lada, W., Olczak, T., Borello, A., Alvani, C., di Bartolomeo, A., *Preparation of Spherical Powders of Hydroxyapatite by Sol-Gel Process*, 1992, Journal of Non-Crystalline Solids, pp. 537-541
- [ERO 76] Eron'yan, M.A., Avarbe, R.G., Nikol'skaya, T.A., *How the Pressure of Nitrogen Affects the Melting Point of ZrN_x (title of translated paper)*, Neorganicheskie Materialy 12 (2), pp. 247-249
- [EVA 63] Evans, P.E., Davies, T.J., *Uranium Nitrides*, 1963, Journal of Nuclear Materials 10, pp. 43-55
- [FRE 72] Freshley, M.D., *A comparison of pellet and vipac nuclear fuels*, 1972, Nuclear Engineering and Design 21, pp. 264-278
- [FU 04] Fu, X., Liang, T., Tang, Y., Xu, Z., Tang, C., *Preparation of UO_2 Kernel for HTR-10 Fuel Element*, 2004, Journal of Nuclear Science and Technology 41 (9), pp. 943-948
- [FÖR 77] Förthmann, R., Blass, G., *Fabrication of Uranium-Plutonium Oxide Microspheres by the Hydrolysis Process*, 1977, Journal of Nuclear Materials 64, pp. 275-280
- [GAN 86] Ganguly, C., Langen, H., Zimmer, E., Merz, E.R., *Sol-Gel Microsphere Pelletization Process for Fabrication of High-Density ThO_2 -2% UO_2 Fuel for Advanced Pressurized Heavy Water Reactors*, 1986, Nuclear Technology 73, pp. 84-95
- [GAN 91] Ganguly, C., Hegde, P.V., Sengupta, A.K., *Preparation and characterisation and out-of-pile property evaluation of (U, Pu)N fuel pellets*, 1991, Journal of Nuclear Materials 178, pp. 234-241

- [GAN 93] Ganguly, C., *Sol – gel microsphere pelletization: A powder – free advanced process for fabrication of ceramic nuclear fuel pellets*, 1993, Bulletin of Material Science 16 (6), pp. 509-522
- [GIB 71] Gibby, R.L., *The effect of plutonium content on the thermal conductivity of (U, Pu)O₂ solid solutions*, 1971, Journal of Nuclear Materials 38, pp. 163-177
- [GRE 73] Greenhalgh, W.O., *Kintecic Measurements for the Carbothermic Synthesis of UN, PuN, and (U,Pu)N* 1973, Journal of the American Ceramic Society 56 (11), pp. 553-557
- [HAG 04] Hagfeldt, C., Kessler, V., Persson, I., *Structure of the hydrated, hydrolysed, and solvated zirconium (IV) and hafnium (IV) ions in water and aprotic oxygen donor solvents. A crystallographic, EXAFS spectroscopic and large angle X-ray scattering study*, 2004, Dalton Transactions 14, pp. 2142-2151
- [HAY 90] Hayes, S.L., Thomas, J.K., Peddicord, K.L., *Material property correlations for uranium mononitride I. Physical properties*, 1990, Journal of Nuclear materials 171, pp. 262-270
- [HAY 12] Haynes, W.M., Ed, “ *Properties of the elements and inorganic compounds*” in *CRC Handbook of Chemistry and Physics, 92nd edition Internet version 2012*, CRC Press/Taylor and Francis, Boca Raton, FL, 2012
- [HED 16a] Hedberg, M., Ekberg, C., *Studies on plutonium-zirconium co-precipitation and carbothermal reduction in the internal gelation process for nitride fuel preparation*, 2016, Journal of Nuclear Materials 479, pp. 608-615
- [HED 16b] Hedberg, M., Cologna, M., Cambriani, A., Somers, J., Ekberg, C., *Zirconium carbonitride pellets by internal sol gel and spark plasma sintering as inert matrix fuel material*, 2016, Journal of Nuclear Materials 479, pp. 137-144
- [HED 16c] Hedberg, M., Streit, M., Ekberg, C., *Effects of carbide impurities on the lattice parameter of mixed zirconium nitrides*, Submitted to Progress in Nuclear Engineering
- [HED 16d] Hedberg, M., Ekberg, C., *A comparative study of nitride purity and Am fabrication losses in PuN materials by the powder and internal gelation production routes*, 2016, Manuscript
- [HEL 78] Hellwege, K.-H., Crystal structure data of inorganic compounds. In *Landolt - Börnstein Numerical Data and Functional Relationships in Science and Technology*, 1978,
http://www.springermaterials.com/docs/pdf/10201501_10.html?queryterms=%22zrn%22, (2016-05-27)
- [HEL 06] Hellwig, Ch., Bakker, K., Ozawa, T., Nakamura, M., Ingold, F., Nordström, L.Å., Kihara, Y., *FUJI: A Comparative Irradiation Test with Pellet, Sphere-pac and Vipac fuels*, 2006, Nuclear Science and Engineering 153, pp. 233-244
- [HOL 69] Holleck, H., Kleykamp, H., *Thermodynamics of Multi-Component Systems Containing UC and PuC a review*, 1969, Journal of Nuclear Materials 32, pp. 1-19

- [HOL 03] Holmberg, K., Jönsson, B., Kronberg, B., Lindman, B., *Surfactants and polymers in aqueous solution 2nd edition*, Chichester, John Wiley & sons Ltd, 2003
- [HUN 10] Hunt, R.D., Montgomery, F.C., Collins, J.L., *Treatment techniques to prevent cracking of amorphous microspheres made by internal gelation process*, 2010, Journal of Nuclear Materials 405, pp. 160-164
- [IAE 15] IAEA, *Nuclear Technology Review 2015*, Vienna, Printed by the IAEA, 2015
- [IDE 03] Idemitsu, K., Arima, T., Inagaki, Y., Torikai, S., Pouchon, M.A., *Manufacturing of zirconia microspheres doped with erbia, yttria and ceria by internal gelation process as part of a cermet fuel*, 2003, Journal of Nuclear Materials 319, pp. 31-36
- [ISL 03] Islam, M.F., Rojas, E., Bergey, D.M., Johnson, A.T., Yodh, A.G., *High Weight Fraction Surfactant Solubilization of Single – Wall Carbon Nanotubes in Water*, 2003, Nano Letters 3 (2), pp. 269-273
- [ISO 09] ISO (International Organization for Standardization), *NUCLEAR FUEL TECHNOLOGY – Dissolution of Plutonium Dioxide-Containing Materials*, 2003, Report number: ISO/DIS 18213-2
- [JAC 07] Jacob, K.T., *Vegard's law: a fundamental relation or an approximation?* 2007, International Journal of Materials Research 98 (9), pp. 776-779
- [JOH 16] Johnson, K.D., Wallenius, J., Jolkkonen, M., Claisse, A., *Spark plasma sintering and porosity studies of uranium nitride*, 2016, Journal of Nuclear Materials 473, pp. 13-17
- [JON 52] de Jong, J.I., de Jonge, J., *The Reaction of Urea with Formaldehyde*, 1952, Recueil, pp. 643-660
- [KAN 74] Kanij, J.B.W., Noothout, A.J., Votocek, O., *The KEMA U(VI)-Process for the Production of UO₂ Microspheres*, 1974, in Sol-Gel Process for Fuel Fabrication. IAEA-161, pp. 185-195
- [KEM 60] Kempter, C.P., Fries, R.J., *189. Zirconium Carbide*, 1960, Analytical Chemistry 32 (4), pp. 570
- [KIN 90] King, C.M., King, R.B., Garber, A.R., Thompson, M.C., Buchanan, B.R., *Magnetic Resonance as a Structural Probe of a Uranium (VI) Sol-Gel Process (U)*, 1990, Materials Research Society: Better Ceramics Through Chemistry IV Symposium
- [KLE 99] Kleykamp, H., *Selection of materials as diluents for burning plutonium fuels in nuclear reactors*, 1999, Journal of Nuclear Materials 275, pp. 1-11
- [LED 92] Ledergerber, G., Kopajtic, Z., Ingold, F., Stratton, R.W., *Preparation of uranium nitride in the form of microspheres*, 1992, Journal of Nuclear Materials 188, pp. 28-35
- [LED 96] Ledergerber, G., *JAERI Review - Internal Gelation for Oxide and Nitride Particles*, 1996, Japan Atomic Energy Research Institute
- [LEI 70] Leitnaker, J.M., Lindemer, T.B., Fitzpatrick, C.M., *Reaction of UC with Nitrogen from 1475° to 1700 °C*, 1970, Journal of the American Ceramic Society 53 (9), pp. 479-481

- [LLO 76] Lloyd, M.H., Bischoff, K., Peng, K., Nissen, H-U., Wessicken, R., *Crystal Habit and Phase Attribution of U(VI) Oxides in a Gelation Process*, 1976, Journal of inorganic nuclear Chemistry 38, pp. 1141-1147
- [LLO 78] Lloyd, M.H., Haire, R.G., *The Chemistry of Plutonium in Sol-Gel Processes*, 1978, Radiochimica Acta 25, pp. 139-148
- [LOR 68] Lorenzelli, R., *Contribution a L'Etude du Systeme (U,Pu)C,N; CEA Report R-3536*; CEA, Fontenay-aux-Roses, France, 1968
- [LOT 68] Lotts, A.L., Wymer, R.G., *Economics and Technology of HTGR Fuel Recycle*, 1968, Report ORNL-TM-2377
- [LOV 06] Loveland, W.D., Morrissey, D.J., Seaborg, G.T., *Modern Nuclear Chemistry*, Hoboken, John Wiley & sons Inc, 2006
- [MAI 01] Maillard, C., Adnet, J.M., *Plutonium(IV) peroxide formation in nitric medium and kinetics Pu(VI) reduction by hydrogen peroxide*, 2001, Radiochimica Acta 89, pp. 485-490
- [MAL 14] Malkki, P., Jolkkonen, M., Hollmer, T., Wallenius, J., *Manufacture of fully dense uranium nitride pellets using hydride derived powders with spark plasma sintering*, 2014, Journal of Nuclear Materials 452, pp. 548-551
- [MAT 86] Matzke, Hj., *Science of Advanced LMFBR Fuels*, Amsterdam, Elsevier Science Publishers, 1986
- [MAT 91] Matzke, Hj., *Fabrication and Testing of Non – Oxide Nuclear Fuels for Fast Breeders*, 1991, Ceramics International 17, pp. 315-323
- [MIT 68]. Mitamura, T., Kanno, M., Mukaibo, T., *Preparation of Uranium Nitrides from Uranium Tetrachloride*, 1968, Journal of Nuclear Science and Technology 5 (2), pp. 60-64
- [MUK 90] Mukerjee, S.K., Dehadraya, J.V., Vaidya, V.N. Sood, D.D, *Kinetic study of the carbothermic synthesis of uranium monocarbide microspheres*, 1990, Journal of Nuclear Materials 172, pp. 37-46
- [MUK 91] Mukerjee, S.K., Dehadraya, J.V., Vaidya, V.N., Sood, D.D., *Kinetics of the carbothermic synthesis of uranium mononitride microspheres*, 1991, Journal of Nuclear Materials 185, pp. 39-49
- [MUK 93] Mukerjee, S.K., Rama Rao, G.A., Dehadraya, J.V., Vaidya, V.N., Venugopal, V., Sood, D.D., *Carbothermic reduction of (UO₃ + C) microspheres to (UO₂ + C) microspheres*, 1993, Journal of Nuclear Materials 199, pp. 247-257
- [MUR 77] Muromura, T., Tagawa, H., *Formation of uranium mononitride by the reaction of uranium dioxide with carbon in ammonia and a mixture of hydrogen and nitrogen – I synthesis of high purity UN*, 1977, Journal of Nuclear Materials 71, pp. 65-72
- [NAE 79] Naefe, P., Zimmer, E., *Preparation of Uranium Kernels by an External Gelation Process*, 1979, Nuclear Technology 42, pp. 163-171
- [NAK 98] Nakajima, K., Arai, Y., Suzuki, Y., *Vaporization behavior of (Np,Pu)N*, 1998, Journal of Alloys and Compounds, pp. 666-669

- [NIS 08] Nishi, T., Itoh, A., Takano, M., Numata, M., Akabori, M., Arai, Y., *Heat capacities of NpN and AmN*, Journal of Nuclear Materials 377, pp. 467-469
- [NOR 12] Nordlund, A., *Introduction to Nuclear Reactors*, Course material Chalmers University of Technology, 2012
- [OET 67] Oetting, F.L., *The chemical thermodynamic properties of plutonium compounds*, 1967, Chemical Reviews 67 (3), pp. 261-297
- [OGA 95] Ogawa, T., Ohmichi, T., Maeda, A., Arai, Y., Suzuki, Y., *Vaporization behaviour of (Pu,Am)N*, 1995, Journal of Alloys and Compounds 224, pp. 55-59
- [OHM 85] Ohmichi, T., Nomura, S., Maeda, A., *Removal of Americium by Its Evaporation during Carbothermic Reduction of Plutonium Dioxide*, 1985, Journal of Nuclear Science and Technology 22, pp. 329-330
- [OI 72] Oi, N., Hirayama, S., Tanabe, I., Muramatsu, A., Kawada, T., *Preparation of High Density Uranium Nitride and Uranium Carbonitride Fuel Pellets*, 1972, Journal of Nuclear Science and Technology 9 (9), pp. 521-527
- [OLS 63] Olson, W.M., Mulford, R.N.R., *The decomposition pressure and melting point of uranium mononitride*, 1963, Journal of physical chemistry 67 (4), pp. 952-954
- [OLS 64] Olson, W.M., Mulford, R.N.R., *The decomposition pressure of plutonium nitride*, 1964, Journal of Physical Chemistry 68 (5), pp. 1048-1051
- [OLS 65] Olson, W.M., Mulford, R.N.R., *The Decomposition Pressure and Melting Point of Thorium Mononitride*, 1965, Journal of Physical Chemistry 69 (4), pp. 1223-1226
- [PAR 11] Parkison, A.J., McDeavitt, S.M., *Hydride Formation Process for the Powder Metallurgical Recycle of Zircaloy from Used Nuclear Fuel*, 2011, Metallurgical and Material Transactions A: Physical Metallurgy and Materials Science 42 (1), pp. 192-201
- [PAU 88] Pautasso, G., Richter, K., Sari, C., *Investigation of the reaction $UO_{2+x} + PuO_2 + C + N_2$ by thermogravimetry*, 1988, Journal of Nuclear Materials 158, pp. 12-18
- [PFE 98] Pfenning, G., Klewe-Nebenius, H., Seelmann-Eggebert, W., *Karlsruher Nuklidkarte*, Karlsruhe, Marktdienste Haberbeck GmbH, 1998
- [PHI 97] Phillips, D.H., Lannutti, J.J., *Measuring physical density with X-ray computed tomography*, 1997, NDT & E International vol. 30, pp. 339-350
- [PIL 89] Pillon, S., *Investigation on U-O-Na and Pu-O-Na phase diagrams*, CEA-R-5489, 1989
- [POP 00] Popov, S.G., Ivanov, V.K., Carbajo, J.J., Yoder, G.L., *Thermophysical properties of MOX and UO₂ fuels including the effects of irradiation*, 2000, ORNL/TM-2000/351
- [POU 03] Pouchon, M.A., Ingold, F., Kopajtic, Z., Tomita, Y., Kono, S., *Fabrication and Characterization of MOX Microspheres for the FUJI Project*, 2003, Proceeding GLOBAL 2003
- [POU 09] Pouchon, M.A., Ingold, F., *Internal Gelation at PSI: The past and the future*, 2009, Proceedings of ICAPP 09, paper 9494

- [RAH 03] Rahaman, M.N., *Ceramic Processing and Sintering 2nd edition*, New York, Marcel Dekkers, 2003
- [RAM 91] Rama Rao, G.A., Mukerjee, S.k., Vaidya, V.N., Venugopal, V., Sood, V.V., *Oxidation and hydrolysis kinetic studies on UN*, 1991, Journal of Nuclear Materials 185, pp. 231-241
- [RIC 06] Richerson, D.W., *Modern Ceramic Engineering properties, processing and use in design*, New York (U.S), Taylor & Francis Group LLC, 2006
- [RIE 11] Riedel, R., Chen, I-W., *Ceramics Science and Technology, Volume 3: Synthesis and Processing*, Hoboken NJ USA, Wiley, 2011
- [RIN 86] Ringström, B. (Editor)., Brohult, S., Blix, H., Grenthe, I., Gustafson, T., Kiessling, R., Leine, L., Lidén, K., Rydberg, J., Ståhl, I., *Kärnenergi i utveckling*, Köping (Sweden), Bonnier Fakta bokförlag AB, 1986
- [RIG 00] Riggs, J.E., Walker, D.B., Carroll, D.L., Sun, Y.P., *Optical Limiting Properties of Suspended and Solubilized Carbon Nanotubes*, 2000, Journal of Physical Chemistry, pp. 7071-7076
- [ROG 03] Rogozkin, B.D., Stepenova, N.M., Proshkin, A.A., *Mononitride Fuels for Fast Reactors*, 2003, Atomic Energy 95 (3), pp. 624-636
- [SAH 10] Saha, B., Acharya, J., Sands, T.D., Waghmare, U.V., *Electronic structure, phonons, and thermal properties of ScN, ZrN and HfN: A first-principles study*, 2010, Journal of Applied Physics 107 (3), art.no. 033715
- [SAW 88] Sawicka, B.D., Palmer, B.J.F., *Density gradients in ceramic pellets measured by computed tomography*, 1988, Nuclear Instruments and Methods in Physics Research A236, pp. 525-528
- [SHE 00] Sherif El - Eskandarany, M., Ashour, A.H., *Mechanically induced gas – solid reaction for the synthesis of nanocrystalline ZrN powders and their subsequent consolidations*, 2000, Journal of Alloys and Compounds 313, pp. 224-234
- [SIL 09] Silva, G.W.C., Yeamans, C.B., Cerefice, G.S., Sattelberger, A.P., Czerwinski, K.R., *Synthesis and Nanoscale Characterization of (NH₄)₄ThF₈ and ThNF*, 2009, Inorganic Chemistry 48, pp. 5736-5746
- [SIL 12] Silva, G.W.C., Weck, P.F., Kim, E., Yeamans, C.B., Cerefice, G.S., Sattelberger, A.P., Czerwinski, K.R., *Crystal and Electronic Structures of Neptunium Nitrides Synthesized Using a Fluoride Route*, 2012, Journal of the American Chemical Society, pp. 3111-3119
- [SKB 11] Svensk Kärnbränslehantering AB, *Long-Term Safety for the Final Repository for Spent Nuclear Fuel at Forsmark*, Technical Report SKB TR-11-01, 2011
- [SMA 05] Smart, L.E., Moore, E.A., *Solid State Chemistry – An Introduction 3rd edition*, Boca Raton, Taylor & Francis, 2005
- [SMI 60] Smiley, W.G., *Oxidation-Reduction Reprocessing of Uranium Carbide Reactor Fuel I. Carbothermic Reduction of UO₂*, 1960, ATOMICS INTERNATIONAL, Report NAA-SR-6976

- [SOM 11] Somers, J., *Minor Actinide Bearing Fuels: Fabrication and Irradiation Experience in Europe*, 2011, Energy Procedia 7, pp. 169-176
- [SOO 10] Sood, D.D., *The role sol-gel process for nuclear fuels-an overview*, 2010, Journal of Sol-Gel Science and Technology
- [STO 64] Storms, E.K., *A Critical Review of Refractories*, 1964, Report Los Alamos Scientific Laboratory LA-2942
- [STO 67] Storms, E.K., *Refractory Materials Volume 2-The Refractory Carbides*, Academic Press, New York (U.S), 1967
- [STR 67] Strausberg, S., *Conversion of U_3O_8 to UC*, 1967, United States Patent Office, Patent number 3,320,034
- [STR 03] Streit, M., Ingold, F., Pouchon, M., Gauckler, L.J., Ottaviani, J.-P., *Zirconium nitride as inert matrix for fast systems*, 2003, Journal of Nuclear Materials 319, pp. 51-58
- [STR 04] Streit, M., *Fabrication and Characterisation of (Pu,Zr)N Fuels*, Doctoral Thesis, ETH Zürich, Zürich, 2004
- [SUZ 98] Suzuki, Y., Arai, Y., *Thermophysical and thermodynamic properties of actinide mononitrides and their solid solutions*, 1998, Journal of Alloys and Compounds, pp. 577-582
- [TAK 01] Takano, M., Itoh, A., Akabori, M., Ogawa, T., Numata, M., Okamoto, H., *Carbothermic synthesis of (Cm,Pu)N*, 2001, Journal of Nuclear Materials 294, pp. 24-27
- [TAK 08] Takano, M., Akabori, M., Arai, Y., Minato, K., *Lattice thermal expansion of NpN, PuN and AmN*, 2008, Journal of Nuclear Materials 376, pp. 114-118
- [TSU 99] Tsukada, T., Venigalla, S., Morrone, A.A., Adair, J.H., *Low-Temperature Hydrothermal Synthesis of Yttrium-Doped Zirconia Powders*, 1999, Journal of the American Ceramic Society 82 (5), pp. 1169-1174
- [VAI 87] Vaidya, V.N., Mukerjee, S.K., Joshi, J.K., Kamat, R.V., Sood, D.D., *A study of chemical parameters of the internal gelation based Sol-Gel process for uranium dioxide*, 1987, Journal of Nuclear Materials 148, pp. 324-331
- [VAI 08] Vaidya, V.N., *Status of sol – gel process for nuclear fuel*, 2008, Journal of Sol-Gel science and Technology 46 (3), pp. 369-381
- [VĀL 14] Vālu, O.S., Beneš, O., Konings, R.J.M., Hein, H., *The high temperature heat capacity of the (Th, Pu)O₂ system*, 2014, Journal of Chemical Thermodynamics 68, pp. 122-127
- [VEG 21] Vegard, L., *Die Konstitution der Mischkristallen und die Raumfüllung der Atome*, 1921, Zeitschrift für Physik, 5, pp.17-26
- [VER 07] Verfondern, K., Nabelek, H., Kendall, J.M., *coated particle fuel for high temperature gas cooled reactors*, 2007, Nuclear Engineering and Technology 39 (5), pp. 603-616
- [WAL 11] Wallenius, J., *Transmutation of Nuclear Waste*, Märsta, Leadcold books and games, 2011

- [WAL 12] Wallenius, J., Suvdantsetseg, E., Fokau, A., *ELECTRA: European Lead – Cooled Training Reactor*, 2012, Nuclear Technology 177, pp. 303-313
- [WEC 13] World Energy Council, *World Energy Resources - 2013 Survey*, 2013, report
- [WIL 76] Wilhelm, H.A., McClusky, J.K., *Method of Preparing Uranium Nitride or Uranium Carbonitride Bodies*, 1976, United States Patent Office, Patent Number 3,953,556
- [WYM 68] Wymer, R.G., *Laboratory and Engineering Studies of Sol-Gel Processes at Oak Ridge National Laboratory*, 1968, Report ORNL-TM-2205
- [YEA 08] Yeamans, C.B., Chinthaka Silva, G.W., Cerefice, G.S., Czerwinski, K.R., Hartmann, T., Burrell, A.K., Sattelberger, A.P., *Oxidative ammonolysis of uranium(IV) fluorides to uranium(VI) nitride*, 2008, Journal of Nuclear Materials 374, pp. 75-78
- [YIM 06] Yim, M.S., Caron, F., *Life cycle and management of carbon-14 from nuclear power generation*, 2006, Progress in Nuclear Energy 48, pp. 2-36
- [YOS 68] Yoshihara, K., Kanno, M., Mukaibo, T., *Preparation of Uranium Nitrides from Uranium Tetrafluoride*, 1968, Journal of Nuclear Science and Technology 5 (12), pp. 643-646